2000

Aspects of the coordination chemistry of oxorhenium(V) and oxorhenium(VII) complexes

David William Lahti
Iowa State University

INFORMATION TO USERS

This manuscript has been reproduced from the microfilm master. UMI films the text directly from the original or copy submitted. Thus, some thesis and dissertation copies are in typewriter face, while others may be from any type of computer printer.

The quality of this reproduction is dependent upon the quality of the copy submitted. Broken or indistinct print, colored or poor quality illustrations and photographs, print bleedthrough, substandard margins, and improper alignment can adversely affect reproduction.

In the unlikely event that the author did not send UMI a complete manuscript and there are missing pages, these will be noted. Also, if unauthorized copyright material had to be removed, a note will indicate the deletion.

Oversize materials (e.g., maps, drawings, charts) are reproduced by sectioning the original, beginning at the upper left-hand corner and continuing from left to right in equal sections with small overlaps.

Photographs included in the original manuscript have been reproduced xerographically in this copy. Higher quality 6" x 9" black and white photographic prints are available for any photographs or illustrations appearing in this copy for an additional charge. Contact UMI directly to order.

Bell & Howell Information and Learning
300 North Zeeb Road, Ann Arbor, MI 48106-1346 USA
800-521-0600

Aspects of the coordination chemistry of oxorhenium(V) and oxorhenium(VII) complexes

by

David William Lahti

A dissertation submitted to the graduate faculty
in partial fulfillment of the requirements for the degree of
DOCTOR OF PHILOSOPHY

Major: Inorganic Chemistry
Major Professor: James H. Espenson

Iowa State University
Ames, Iowa
2000

Graduate College

Iowa State University

This is to certify that the Doctoral dissertation of

David William Lahti

has met the dissertation requirements of Iowa State University

Signature was redacted for privacy.

Major Professor

Signature was redacted for privacy.

For the Major Program

Signature was redacted for privacy.

For the Graduate College

TABLE OF CONTENTS

GENERAL INTRODUCTION

Introduction

The chemistry of organorhenium oxides is extensive, and a lot of this work has been done during the past 10 years.[1] Catalysis drives this area of research. The molecule methyltrioxorhenium(VII) (CH_3ReO_3), or MTO, is among the most important or popular species in this arena.[1] Among the most desirable features of MTO, that has allowed its chemistry to flourish, are its solubility in numerous common solvents, including water, while not having sensitivity to dioxygen. There are also convenient ^1H NMR signals, from the methyl group, for itself and many of its derivatives, as well as a useful electronic spectrum. Reviews on this topics have been published.[2,3] MTO was first observed in the late 1970's by Beattie and Jones[4] and was largely left unexplored until the efforts of Herrmann and coworkers realized ways to improve the synthesis in the early 1990's.[5,6] These two methods both rely on dirhenium heptoxide and tetramethyl tin as the starting reagents, eq 1, which shows the second of these procedures which is yet improved from the first.

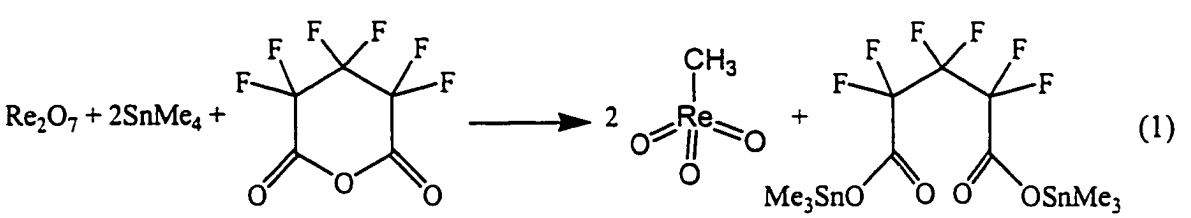

(1)

Since the direct alkylation route of dirhenium heptoxide causes a 50% loss of rhenium atoms due to formation of trialkylstannyl perrhenate, the second route, above, uses trifluoroacetic anhydride to suppress the rhenium containing byproducts, yet the drawback now is the expensive anhydride.[7] An even newer route, reported in 1997, is more atom efficient and utilizes simple perrhenate salts as the source of rhenium[7] and has been used

with success in this group recently. The other major advantage of this new route is that it uses a form of rhenium which is not sensitive to water and only requires one additional and inexpensive reagent, Me_3SiCl, and tetramethyl tin as before. This reaction, which can be done in one pot, is shown with the presumed intermediates, eq 2.

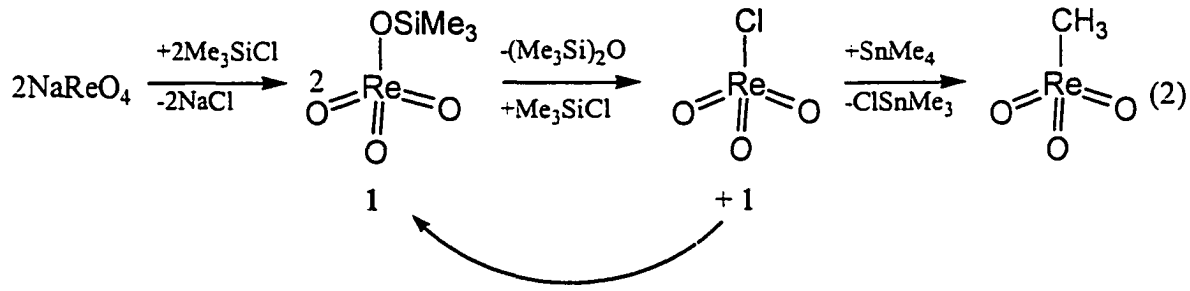

The recent preparation of a new family of dithiolato-oxo rhenium compounds, $\{CH_3(O)Re(SCH_2C_6H_4S)\}L$ or **M–L**, where **L** is a Lewis base, recently have been shown to be a useful group of catalysts for a variety of reactions.[8] A notable example is the catalytic removal of oxygen atoms from pyridine-N-oxides, to yield free pyridines, under mild conditions. Since catalysis, like many enzymes for that matter, typically require coordination or binding of a substrate to an open binding site of a metal, these **M-L** materials have the advantage of an open coordination site, that can be attacked by a basic ligand, is built right in; the molecule is five coordinate. This open site is in a position *trans* to the oxo ligand, shown below, where L is $MePh_2P$.

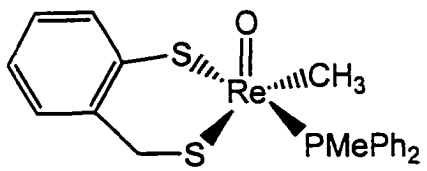

M-$PMePh_2$

It is observed that the ancillary ligand **L**, $PMePh_2$ in this case, is in a position *trans* to the phenolic sulfur of the dithiol chelate. The sulfur chelate is strongly bonded, as are the oxo and methyl ligands. Further, this is the ligand that is subject to displacement by attacking ligands, eq 3, illustrates a good example of a specific reaction, which I have studied. This is a noteworthy example since both $M–PPh_3$ and $M–PMePh_2$ have been characterized by x-ray crystallography, so the molecular structures are known.

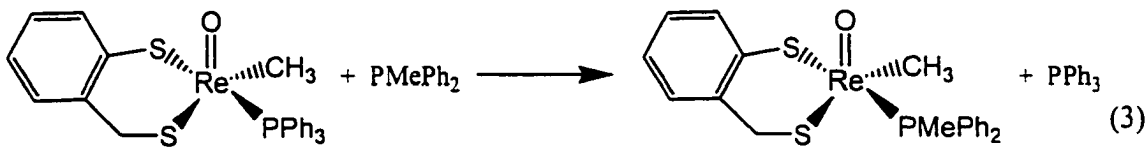

M-PPh_3 M-$PMePh_2$ (3)

During catalysis lots of species that could be ligands are present, especially when pyridine, a good Lewis base, is a product. Thus ligand substitution around rhenium becomes very important to understand since it is a first step in the catalystic reactions. Thus, kinetics and mechanistic studies must be done on a more basic level. Once a better understanding of this process is known, it will aid in assigning mechanisms of the catalytic reactions. The first thing to consider is that ligand exchange reactions can proceed via numerous mechanism, which at the limits are Associate (or A type) or Dissociative (or D type). Studies of these ligand exchange reactions and their kinetics and mechanism will be reported in this thesis. Further, a turnstile type mechanism in invoked to occur while ligands are exchanging around the complexes of the M–L type. This mechanism has recently been proposed for palladium complexes which undergo an intramolecular isomerization.[9]

The results of ligand exchange studies can be broken down into two groups. Specifically, the first group of reactions were observed to follow monophasic kinetics or, said another way, follow a single exponential decay. This monophasic nature is supported by lack

of any observable intermediates by ^{1}H NMR. The reactions which are described by eq 4, show M-L^1 reacting with L^2, in a first order process with rate constant k_1, while forming M-L^2 while L^1 is displaced. They appear to give the product right away.

$$M\text{-}L^1 + L^2 \xrightarrow{k_1} M\text{-}L^2 + L^1 \qquad (4)$$

After some thought, it seemed difficult to draw a mechanism for this reaction since the entering ligand and departing ligand ought enter and leave from the same position, if the principle of microscopic reversibility is to hold. Said another way, the L^1 ligand can not simply depart from the equatorial plane as L^2 attacks *trans* to oxo to form a pseudo octahedral transition state complex; only later to allow L^2 to swing up to occupy the position *trans* to the phenolic sulfur once held by L^1. This is a problem that my research addresses, as it seems an intermediate should be present, especially given the results of the other type of reactions.

The second class of reactions were actually found to follow "biphasic kinetics" and have an intermediate, called **I**, eq 5. Each step has rate constants equal to k_1 and k_2, respectively. All of these reactions were found to have a dependence on the concentration of the new ligand, L^2, to the first power: a first order dependence. Multiple approaches were taken to elucidate this mechanism and assign the rate constants properly, which is not always trivial for a biphasic reaction scheme.

$$M\text{-}L^1 \xrightarrow[k_1]{[L^2]} I \xrightarrow[k_2]{[L^2]} M\text{-}L^2 \qquad (5)$$

Biphasic reaction schemes are only observable when the rate constants for the first and second stage are comparable, given a large excess of one reagent. Certainly the rate

constants must be less than one order of magnitude apart and probably should be within no a factor of about six. Theoretically, a reactions that appears monophasic could actually be biphasic, like eq 5, if the second process, for example, was found to be much more rapid than the first; the intermediate reacts and disappears as soon as it is formed, eq 6. If this were the case, only k_1 would be measured. Thus, reactions that show a monophasic dependence were re-examined since it seemed like they should have a comparable mechanism.

$$M\text{-}L^1 + L^2 \xrightarrow{k_1} I \xrightarrow[\text{very fast}]{[L^2]} M\text{-}L^2 \qquad (6)$$

By using pyridine ligands, as L^1 ligands, it was possible to increase that rate of the first step to look to see if an intermediate could be seen. In fact, evidence for an intermediate was collected, and these results are also reported in the thesis. Since this allowed the second rate constant, k_2, was determined, it could be compared to k_1 for the monophasic reactions with the same L^2. It was found that k_2 is a factor of 200 and 50 for $MePh_2P$ and Me_2PhP, respectively faster, which explains why the first reactions were observed to be monophasic.

The new **M-L** complexes that have been described have been realized as a consequence of a desire to achieve sulfur atom transfer with MTO.[10] It was the discovery that MTO treated with H_2S became much better at removing sulfur atoms from episulfides to form triphenylphosphinesulfide in the presence of sacrificial triphenylphosphine.[10] This rhenium dimer [$\{CH_3(O)Re(SCH_2C_6H_4S)\}_2$], or **D**, complex was prepared since it has a mixture of oxo and sulfur ligands, the presumed result of the MTO/H_2S mixture.[11] The species, **D**, was found to be similar to the dimeric species [$\{CH_3(O)Re(SPh)_2\}_2$], which has been prepared in the past from MTO and thiophenol by Herrmann and coworkers.[12] **D** can

undergo monomerization with Lewis bases, to form two equivalent of **M-L** species, eq 7. The Re-S coordinate bonds are broken during this monomerization process.

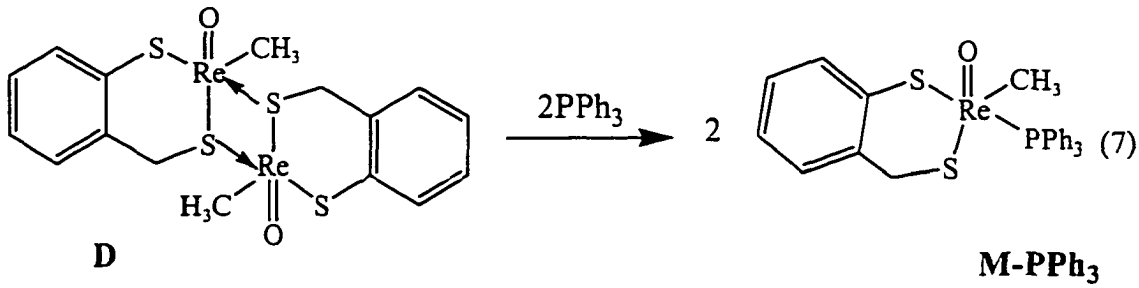

(7)

The kinetics and mechanism of monomerization of the dimer, **D**, has been reported earlier with selected pyridines and substituted trialkyl phosphine ligands.[13] The reaction scheme and been proposed, eq 8. The intermediate species are depicted in figure 1.

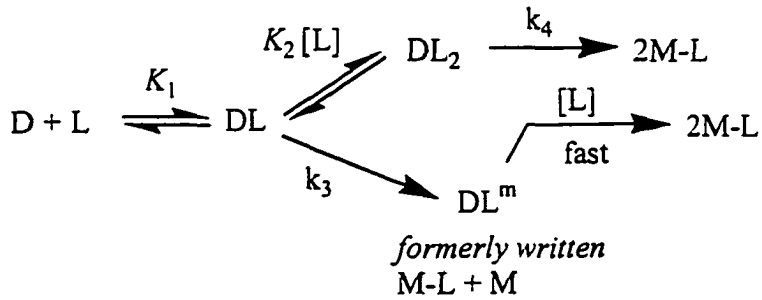

(8)

The following rate law can be constructed, which can support the current data that has been collected and is in the agreement with the above scheme, eq 9. The expression can be simplified if $K_1[L]$ and $K_1K_2[L]$ are dropped from the denominator. The expression for k_{obs} can be derived by making $k_a = k_3K_1$ and $k_b = k_4K_1K_2$, eq 10. This equation has a 'first order' and 'second order' term relative to the concentration of the ligand. I have used a variety of phosphines for studying the kinetics and mechanistic study on monomeriztion of **D** with ligands that have different cone angles and basisity.

$$\frac{d[\mathbf{ML}]}{dt} = 2\frac{k_3K_1[L] + k_4K_1K_2[L]^2}{1 + K_1[L] + K_1K_2[L]^2}[\mathbf{D}] \qquad (9)$$

$$k_{obs} = 2(k_a[L] + k_b[L]^2) \qquad (10)$$

Since there is no evidence for free or $[CH_3(O)Re(SCH_2C_6H_4S)]$ or **M** (produced down the first-order path, or via k_3) what was previously written M-L + M will now be called DL^m. The species DL^m has one coordinate Re–S bond broken, and can presumable undergo a fast reaction with a phosphine to break the remaining Re–S bond, figure 1.

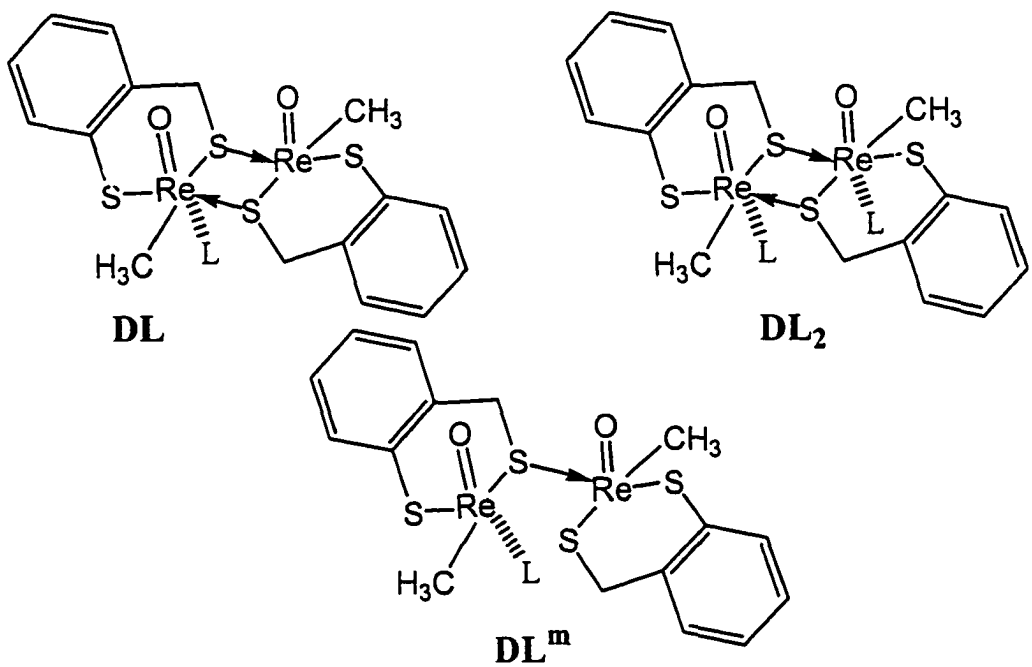

Figure 1. Structures of various rhenium(V) compounds.

Support for **DL** and $\mathbf{DL_2}$ comes from two structures had have been determined. The first, and previously reported, is an adduct of **D** and dmso, which forms **D-dmso** and supports **DL**. A hydroxide bridging adduct species of **D** has been prepared, $[Bu^n_4N][\{MeReO(mtp)\}_2(\mu\text{-}OH)]$. Figure 2 shows the anionic portion which contains

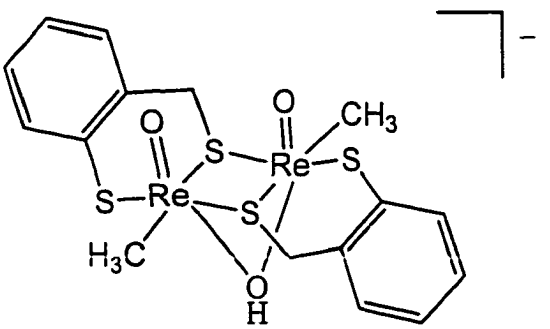

$[\{MeReO(mtp)\}_2(\mu\text{-}OH)]^-$

Figure 2. The bridging hydroxide structure of compound $\{MeReO(mtp)\}_2$.

rhenium. While this compound does not have the same stoichiometry as the intermediate **DL_2**, in terms of binding, it offers support of its existence.

The fact that **D** and **M-L** both have a methyl and oxo ligand is not by chance, as **D** is first made from MTO.[11] This reaction is shown in eq 8. The rhenium has been reduced here from Re(VII) in MTO to Re(V) in the **D**, which is why two equivalents of disulfide have been produced from half of the dithiol starting reagent, 2-methylmercapothiophenol.

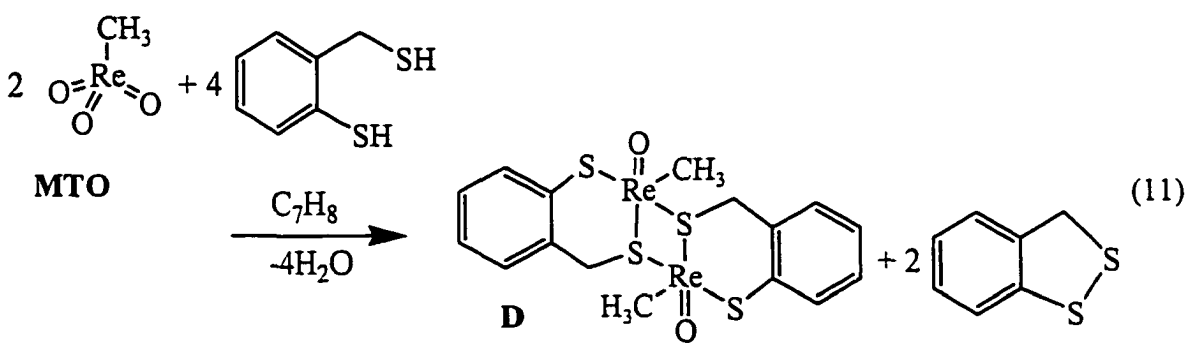

MTO **D** (11)

MTO is most famous for its ability to active hydrogen peroxide and efficiently and rapidly deliver an oxygen atom from hydrogen peroxide to a substrate, an oxygen atom acceptor, eq 10.

$$H_2O_2 + X \longrightarrow XO + H_2O \qquad (12)$$

To do so, it can form a monoperoxo and diperoxo species, denoted **A** and **B**, respectively, eq 13. It is these species that actually are the catalytically active form, MTO itself does not donate one of its oxygen atoms to substrates. Typically, **A** and **B** have comparable reactivity.[3]

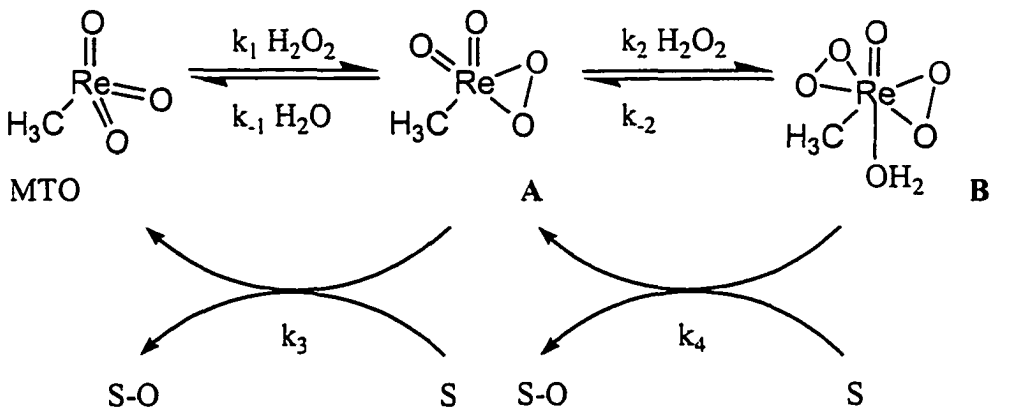

(13)

The final chapter will present a paper in which the topic oxidation of organic sulfoxides with MTO and hydrogen peroxide, HP. It was discovered in this work that only **B** can efficiently oxidized sulfoxide and **A** has virtually no reactivity toward them, eq 14. The reason such a study was preformed, is that it adds a nice compliment of results to the previous kinetic study of the oxidation of sulfides with MTO and HP.[14] Further, it examines whether there is a change in mechanism for this process, as was found for the oxidation of organic sulfines.[15]

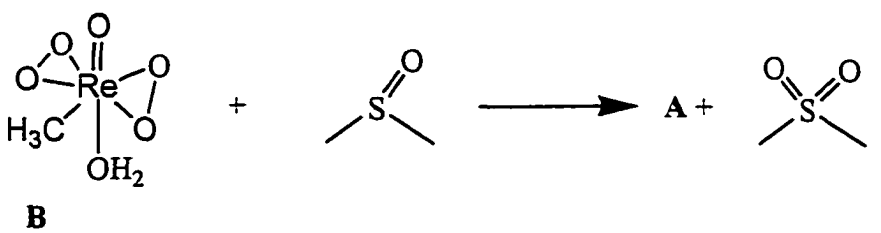

(14)

Dissertation Organization

The dissertation consists of four chapters which are written as journal papers. Chapter 1 corresponds to manuscript submitted for publication to the *Journal of the American Chemical Society*. This paper concerns ligand exchange reactions around five-coordinate rhenium(V) compounds. Chapter 2 corresponds to a manuscript describing an new hydroxide bridging species derived from the dimer, **D**, which will be submitted for publication to *Inorganic Chemistry*. Chapter 3 corresponds to a paper concerning the products made from treating rhenium(V) compounds with chelating phosphorus containing ligands. Chapter 4 reports on the oxidation of sulfoxides with MTO and hydrogen peroxide, which has been published in *Inorganic Chemistry*.[16] Each chapter is self-contained with its own equations, figure, tables and references. Following the last chapter is a general conclusion. Except for the X-ray structural analysis, all of the work done and results presented were performed by the author, David W. Lahti.

References

(1) Romao, C. C.; Kuhn, F. E.; Herrmann, W. A. *Chem. Rev.* **1997**, *97*, 3197-3246.

(2) Herrmann, W. A.; Kuhn, F. E. *Accounts of Chemical Research* **1997**, *30*, 169-180.

(3) Espenson, J. H. *Chem. Comm.* **1999**, 479-488.

(4) Beattie, I. R.; Jones, P. J. *Inorg. Chem.* **1979**, *18*, 2318.

(5) Herrmann, W. A.; Romao, C. C.; Kiprof, P.; Behm, J.; Cook, M. R.; Taillefer, J. *J. Organomet. Chem.* **1991**, *413*.

(6) Herrmann, W. A.; Kuhn, F. E.; Fischer, R. W.; Thiel, W. R.; Romao, C. C. *Inorg. Chem.* **1992**, *31*, 4431.

(7) Herrmann, W. A.; Kratzer, R. M.; Fischer, R. W. *Angew. Chem., Int. Ed. Eng.* **1997**, *36*, 2652-2654.

(8) Wang, Y.; Espenson, J. H. *Organic Letters* **2000**, *2*, 3525.

(9) Casares, J. A.; Espinet, P. *Inorg. Chem.* **1997**, *36*, 5428-5431.

(10) Jacob, J.; Espenson, J. H. *Chem. Comm.* **1999**, 1003-1004.

(11) Jacob, J.; Guzei, I. A.; Espenson, J. H. *Inorg. Chem.* **1999**, *38*, 1040-1041.

(12) Takacs, J.; Cook, M. R.; Kiprof, P.; Kuchler, J. G.; Herrmann, W. A. *Organometallics* **1991**, *10*, 316-320.

(13) Lente, G.; Guzei, I. A.; Espenson, J. H. *Inorg. Chem.* **2000**, *39*, 1311-1319.

(14) Vassell, K. A.; Espenson, J. H. *Inorg. Chem.* **1994**, *33*, 5491.

(15) Huang, R.; Espenson, J. H. *J. Org. Chem.* **1999**, *64*, 6374.

(16) Lahti, D. W.; Espenson, J. H. *Inorg. Chem.* **2000**, *39*, 2164-2167.

CHAPTER I. ISSUES OF MICROSCOPIC REVERSIBILITY AND AN ISOMERIC INTERMEDIATE IN LIGAND SUBSTITUTION REACTIONS OF FIVE-COORDINATE OXORHENIUM(V) DITHIOLATE COMPLEXES

A paper submitted to the *Journal of the American Chemical Society*.

David W. Lahti and James H. Espenson

Abstract

Ligand substitution reactions between five-coordinate oxorhenium(V) dithiolates, $[CH_3ReO(SCH_2C_6H_4S)X]$, and entering ligands Y have been studied in detail; Y is a phosphine and X is a phosphine (usually) or a pyridine. Many of them occur in two distinct stages, although some merge to a single kinetic term when the successive rate constants are quite different in value. The biphasic reaction give clear evidence for the intervention an intermediate which rises to a level that it can be detected directly by electronic and NMR spectroscopy. Even the monophasic reactions follow this pattern, when the first rate constant is made larger by substitution of X by a better leaving group. Just for the phosphines, the range of rate constants is remarkably large; in the first stage, k spans the range 10^{-4}–10^{1} L mol^{-1} s^{-1} at 25 ° in benzene; in the second, which also shows a first-order dependence on the concentration of the entering ligand, the range is 10^{-4}–10^{3} L mol^{-1} s^{-1}. Spectroscopic evidence shows that the intermediate has the same composition as the product; the metastable form is designated as MeReO(mtp)Y*. The structures of all the isolated products have a single stereochemical pattern: Me and $-SCH_2$ lie in trans positions, as do Y and –SAr. This is believed to be reversed in the transient, Y and $-SCH_2$ occupying trans position. Further

support for this assignment comes from the ^{31}P splitting of the ^{1}H NMR spectrum. It shows further splitting indicative of unusual four-bond coupling from a W-pattern of the hydrogen and phosphorus atoms. The intermediate does not undergo an intramolecular rearrangement to the final product; instead, it reacts with a ligand of the same type, clearly an intermolecular rearrangement. The activation parameters were determined for selected reactions and the results support a mechanism with considerable associative character, as the $\Delta S^{\ddagger}$ values are ca. -125 J K^{-1} mol^{-1}. To account for the intervention of the isomer while honoring the principle of microscopic reversibility, a mechanism is proposed involving a C_3 rotation of a specific group of three ligands in the six-coordinate transition state. Entering ligand must enter from the vacant coordination position trans to the Re=O group; a means must be devised for leaving group X to gain that position. Turnstile rotation of the groups X, Me, and Y can accomplish the needed transposition; the transition state passes through an approximate trigonal prismatic configuration. In so doing, a different and less stable isomer is formed. A second reaction, between $MeReO(SCH_2C_6H_4S)Y^*$ and Y, then ensues by the *same* mechanism. This turnstile operation generates the product in the stable isomeric form. Results are also presented from a study of monomerization of the dimeric rhenium species, $\{CH_3ReO(SCH_2C_6H_4S)\}_2$, with phosphines of various size and basicity. The results support a mechanism with two intermediates on the pathway to form two equivalents of $MeReO(SCH_2C_6H_4S)X$.

Introduction

Oxorhenium compounds are known to catalyze oxygen-atom transfer reactions between closed shell molecules. Thus, as has been reviewed,[1-3] $MeReO_3$ (MTO) is an active catalyst for the oxidation of many different substrates by hydrogen peroxide:

$$X + H_2O_2 \rightarrow XO + H_2O \qquad (1)$$

where $X = R_2S$,[4] PR_3,[5] alkenes, hydroxylamines, anilines, etc.[1] Also, the couple $MeReO_3/MeReO_2$ catalyzes the reduction of oxoanions, including perchlorate ions, in aq. solution:[6,7]

$$ClO_4^- + 4\ H_3PO_2 \rightarrow Cl^- + 4\ H_3PO_3 \qquad (2)$$

The chemistry of oxorhenium compounds has been developed extensively in the past decade.[2,8,9] The deoxygenation of pyridine N-oxides[10] is catalyzed by the Re(V) compound $MeReO(mtp)PPh_3$ (Chart 1), eq 3. Here, $mtpH_2$ is 2-(mercaptomethyl)thiophenol; many such compounds are now known and characterized, with L = phosphine, pyridine, thioether, and similar Lewis bases.[11-13]

$$X\text{-}C_5H_4NO + PPh_3 \rightarrow X\text{-}C_5H_4N + Ph_3PO \qquad (3)$$

The success of such catalytic conversions rests in part on the replacement of one ligand for another, particularly the replacement of a existing ligand by the substrate. Thus, to understand the mechanism for catalysis we need to characterize ligand substitution reactions. The MeReO(mtp)L compounds adopt an approximate square-pyramidal structure with the oxo group in the axial position; of those characterized to date, in every case the methyl group lies trans to the benzylic sulfur of mtp.[11-13] This thermodynamic preference for a single

stereoisomer proves to be an important feature of their substitution chemistry, as developed in the course of this research. We have undertaken studies the following reaction

$$MeReO(mtp)X + Y \rightarrow MeReO(mtp)Y + X \qquad (4)$$

Previous work on low-valent oxorhenium compounds has shown that the reaction adopts an associative mechanism.[14] This aspect will be dealt with in the present reactions but as it turns out, some important issues are raised here that, to our knowledge, have not been addressed before. Three interrelated issues are: (1) Can L' enter from the lower, vacant axial position, L leaving from an equatorial position? Given the requirements of microscopic reversibility, this appears to be impermissible. (2) Related to this, can a "wedge" structure be formed in an intermediate or transition state, much as has been invoked for square-planar complexes? This species, however, lacks a horizontal symmetry plane, so considerations of microscopic reversibility again enter, ruling out the wedge structure so often invoked for square-planar substitution reactions. In fact, our data will show that the system adopts a different and somewhat more complicated mechanism. The structure of these complexes ligand access to the vacant sixth coordination position trans to the oxo group. The mechanism must, however, satisfy certain requirements, principally that it be symmetric with respect to forward and reverse reactions. (3) Can we show the generality of the finding that MeReO(mtp)PPh3* is an intermediate in the reaction between MeReO(mtp)Py and PPh3?[12] In this study we have also shown that a transient, designated MeReO(mtp)Y*, can be detected in kinetics and in spectroscopy with many of the combinations of leaving and entering ligands. With other ligand pairs, however, the intervention of MeReO(mtp)Y* has been inferred, for reasons to be presented. Here, the notation MeReO(mtp)Y* designates an

isomer of MeReO(mtp)Y; we suggest that the methyl group is trans to the phenolic sulfur in the intermediate. We will provide support that system adopts a *turnstile* mechanism[15-19] to explain our data.

Also bearing on mechanistic issues in catalysis, it should be noted that the dirhenium compound {MeReO(mtp)}$_2$ (**D**, Chart 1) is monomerized upon reaction with the same set of ligands according to this *reversible* reaction:[13,20a]

$$\mathbf{D} + 2\,\mathrm{L} \rightleftharpoons 2\,\mathbf{M}\text{–}\mathrm{L} \qquad (5)$$

It, too, starts with attack of L at either (sometimes both) of the equivalent, vacant axial sites. Some of the same issues are involved in the mechanism of monomerization, not the least of which are the question of the possible involvement of MeReO(mtp)Y* and an assessment of the extent to which any MeReO(mtp)Y is formed directly.

Chart 1

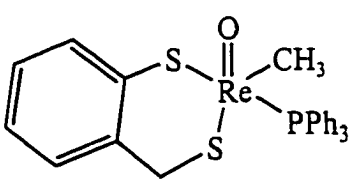

MeReO(mtp)PPh$_3$

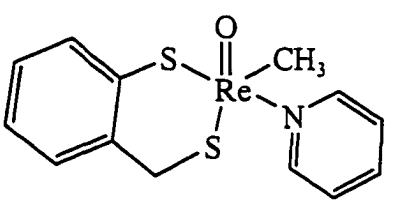

MeReO(mtp)Py

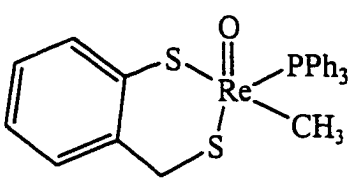

MeReO(mtp)PPh$_3$*

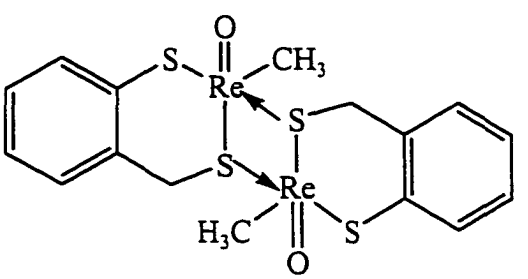

{MeReO(mtp)}$_2$ **D**

Experimental

Reagents. MTO was prepared from sodium perrhenate according to a published procedure.[20b] The dimeric complex $\{MeReO(mtp)\}_2$ was prepared from MTO and $mtpH_2$ as previously reported.[11] The dimer was the source of the monomeric phosphine complexes, obtained from mixing a 2.1:1 molar ratio of phosphane to dimer in toluene, resulting in $MeReO(mtp)PR_3$. The solvent was removed and the compound purified by recrystallization from methylene chloride–hexanes after cooling to –10 °C. This procedure was successful for the previously-prepared compound with PPh_3, as well as for new compounds that are analogues of it, with $PMePh_2$, $PCyPh_2$, $PPhCy_2$, $P(4\text{-}ClC_6H_4)_3$, $P(4\text{-}FC_6H_4)_3$ and $P(4\text{-}MeC_6H_4)_3$.

Previously, $MeReO(mtp)PR_3$ complexes of PPh_3 and other phosphines were characterized spectroscopically and crystallographically.[11] Each complex was characterized by ^1H, ^{31}P, and UV/Visible spectroscopy. One can see from Figure 1 that $MeReO(mtp)PR_3$ complexes are characterized by a weak absorption maximum near 600 nm (ε ~200 L mol^{-1} cm^{-1}) and a much stronger shoulder near 400 nm (ε ~1500 L mol^{-1} cm^{-1}). Extinction coefficients and NMR data are presented for numerous $MeReO(mtp)PR_3$ complexes in Tables S–1 and S–2. The difference in intensity between the 600 nm band of reactant and product is too low in intensity to be useful for kinetics. Thus most studies were carried out in the vicinity of 400 nm.

The isolated $MeReO(mtp)PR_3$ complexes were used directly as the starting materials in the kinetics determinations. Because pyridine complexes coordinate more weakly than phosphines, an isolated MeReO(mtp)Py complex will dissociate to considerable extent, giving rise to the dimer. For that reason, the reactions of MeReO(mtp)Py complexes were

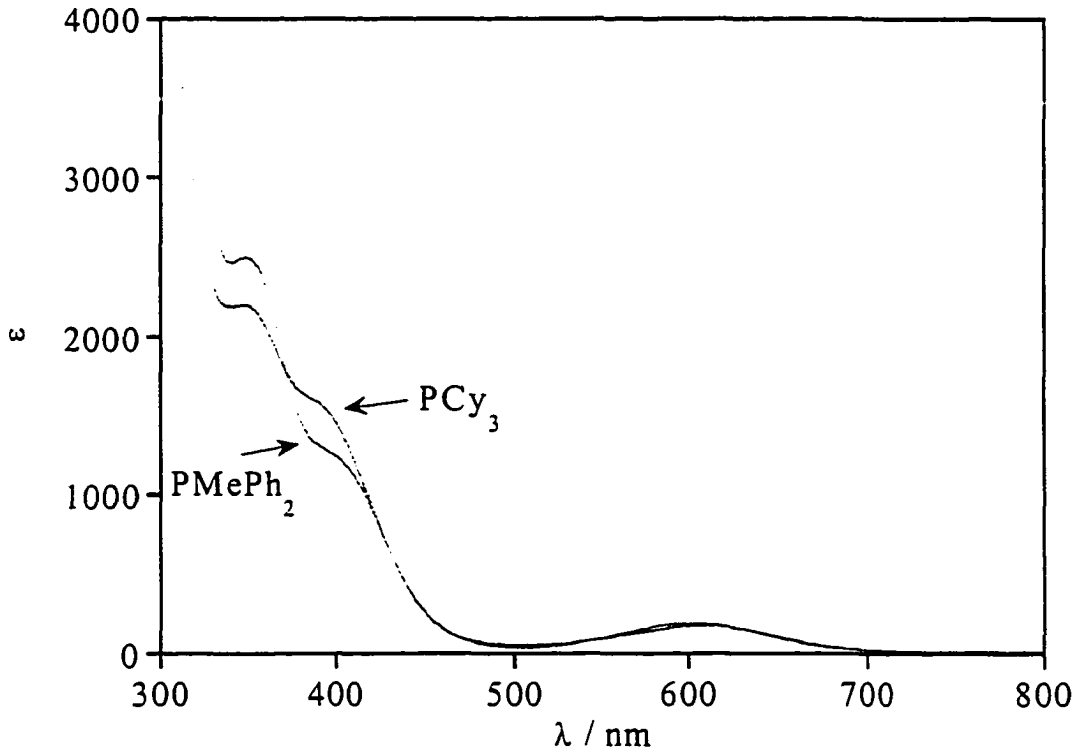

Figure 1. UV–visible spectra of two compounds MeReO(mtp)–PR_3, with $PMePh_2$ and PCy_3. The difference at 500–700 nm is too small to be useful, whereas that near 400 nm provided a precise measure of the reaction progress.

carried out in the presence of added pyridine to prevent formation of $\{MeReO(mtp)\}_2$ by the reverse of reaction 5. It was shown that a 10-fold increase in the concentration of free pyridine was immaterial. Benzene was used as the solvent for reaction kinetics.

Kinetics. A Bruker DRX–400 spectrometer was used to record NMR spectra. Chemical shifts were recorded relative to tetramethylsilane or the residual proton peak of the deuterated solvent. Shimadzu 3101 and 2501 spectrophotometers were used for optical spectra and to monitor reactions that lasted longer than ca. 30 s. Two stopped-flow (SF) instruments were used for more rapid reactions; one is a single-wavelength Applied Photophysics Laboratories (APL) instrument that was also used in sequential mixing experiments, the other an OLIS SF apparatus with a rapid-scanning monochromator and global fitting programs The SF data obtained with the OLIS instrument was collected over a 230 nm range, usually 310–540 nm. That window was sometimes narrowed to 350–475 nm when little absorbance change could be detected outside that range. Ligand exchange reactions usually used the entering ligand at 1–40 mM, a much higher concentration than that of the starting complex, typically 80 μM. Reactions of MeReO(mtp)Py (M–Py) complexes also contained free pyridine at a concentration of about 1–5 mM. Because the formation constants are K (M–PR_3) >> K (M–Py), these reactions proceeded to completion and their rates were independent of the pyridine concentration over the range investigated. The data were analyzed by single-exponential (pseudo-first-order) or biexponential equations, as needed.

A sequential SF experiment with the APL instrument was carried out in which the two components, MeREO(mtp)(4-$Bu^tC_5H_4N$) and $PMePh_2$, were mixed as usual. After a selected time (usually 3.0 s) in the "aging loop" a final reagent (PMe_2Ph) was mixed

automatically with the first two. Data from five replicates were averaged to obtain the final rate constant. Similar experiments with different reagents that allowed for a longer delay (ca. 120 s) were performed by rapidly introducing freshly-prepared solutions into the OLIS instrument, such that the first measurement could be taken just at 120 s.

The two equations used for fitting most absorbance–time data are those for first-order kinetics, eq 6, and biexponential kinetics, eq 7, as in the case where two pseudo-first-order reactions occur in sequence.

$$Abs_t = Abs_\infty + (Abs_0 - Abs_\infty)e^{-k\cdot t} \quad (6)$$

$$Abs_t = Abs_\infty + \alpha e^{-k_\alpha \cdot t} + \beta e^{-k\beta \cdot t} \quad (7)$$

Isolation and Crystallographic Studies. The compound MeReO(mtp)$PMePh_2$ was prepared from 30 mg of $\{MeReO(mtp)\}_2$ in benzene and 2.1 eq $PMePh_2$. The solution was allowed to evaporate over 2 d, giving bright green crystals in 80% yield. Elem. anal.: found C 44.72 found (44.12 calcd.), H 3.87 (3.88); S 10.2 (11.2).

The crystal evaluation and data collection were performed on a Bruker CCD–1000 diffractometer with Mo–Kα (λ 0.71073 Å) radiation. The distance from the diffractometer to the crystal was 5.08 cm. All non-hydrogen atoms were refined with anisotropic displacement coefficients. The hydrogen atoms were included in the structure factor calculation at idealized positions and were allowed to ride on the neighboring atoms with relative isotropic displacement coefficients. The software and sources of the scattering factors are contained in the SHELXTL program library, version 5.1[21] The absorption correction was based on fitting a function to the empirical transmission surface as sampled by multiple equivalent measurements.[22]

Results

X-ray crystallography. Previous structures of MeReO(mtp)L complexes have been determined: L = PPh_3,[11] Py,[12] and 1,1,3,3-tetramethylthiourea,[13] 4-acetylpyridine[13] and 1,3-diethylthiourrea.[12] With that, further structural determinations might seem redundant, were it not for the way in which the mechanistic results of this study pointed towards an intermediate that might be an isomeric form. Thus the structure of the compound MeReO(mtp)$PMePh_2$ was determined by single crystal x-ray diffraction. The crystallographic information is summarized in Tables S–3-to-7 in the Supporting Information. The molecular structure is depicted in Figure 2, with a few key bond distances and angles given in its caption. Complete information is given in Table S–5 and Figure S-1. This structure is analogous to the five preceding ones. The groups about rhenium form an approximate square pyramid[23] with the oxo group at the apex. All four compounds adopt the same structural format: the CH_3 group is trans to the S atom attached to the benzylic carbon; the phenolic S lies trans to the Lewis base, here the P atom of $PMePh_2$. This holds irrespective of the electronic and steric attributes of the coordinated ligand.

From this data base we postulate, therefore, that all stable compounds of this family have analogous structures. That is to say, this structure is the thermodynamically preferred one for all phosphine and pyridine ligands. This argument is key to other assignments that we are making as to the probable structure of a metastable intermediate detected by kinetics and spectroscopy. We suggest that the intermediate has the CH_3 group and ligand reversed.

Initial Observations. We have examined reactions of the compounds MeReO(mtp)X, where X is used to represent the leaving ligand, phosphine (usually) or pyridine (occasionally). Upon reaction with an entering group Y, a different phosphine,

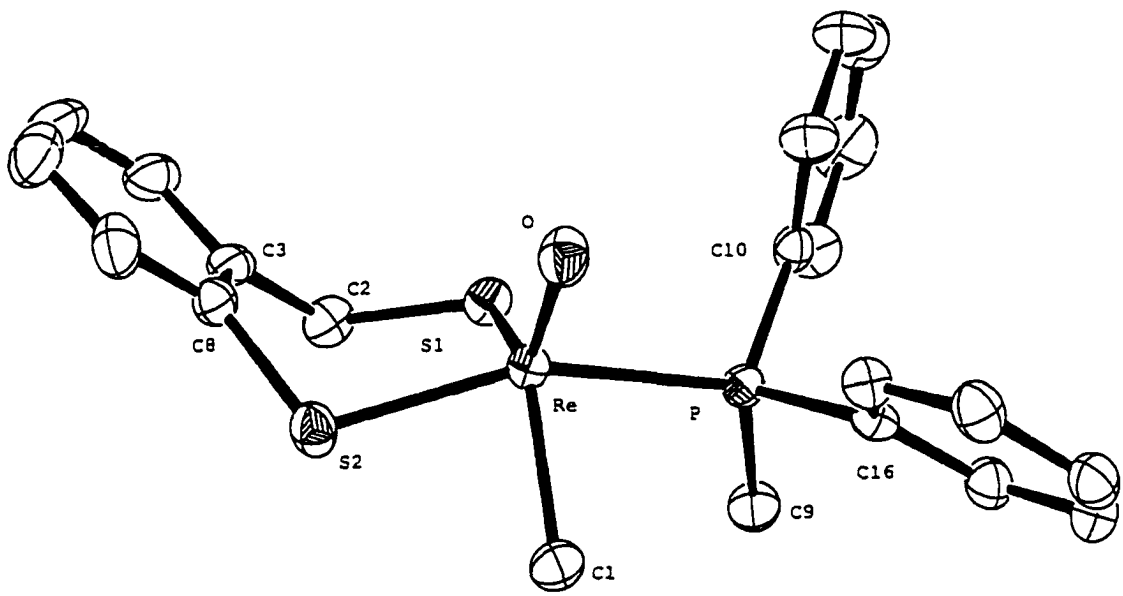

Figure 2. Perspective view of the rhenium compound MeReO(mtp)$PMePh_2$ with thermal ellipsoids at the 30% probability level. Selected bond lengths (pm) and angles (deg): Re(1)–O(1), 168.4; Re(1)–C(1), 213.2; Re(1) –P, 245.4; Re(1) –S(1), 227.6; Re(1)–S(2), 232.1; S(1)–C(2), 184.9; S(2)–C(8), 178.2; O(1)–Re–C(1), 115.8; O(1)–Re–S(1), 119.9; C(1)–Re–S(2), 123.73; O–Re–S(2), 106.5, S(1)–Re–S(2), 90.37, C(1)–Re–S(2), 80.22. Additional structural parameters are given in Table S–5.

MeReO(mtp)Y is formed. This seemingly simple transformation has proved to be more intricate than this, however, and is rich in new mechanistic insights. In many cases the kinetics and spectroscopy afford direct evidence for the intervention of an intermediate. In others, the intermediate could not be seen but we will demonstrate that it is mostly likely disguised but not absent.

It is instructive first to examine one particular combination, X = PPh_3 and Y = $PCyPh_2$ (Cy = cyclohexyl). When followed spectrophotometrically with [Y] >> [MeReO(mtp)X], the absorbance at 400 nm first rises and then falls, Figure 3. The same experiment monitored by ^{1}H NMR spectroscopy shows the buildup of a resonance at 5.1 ppm that later disappears. Analysis of the absorbance-time data, given the large excess of the entering ligand, was made by bi-exponential kinetics, which gave excellent fits at each set of concentration conditions. The pair of pseudo-first-order rate constants so determined are designated k_α and k_β, describing their relative numerical values. We defer momentarily a specification as to which rate constant is the first or second in the sense of the chemical reaction scheme (this is the context for which the designations k_1 and k_2 are reserved). The kinetics determinations were carried out at several concentrations of $PCyPh_2$. Figure 4 shows that k_α and k_β are both linear functions of [Y] that extrapolate to the origin. Thus both stages and not only the first is a *displacement* process. An abbreviated scheme is therefore:

$$\mathbf{M}\text{-X} \xrightarrow[k_1]{Y} X + \text{Int}; \quad \text{Int} \xrightarrow[k_2]{Y} Y + \mathbf{M}\text{-Y} \qquad (8)$$

Spectroscopic data indicate that the intermediate contains [MeReO(mtp)] (or **M**) and Y, but not X, as written in eq 8. The doublet pattern for CH_3 in the ^{1}H NMR spectrum shows

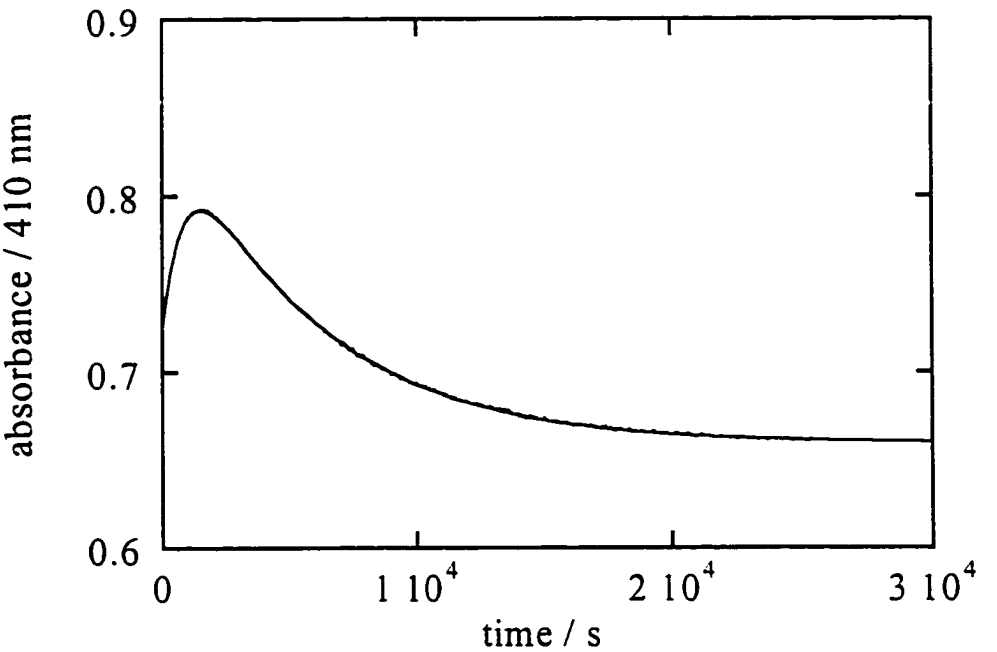

Figure 3. The absorbance-time data for a reaction between 0.58 mM MeReO(mtp)PPh_3 and 45 mM $PCyPh_2$ at 298 K in benzene. A fit to biexponential kinetics gave these rate constants: $k_\alpha = 1.15 \times 10^{-3}\ s^{-1}$ and $k_\beta = 1.83 \times 10^{-4}\ s^{-1}$.

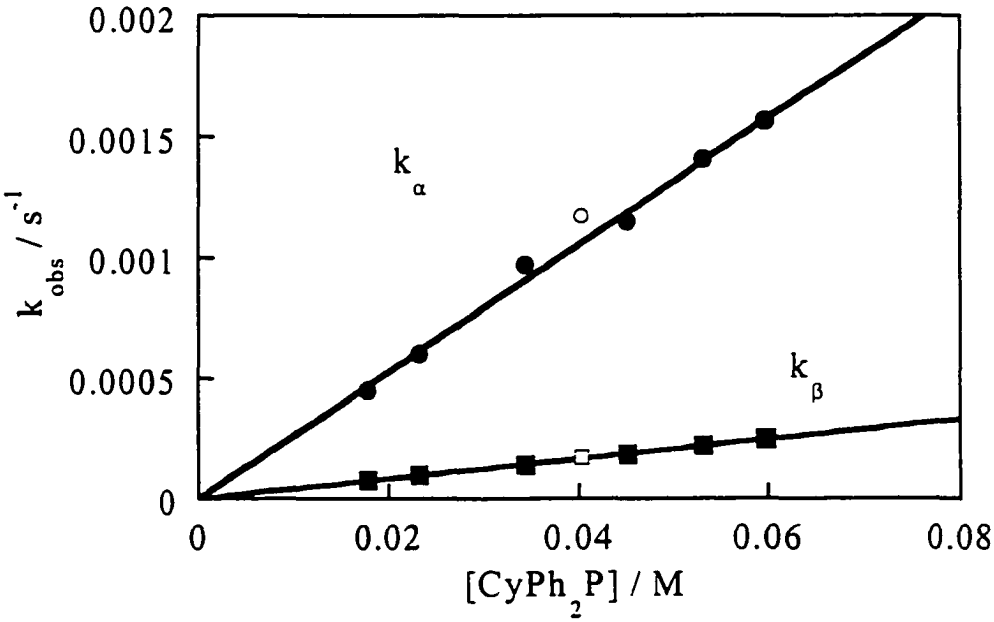

Figure 4. The plots show values of k_α (circles) and k_β (squares) against [PCy_2Ph], including data taken at two wavelengths, 360 nm (filled symbols) and 410 nm (cross-hatched symbols). The least-squares slopes are 2.4×10^{-2} and 4.2×10^{-3} L mol^{-1} s^{-1}.

that **M–X**, **M–Y** *and the intermediate* contain a single phosphorus atom coordinated to Re; a more complex pattern would have been seen if X and Y had both remained coordinated in the intermediate species.

Successive Displacement Reactions. For the other X, Y pairs whose reactions follow bi-exponential kinetics, the pattern is the same. For each ligand pair it is possible to evaluate its two first-order rate constants and substantiate that both vary linearly with the concentration of Y. The resulting data take the form of second-order rate constants, designated k_α and k_β, as summarized in Table 1. Three entering ligands were used, Y = $PCyPh_2$, PCy_2Ph and $P(4\text{-}MeC_6H_4)_3$. For each, one member of the pair of rate constants for each X ligand has the same value, within the precision of resolving the pair of values from bi-exponential fitting. Irrespective of whether the constant member is a value of k_α or k_β, we designate it as k_2. This assignment rests on the fact that the second-stage reaction does not retain any involvement of X (see eq 8). To reiterate this important point: according to eq 8, every reaction of a given Y has the second chemical step identical for all X ligands. Thus its rate constant k_2 must be the same for each X ligand. The data in Table 1 show that constancy reasonably well and thus lend support to the reaction model.

NMR Studies of the Intermediate. On the basis of this assignment, ^1H NMR spectroscopy was used to examine the reaction, particularly to provide confirmatory evidence for the existence and composition of an intermediate. The reaction between $MeReO(mtp)PPh_3$ and $PCyPh_2$ gave rise to new resonance at 5.1 ppm that developed and then disappeared; see Figure S–2. Since its intensity is not large, it is clear that the intermediate never attains a high concentration. The spectrophotometric data afforded rate constants of 2.6×10^{-2} and 4.1×10^{-3} s^{-1}. The assignment made earlier was $k_2 = 2.6 \times 10^{-2}$

Table 1. Rate constants for the biphasic ligand exchange reactions at 25 °C. The ligand on rhenium initially is X, and the new (entering) ligand is denoted Y.

entry	X	sorted by k_α and k_β ($L\ mol^{-1}\ s^{-1}$)		sorted by k_1 and k_2 ($L\ mol^{-1}\ s^{-1}$)	
Part A: Y = $PCyPh_2$					
1	$P(4\text{-}MeC_6H_4)_3$	0.021	0.0016	0.0016	0.021
2	PPh_3	0.026	0.0041	0.0041	0.026
3	$P(4\text{-}ClC_6H_4)_3$	0.035	0.023	0.035	0.023
4	$P(4\text{-}FC_6H_4)_3$	0.037	0.024	0.037	0.024
5	Cl^-	0.52	0.024	0.52	0.024
6	$PMePh_2$	~0.05[a]	~0.09[a]		
					av 0.024
Part B: Y = PCy_2Ph					
7	$P(4\text{-}MeC_6H_4)_3$	2.7×10^{-4}	1.0×10^{-4}	1.0×10^{-4}	2.7×10^{-3}
8	PPh_3	4.4×10^{-4}	1.9×10^{-4}	4.4×10^{-4}	1.9×10^{-4}
9	$P(4\text{-}ClC_6H_4)_3$	5.5×10^{-3}	2.5×10^{-4}	5.5×10^{-4}	2.5×10^{-4}
					av 2.4×10^{-4}
Part C: Y = $P(4\text{-}MeC_6H_4)_3$					
10	PPh_3	0.021	0.0016		
11	$P(4\text{-}ClC_6H_4)_3$			0.055	0.033
12	$PMePh_2$			0.021	0.0016
					av. 0.051

a) result from poor fitting

s^{-1}, made on the basis that k_2 would be the same for all X, is thus confirmed. Only when the second rate constant is much larger than the first will the intermediate be held at a low concentration. From these values the maximum extent of buildup of the intermediate is:

$$\frac{[\text{Int}]_{max}}{[\text{MeReO(mtp)PPh}_3]_0} = \left(\frac{k_2}{k_1}\right)^{\frac{k_2}{k_1 - k_2}} \qquad (9)$$

which is 11% in this instance. This agrees with the value obtained from integration of the NMR spectra, ca. 10% intermediate at the maximum. The results of a similar reaction between MeReO(mtp)(4-ClC_6H_4)$_3$ and $PCyPh_2$ gave rise to 45% buildup of the intermediate observed, as depicted in Figure 5, in agreement with the calculation from eq 9 given the assignment of reaction steps in Table 1. Figures S–3 and S–4 show the time evolution of the intensities of each product, starting material, and intermediate attained by integration of the NMR experiments shown in Figures 5 and S–2, respectively. The NMR spectrum of the intermediate is quite distinct. The CH_3 resonance is split into a doublet by a single ^{31}P from Y; X is absent in the spectrum of the intermediate, consistent with eq 8.

Reactions Showing Single-Stage Kinetics. Absorbance-time data from a number of other groups of reactions between MeReO(mtp)X and Y are accurately fit by simple first-order kinetics. With X = PPh_3 and Y = $PMePh_2$, for example, the time course for product buildup is defined with $k = 2.02 \times 10^{-3}$ s^{-1} in benzene at 25.0 °C. Figure 6 illustrates the data and the least-squares fitting. The occurrence of monophasic kinetics is not an isolated instance, as shown for the 10 entries in Table 2; in these cases no intermediates were detected by NMR. Figure S–5 shows the linear relationship between the concentration of $MePh_2P$ and

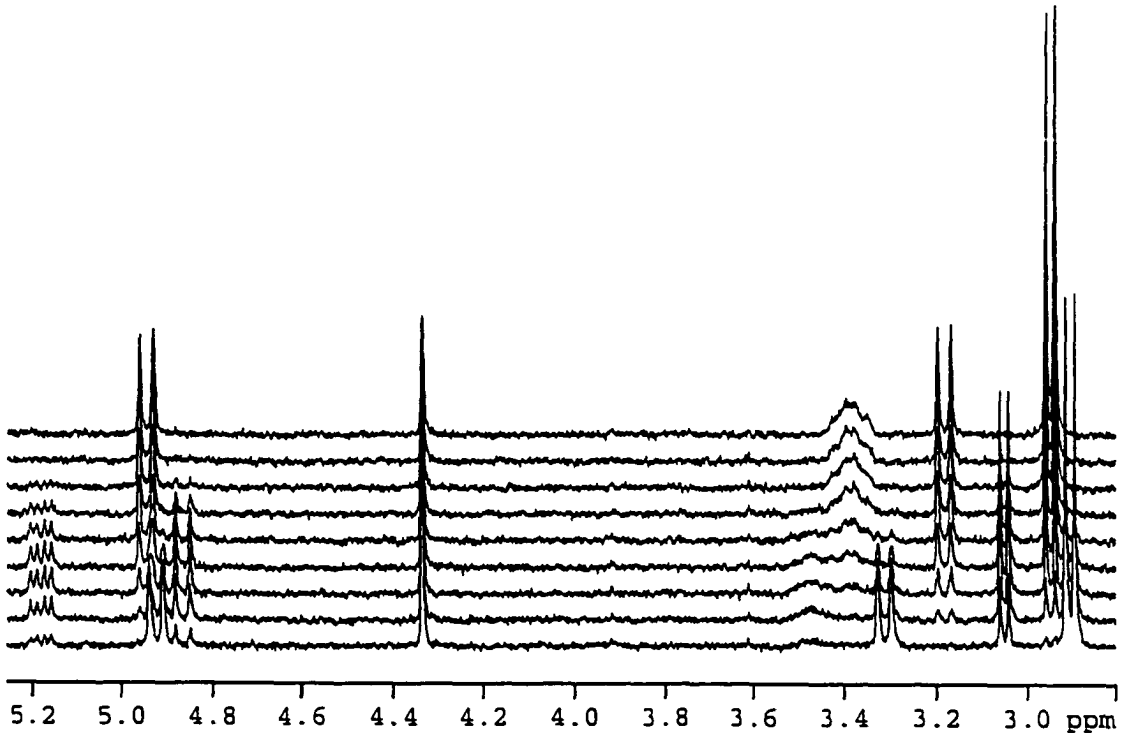

Figure 5. A series of stacked ^{1}H NMR spectra recorded during the reaction of 3.5 mM MeReO(mtp)P(4-$ClC_6H_4)_3$ and 36 mM $PCyPh_2$ in C_6D_6 at 25 °C. The peaks of the intermediate have resonances at 2.99 (CH_3-Re), 5.1 and ca. 4.9 (two CH_2 protons) ppm.

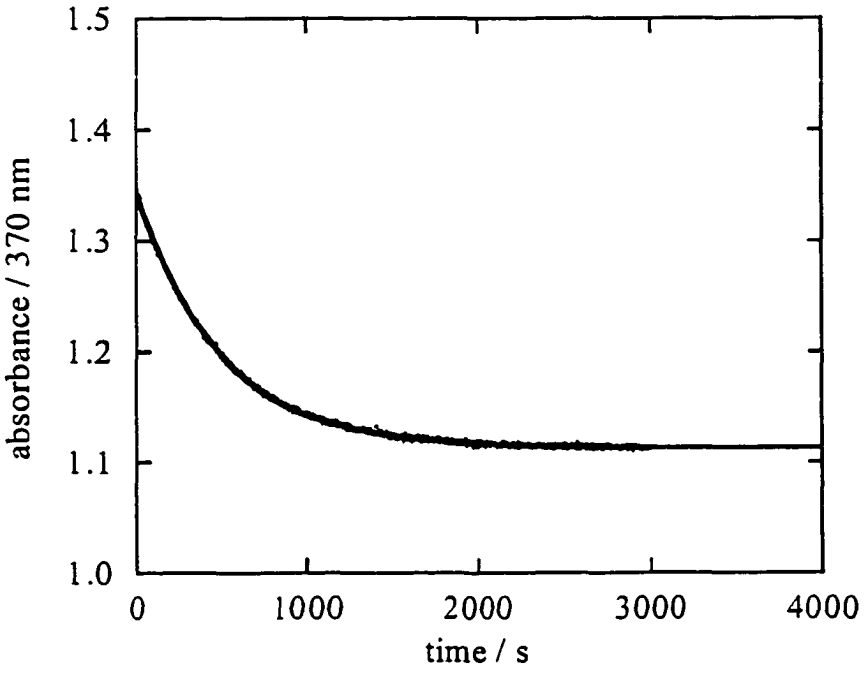

Figure 6. The absorbance-time course of a reaction between 0.66 mM $MeReO(mtp)PPh_3$ and 7.83 mM $PMePh_2$ in benzene at 25.0 °C. The reaction follows first-order kinetics, with k = 2.02×10^{-3} s^{-1}.

Table 2. Rate constants from monophasic ligand exchange reactions at 25 °C. The displaced ligand is X and the new entering ligand is Y.

entry	X	Y	k^a ($L\ mol^{-1}\ s^{-1}$)
1	$P(4\text{-}ClC_6H_4)_3$	$PMePh_2$	2.83 ± 0.02
2	$P(4\text{-}FC_6H_4)_3$	$PMePh_2$	1.10 ± 0.02
3	PPh_3	$PMePh_2$	0.282 ± 0.005
4	PPh_3	$P(MeO)Ph_2$	0.126 ± 0.003
5	$P(p\text{-tolyl})_3$	$PMePh_2$	0.089 ± 0.001
6	$PCyPh_2$	$PMePh_2$	0.062 ± 0.001
7	PCy_2Ph	$PMePh_2$	0.0220 ± 0.0003
8	PCy_3	$PMePh_2$	0.0018 ± 0.0001[a]
9	PPh_3	PMe_2Ph	23.0 ± 0.1
10	$PMePh_2$	PMe_2Ph	37 ± 1

a) believed to be k_1 in eq 8
b) results from an NMR experiment, other from UV-visible kinetics

the observed rate constant for its reaction with $MeReO(mtp)PPh_3$, with some NMR data included as well, Figure S-6.

Rather than invoke a different reaction scheme for this set, we have explored the possibility that those cases following first-order kinetics reflect just one limit of the general two-stage scheme in eq 8, except that one step is much faster than the other. The limit cannot be obtained with $k_2 << k_1$, for then the value of k for each grouping in Table 2 would represent k_2, and the same value, independent of the identity of X, would have been found. If the original premise is correct, then reduction of bi-exponential to first-order kinetics must be the consequence of the reverse inequality, $k_2 >> k_1$. That is, the experiments would record

the values of k_1, a quantity varying with X and Y; the contribution of the k_2 reaction would have been lacking since that step was relatively much faster.

A Better Leaving Group. To pursue the issue just alluded to, we chose to use as the starting compound a complex with X = 4-Bu^{t}C$_5$H$_4$N. Earlier work[12] has shown that pyridine complexes are much more labile than phosphines. Experiments were carried out on three MeReO(mtp)NC$_5$H$_4$R derivatives and two phosphines. Figures S–7 and S–8 show juxtaposed spectra for such an experiment and a single wavelength kinetic trace extracted from these data, which shows bi-exponential kinetics, respectively. Table 3 summarizes these rate constants. The smaller values can be identified as belonging to the second stage; MeReO(mtp)Y* + Y has k_2 = 53 L mol^{-1} s^{-1} (Y = PMePh$_2$) and 1.1 × 10^3 L mol^{-1} s^{-1} (Y = PMe$_2$Ph).

The significance of these rate constants can be appreciated by reference to Table 2. In reactions with these phosphines as Y only a single stage was seen. For reasons already stated, the derived rate constants are the values of k_1. The range of k_1 values is 0.0018–2.8 L mol^{-1} s^{-1} for Y = PMePh$_2$. Naturally then, with k_2 = 53 L mol^{-1} s^{-1}, the second stage is so much more rapid than the first that it went undetected. The same considerations apply to the case Y = PMePh$_2$.

These data confirm that all the reactions investigated follow the same two-step scheme. Of the three cases with kinetics that do not conform to a two-stage reaction, the two dealt with in this section can be seen to simplify to first-order kinetics only because of inequalities in the rate constant values.

Diverting the Intermediate. The data have shown that the second reaction, between MeReO(mtp)Y* and Y, gives the final product MeReO(mtp)Y. The most reasonable

interpretation of this finding is to suggest that this step is also a displacement of one Y by another. To demonstrate this, a system was found in which a third ligand Z could be introduced. For this purpose, MeReO(mtp)4-Bu^{t}NC$_5$H$_4$N and PMePh$_2$ were first mixed in the stopped-flow apparatus. After a specified delay time of 3.0 s, calculated from the rate constants in Tables 1–3, so as to maximize the concentration of the intermediate, the third reagent, Z = PMe$_2$Ph, was introduced. The absorbance-time trace was then monitored at 390.

Table 3. Rate constants for the biphasic ligand exchange reactions at 25 °C that involve various Me(O)Re(mtp)-pyridine compounds, M-X, and entering ligands, Y.

X	Y	$k_a = k_1$ (L mol^{-1} s^{-1})	$k_b = k_2$ (L mol^{-1} s^{-1})[a]
C_5H_5N	$PMePh_2$	1940	52
4-$MeOC_5H_4N$	$PMePh_2$	1044	53
4-Bu^{t}C$_5$H$_4$N	$PMePh_2$	1089	52.8
C_5H_5N	PMe_2Ph	~2 × 10^5 [b]	~1430 [b]
4-Bu^{t}C$_5$H$_4$N	PMe_2Ph	82500	1100

a) k_2 refers to the reaction between MeReO(mtp)Y* and Y
b) denote that rate constant are approximate

Scheme 1 depicts the reactions. Analysis of the kinetic data for this stage shows that the apparent first-order rate constant is directly proportional to [PMe$_2$Ph], as shown in Figure 7. The rate constant for MeReO(mtp)PMePh$_2$* and PMe$_2$Ph is 1.7 × 10^3 L mol^{-1} s^{-1}. The slower stage in the kinetics originates from the independently-known reaction of MeReO(mtp)PMePh$_2$ with PMe$_2$Ph. This is the single example of a reaction in which a ligand displaces a different ligand from the intermediate.

Scheme 1. A reaction sequence showing the generation of the intermediate and it reacting with two non-equal ligands.

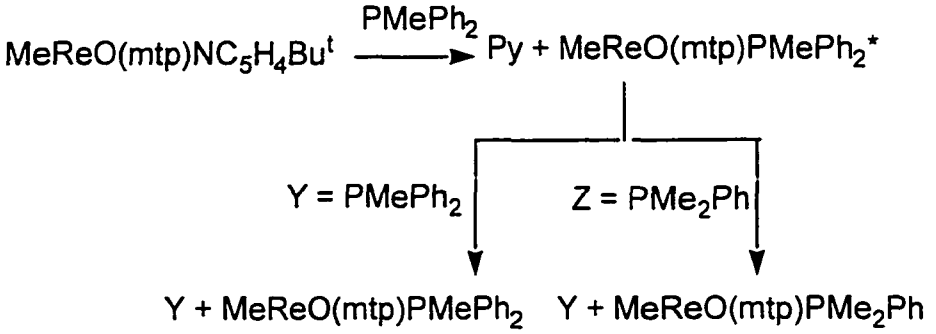

A second experiment explicitly for the intermediate was carried out between MeReO(mtp)4-Bu^{t}C$_5$H$_4$N and Me$_2$bpy (4,4'-dimethyl-2,2'-bipyridine). Pyridine complexes exist in an approximate 9:1 ratio of isomers favoring **M**–L over **M**–L*, unlike phosphine complexes for which the **M**–L* isomer remains below the detection limit at equilibrium. This reaction gave two isomers:

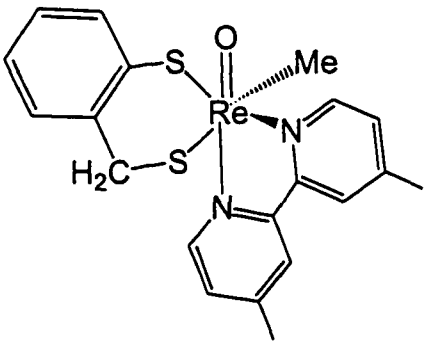

MeReO(mtp)(Me$_2$bpy)

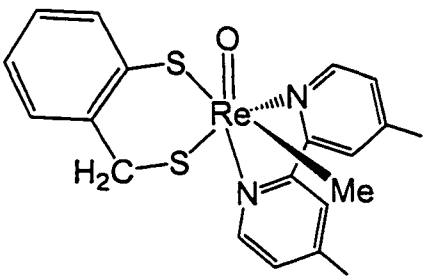

MeReO(mtp)(Me$_2$bpy)*

Our characterization of the two reagents and two products can be made on the basis of the ^{1}H NMR spectra, on the basis of their chemical shifts as calibrated by similar isomers with phosphine ligands. The two methylene protons of the mtp ligand appear as two

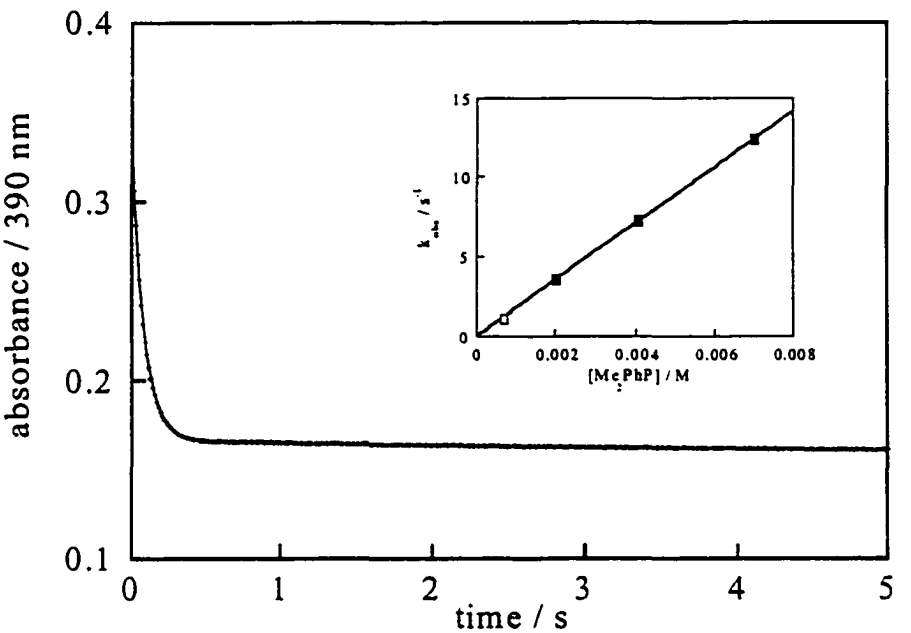

Figure 7. The time course of a reaction between 80 μM MeReO(mtp)$PMePh_2$* 7.0 mM PMe_2Ph at 25 °C in benzene. The fit of these data to bi-exponential kinetics gave these rate constants, 12.3 s^{-1} and 0.17 s^{-1}. The inset shows that the larger rate constant is linearly dependent on the concentration of PMe_2Ph.

doublets, the separation between which prove to be indicative of the isomer obtained. On the basis of such comparisons, we can readily suggest structural assignments given.

Activation Parameters. Several biphasic reactions were recorded as a function of temperature. Bi-exponential fitting was used to resolve the two components. The resulting first-order rate constants were divided by the concentration of the entering rate constants. generating the values of the rate constants for the first and second stages, k_1 and k_2. The temperature dependence of each of these rate constants was analyzed in terms of the transition state theory equation, resulting in values of the entropy and enthalpy of activation. Thus two sets of parameters result, one for the reaction of the stable stereoisomer, MeReO(mtp)X, the other for the metastable form MeReO(mtp)Y*. The results are presented in Table 4 and an Eyring plot is presented, Figure S–9.

Table 4. Rate constants and activation parameters for selected ligand exchange reactions.

X	Y	k_{298} / L mol^{-1} s^{-1}	$\Delta H^{\ddagger}$ / kJ mol^{-1}	$\Delta S^{\ddagger}$ / J mol^{-1} K^{-1}
Part A: Stable compounds				
4-Bu^{t}C$_5$H$_4$N	Me_2PhP	8.25×10^4	8.1 ± 0.9	-124 ± 3
4-Bu^{t}C$_5$H$_4$N	$MePh_2P$	1.09×10^3	17.7 ± 1.0	-127 ± 3
PPh_3	Me_2PhP	2.3×10^1	26.9 ± 0.5	-128 ± 2
PPh_3	$CyPh_2P$	4.1×10^{-3}	47.6 ± 2.0	-130 ± 4
Part B: Metastable intermediates[a]				
Me_2PhP*	Me_2PhP	1.1×10^3	19.5 ± 0.7	-121 ± 3
$MePh_2P$*	$MePh_2P$	5.3×10^1	18.2 ± 1.0	-151 ± 3
$CyPh_2P$*	$CyPh_2P$	2.6×10^2	25.5 ± 2.0	-189 ± 6

a) The one case in which the intermediate reacts with a ligand different from the coordinated one: MeReO(mtp)P$MePh_2$* and PMe_2Ph, give $k = 1.78 \times 10^3$ L mol^{-1} s^{-1}.

Monomerization. An extensive set of data has been obtained pertaining to the rate of the following reactions:[12]

$$\{MeReO(mtp)\}_2 + 2\ PR_3 \rightarrow 2\ MeReO(mtp)PR_3 \qquad (10)$$

The rate law found from earlier work and confirmed for additional phosphines in this study is:

$$\frac{d[MeReO(mtp)PR_3]}{dt} = 2\times[\{MeReO(mtp)\}_2]\times\left(k_a[PR_3]+k_b[PR_3]^2\right) \qquad (11)$$

Table 5 presents the new data along with information form the earlier study. Figure S-10 shows the relationship between k and [$CyPh_2P$] for the monomerization reaction. To a rough approximation, the first term is adopted preferentially by phosphines of smaller size (cone angle) and vice-versa. The situation is not straightforward, however: note that $P(OMe)_2Ph$, for which k_a carries the entire reaction, lies at one end of the selectivity range, whereas $P(OMe)Ph_2$ lies at the other. We calculated relative importance of each pathway as a function of phosphine complexes for several PR_3 ligands (Figure S-11). The poorly donating PPh_3 primarily reacts though the first-order pathway.

Table 5. The kinetic information for monomerization of by $\{MeReO(mtp)\}_2$ phosphines.

ligand	k_a	k_b	$-\Delta H_{HP}$ kcal/mol	cone angle	k_b/k_a
$P(MeO)_2Ph$	12.4 ± 0.3	ca. 0		120	0
PPh_3[a]	0.0082	0.052	21.2	145	6.4
PCy_2Ph	0.029 ± 0.003	1.7 ± 0.3		162	58
$PCyPh_2$	0.060 ± 0.004	6.2 ± 0.4		153	103
PCy_3	0.13 ± 0.04	15 ± 2	33.2	170	115
$PMePh_2$	3.5 ± 0.6	2100 ± 150	24.7	136	600
$P(MeO)Ph_2$	0.7 ± 0.2	590 ± 40		132	842

a) From ref. 12

For certain Y ligands, $\{MeReO(mtp)\}_2$ gave some (**M**–Y)* along with (**M**–Y), especially for those ligands with a slower **M**–Y* + Y reaction. With $PMePh_2$ and PMe_2Ph, **M**–Y* could not be detected by ^1H NMR. Larger ligands gave initial yields of the intermediate of 18% ($PCyPh_2$) and 25% (PCy_2Ph). Further studies are needed, however, as these data are quite limited.

Discussion

Experimental Findings. A succinct recapitulation of the experimental observations is given to guide the discussion. The reaction between MeReO(mtp)X (**M**–X) and Y gives the eventual product **M**–Y; both compounds have the same geometry. These reactions often follow bi-exponential kinetics. In the first stage **M**–X and Y form an intermediate **M**–Y* with the same composition as **M**–Y. That both have a 1:1 ratio of Re:Y and X is absent. In the second stage, **M**–Y* reacts with a *second* Y to form the stable product **M**–Y. The rate of each step in the sequence is directly proportional to the concentration of Y. The rate constant for the second stage (between **M**–Y* and Y) is independent of the identity of X in the parent complex. A certain subset of these reactions seems to occur in a single stage, but that was shown to be a consequence of the inequality $k_2 >> k_1$. With Py as the leaving group and Y the same, the first stage was much faster; again following bi-exponential kinetics. The rate constant of the slower stage is the value of k_2 for the reaction of **M**–Y* and Y, previously disguised. The values of both k_1 and k_2 depend on the identities of the leaving and entering ligands.

Issues of Mechanism. As to the molecular mechanism, this system poses some intricate questions that go beyond the reaction scheme presented in eq 8. A complete mechanism must at the very least account for the need for a two-stage mechanism,

accommodate the precepts of microscopic reversibility, address the existence of an intermediate that can be detected and trapped, account for the trends in reactivity for each step in the mechanism and satisfy the requirement for chemically-reasonable species along the reaction coordinate.

The Intermediate is an Isomer. The spectroscopic data point to **M**–Y* being an isomer of the stable **M**–Y; the suggested structural formula is given in Chart 1. Both **M**–Y* and **M**–Y complexes show a doublet resonance in the ^{1}H NMR spectrum for the C*H*$_3$Re group when Y is a phosphine from splitting by ^{31}P. The ^{31}P NMR spectrum reveals that both peaks of both forms have similar but recognizably different chemical shifts. This shows that only one phosphorus atom is coordinated because a more complex splitting pattern is found with Y = 1,2-bis(diphenylphosphino)benzene. Its chelating phosphorus atoms are inequivalent, and a complex family of multiplets is the resultant.

The inequivalent methylene protons of mtp appear as doublets with J ~ 12 Hz, from coupling between the diastereotopic hydrogens. Both resonances in the **M**–Y* lie downfield of those in **M**–Y. The separation between the doublets in **M**–Y* is 0.2–0.75 ppm, compared to 1.1–1.7 ppm in **M**–Y. Once established, this pattern can serve as a diagnostic tool of structure in compounds for which the assignment is less evident.

In every instance in which the ^{1}H NMR spectrum of **M**–Y* (here, Y has a P donor atom) could be recorded, a further splitting of one (but not both) of the methylene protons of mtp in the ^{1}H NMR spectrum of was found, making it appear as a doublet of doublets, table 7. The secondary coupling has J ca. 4.5 Hz. This secondary splitting was absent, however, for the more stable isomer, which shows both protons as simple doublets:

Table 7. The chemical shift of the methylene protons of the mtp ligand of selected Me(O)Re(mtp)L compounds in C_6D_6.

Chemical shifts (ppm) for CH_2	MeReO(mtp)L		MeReO(mtp)L*	
L = $PCyPh_2$	4.90 (d)	3.13 (d)	5.10[a]	4.80 (d)
L = PCy_2Ph	5.05 (d)	3.39 (d)	5.16[a]	4.68 (d)
L = Me_2bpy	5.27 (d)	4.15 (d)	5.45 (d)	4.72 (d)
L = 4-$Bu^tC_5H_4N$	4.79 (d)	3.78 (d)	5.21 (d)	4.89 (d)

a) doublet of doublets

Broadband decoupling of ^{31}P centered at 25 ppm removed the secondary splitting; it is thus shown to arise from a coupling to ^{31}P. The original and decoupled spectra are presented in Figure 8. That it should occur in the isomer in which the methylene group is bonded to the S trans to P, but not in that with a cis arrangement, suggests to us an unusual four-bond coupling pattern. A few precedents in organic compounds can be cited.[24-26] Further, a coupling pattern to dissimilar from that seen in these experiments has been observed for one H atom of a metal-coordinated SH_2; one H appears as a doublet of doublets (the first coupling from diastereotopic hydrogens) owing to an ancillary phosphine ligand that is also coordinated to the metal.[27]

Long range (four-bond) couplings may occur when a W-configuration exists. Such an arrangement can be drawn here, involving H_aH_b–C–S–Re–P. Its two three-atom components form a dihedral angle of ca. 160°; planarity is not a requirement, however. This is the arrangement of atoms by which H_a couples to phosphorus:

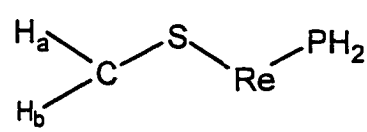

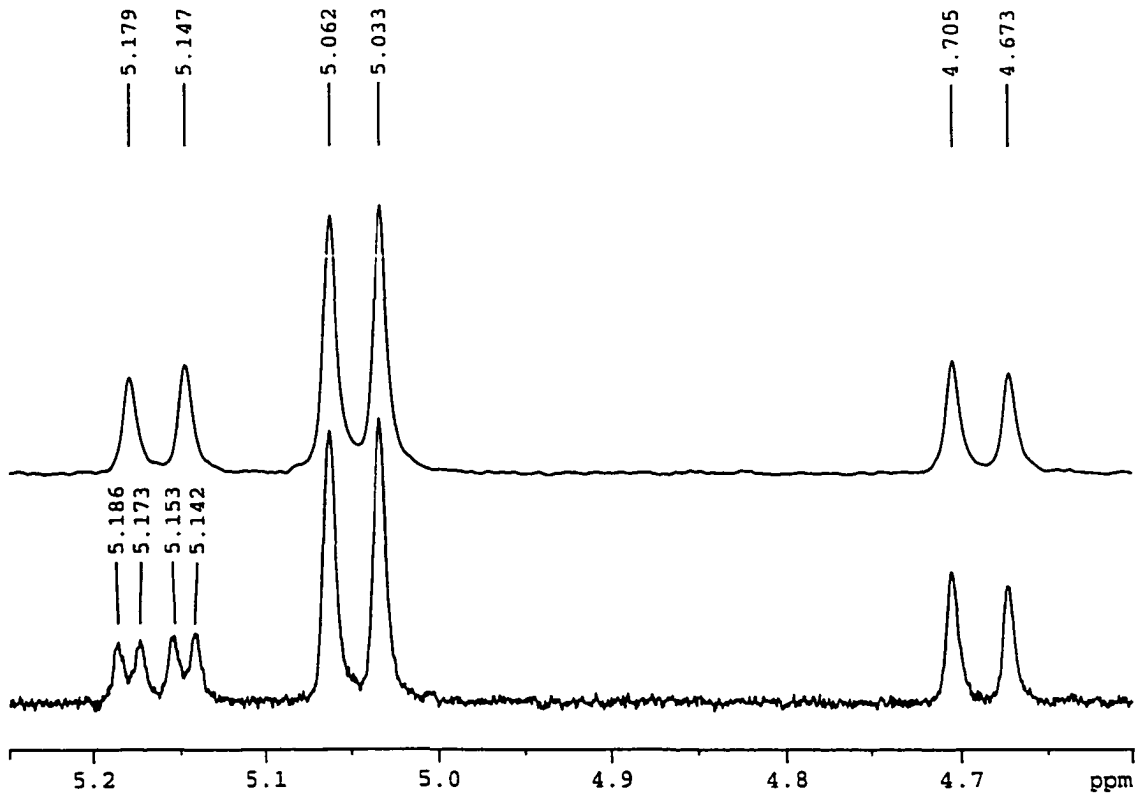

Figure 8. ^{1}H and $^{1}H\{^{31}P\}$ NMR spectra of a solution containing both isomers of $MeReO(mtp)PCy_2Ph$ are shown over a narrow range of chemical shifts. The doublet at 5.04 ppm is from one of the methylene protons of the more stable isomer. The other resonances arise from the pair of methylene protons of $MeReO(mtp)PCy_2Ph^*$. The downfield resonance appears as a doublet of doublets owing to four-bond coupling to ^{31}P; that resonance becomes a doublet as well upon broadband decoupling.

The Turnstile Mechanism. To account for the various issues raised, we suggest the sequence of events depicted in Scheme 2.

Scheme 2. Proposed reaction pathway for ligand exchange.

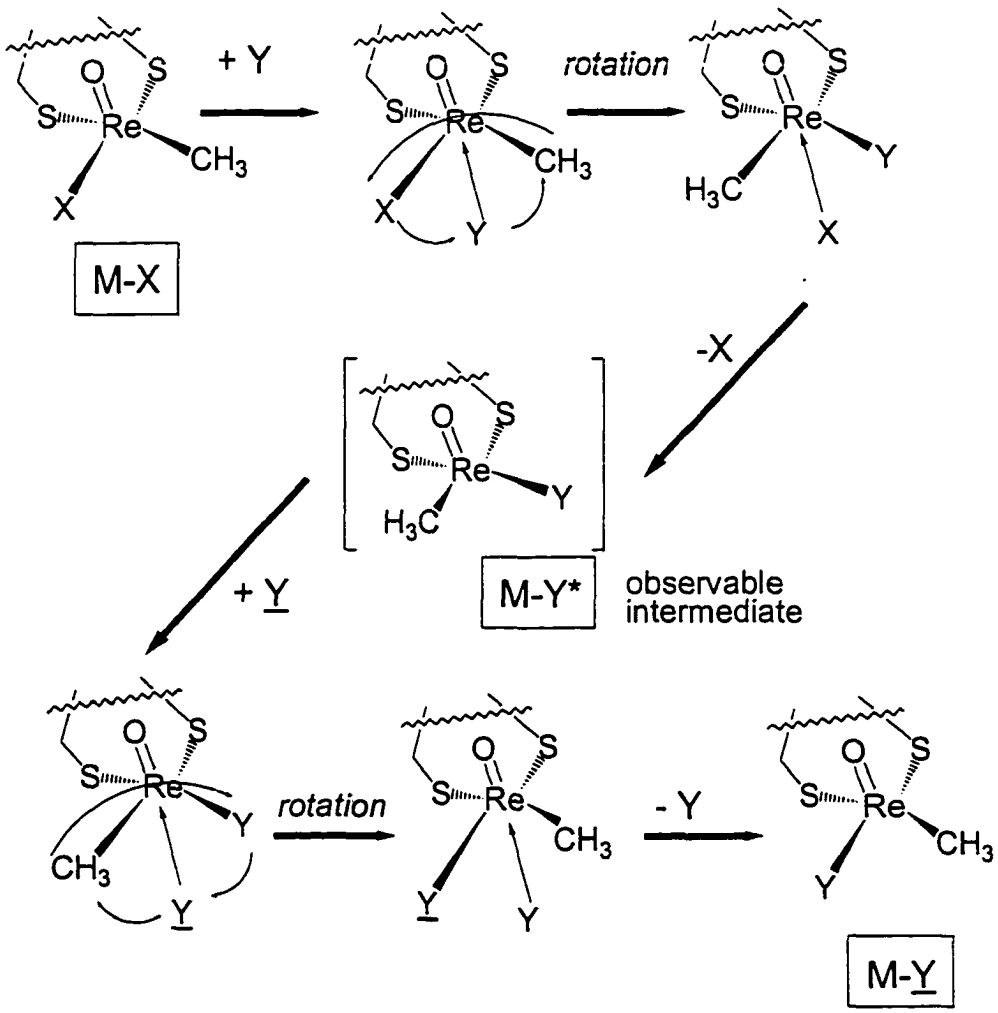

(1) The entering nucleophile attacks rhenium at the only reasonably-available site, the open coordination position trans to the oxo group, to yield an intermediate proposed to have a six-coordinate, approximately octahedral, structure. The interaction between Re and Y in this position must be weak, because monodentate ligands are

not known to form six-coordinate structures in this group of compounds. It can be presumed that Y repeatedly enters and leaves prior to the next step.

(2) The six-coordinate intermediate lies on the pathway for substitution; it must be transformed into a substance in which Y becomes strongly attached to rhenium as the bond to X weakens. Imagine this is accomplished by a rotation about one particular pseudo-C_3 axis of the octahedron; this axis has the donor atoms of X and Y and the CH_3 group. This is termed a *turnstile* rotation. At a rotation angle of ca. 60°, the molecule passes through an approximate trigonal prismatic geometry. This is not an unreasonable, because trigonal prismatic geometry is not too badly destabilized by the d^2 electronic configuration of Re(V). Instances of this geometry have been well established, including several rhenium compounds.[28-31]

(3) As rotation continues to ca. 120°, an approximately octahedral configuration is restored, which may take any of three forms. Trivially, the rotation would restore X, Y, and CH_3 to their original forms and no net change would be realized. A second nonproductive event would be to place the CH_3 group trans to oxo; the strong Re–C covalent bond will not break, so further rotation presumably ensues. The rotation that puts X in the position trans to the oxo group gives the important intermediate that lies along the reaction coordinate. X then leaves from that position. It is the one at which Y entered; this premise goes a long way towards satisfying microscopic reversibility.

(4) The species so formed has the composition MeReO(mtp)Y*, to the formula of which has been added the asterisk denoting it as the detectable intermediate. Examination

of the structural formulas in Scheme 1 reveals that turnstile rotation indeed produces a stereoisomer different from the stable form.

(5) Because MeReO(mtp)Y* is not the stable form, as judged by crystal structures of various isolated complexes, it must undergo further rearrangement. This is accomplished not by a unimolecular process, but by a bimolecular one. A second entering ligand Y attacks the intermediate, as required by the form of the rate law.

(6) It is only logical to presume that the second stage reaction adopts the same mechanism as the first. Following the structural formulas in Scheme 1, it can easily be seen that the same sequence of events produces the more stable isomer of MeReO(mtp)Y.

Six-coordination. In view of the proposal that Y adds to the vacant position trans to the oxo group, it is important to learn whether stable compounds exist with a six-coordinate geometry. None has been found with any monodentate ligand examined. Only when the chelate effect is invoked are such compounds obtained. In addition to the data reported here, examples of six-coordinate MeReO(mtp)(LL) compounds are known with 1,2-bis(diphenylphosphino)benzene[32] and with bipyridine ligands such as Me_2bpy in this work and various other bpy and phen ligands.[33]

The presumably concurrent reactions of Me_2bpy were carried out with a mixture of the isomers MeReO(mtp)$NC_5H_4Bu^t$* and MeReO(mtp)$NC_5H_4Bu^t$ that remain in equilibrium. These isomers equilibrate fairly rapidly,[34] the ^{1}H NMR spectra shown equilibrium proportion of about 10% of the less favored isomer. From the pattern of chemical shifts (Table S–8), two products were identified, MeReO(mtp)(Me_2bpy)* (90%) and MeReO(mtp)(Me_2bpy) (10%), as in Scheme 3.

Scheme 3. Reactions forming isomeric bipyridine complexes.

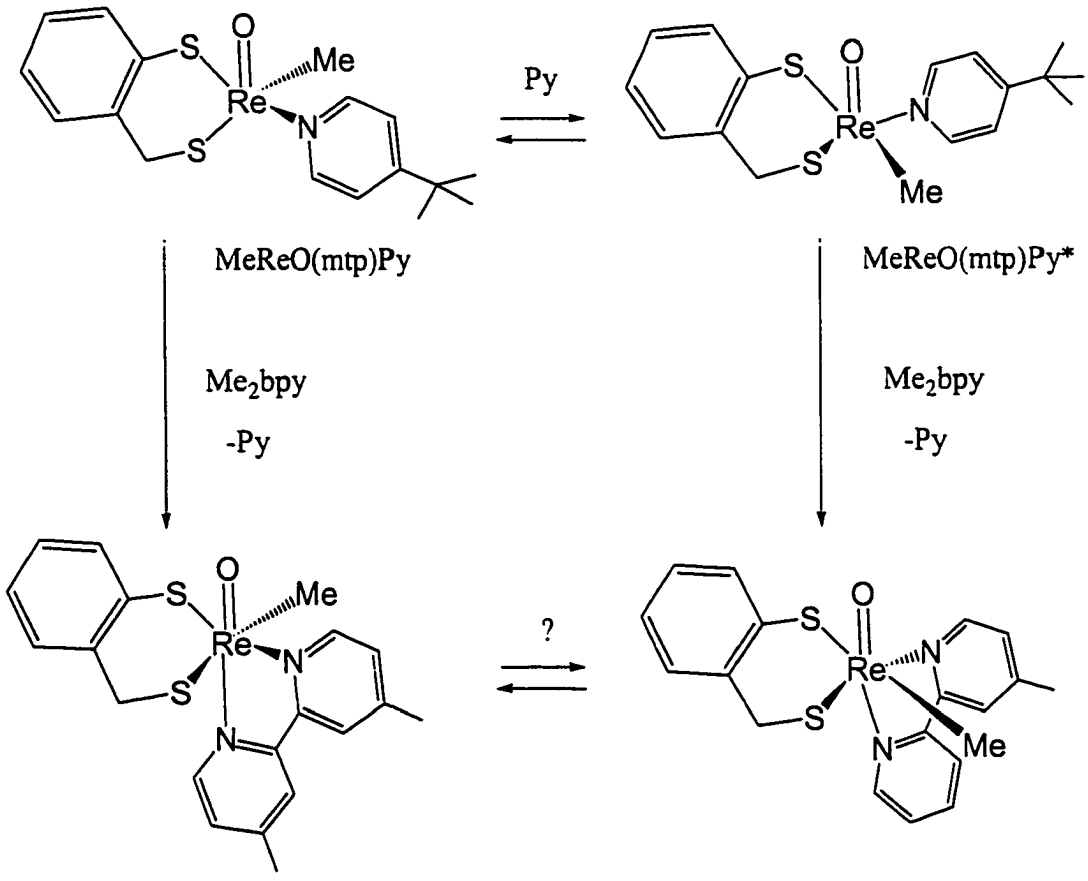

Because of equilibration between the two parent compounds within t <1 min, this result can be interpreted to mean that both reactions with Me_2bpy have nearly the same rate constant, such that the product distribution is close to that of the parents. We ask if this is reasonable, because PMe_2Ph reacts differently with MeReO(mtp)$PMePh_2$* ($k = 1.7 \times 10^3$ L mol^{-1} s^{-1}) and MeReO(mtp)$PMePh_2$ ($k = 37$ L mol^{-1} s^{-1}). In defense of the original precept for pyridine ligands, however, it should be noted that all phosphine ligands give rise to an undetectably low concentration of the isomer. Thus reactions of the isomeric phosphine complexes proceed with substantially different driving forces, a factor that may account for

the kinetic advantage of one isomer. The pyridine complexes, on the other hand, differ in stability by only ΔG° ~5 kJ mol^{-1} in favor of **M**–Py, and the two isomers thus might differ little in reactivity.

A counter-argument can be offered, however that the chelated bpy products come to equilibrium on their own. In that case, the product ratio is a simple reflection of a 9:1 equilibrium ratio of the two isomers of MeReO(mtp)(Me_2bpy). That suggestion is untenable, however, because the less stable isomer is in the large majority. Under these conditions, no evidence was obtained for unimolecular interconversion of the isomers of MeReO(mtp)(Me_2bpy). The reaction in Scheme 3 with an arrow marked "?" does not occur, according to this interpretation. The cis-trans isomerization of Me_2ReO(bpy)Cl[8] perhaps adopts a turnstile mechanism as well, contrary to the suggested mechanism in which one arm of the bpy chelate was proposed to dissociate.

The Rate Constants and their Activation Parameters. The mechanism is associative, as shown by the first-order dependence on ligand Y in a step that gives rise to a six-coordinate intermediate in a fast prior-equilibrium. The rate controlling step is the turnstile rotation. To show the effects of changing X and Y, the rate constants for selected reactions are presented in a different arrangement in Table 6. The best Lewis bases are the most reactive nucleophiles Y; their influence is substantial as represented both by the strength of the equilibrium interaction and by the increase in bonding strength as the stronger ligand Y turns into an equatorial position. The leaving group X has the opposite effect, the weakest nucleophiles reacting more rapidly. For X, however, the effect should be confined to the turnstile step, as X rotates into the lower axial position at which its bonding is weaker.

Table 6. Rate Constants as a Function of Leaving (X) and Entering (Y) Groups.

Part A: MeReO(mtp)X + Y					
Y →	PMe_2Ph	$PMePh_2$	$PCyPh_2$	PCy_2Ph	$P(p\text{-tolyl})_3$
X ↓					
Cl^-			0.52		
$PMePh_2$	37.0		~0.09		0.0016
$P(4\text{-}ClC_6H_4)_3$		2.83	0.037	0.0055	0.033
$P(4\text{-}FC_6H_4)_3$		1.10	0.035		
PPh_3		0.282	0.0041	0.00044	0.0023
$PCyPh_2$		0.062			
PCy_2Ph		0.022			
PCy_3		0.0018			
Part B: MeReO(mtp)Y* + Y					
Y →	PMe_2Ph	$PMePh_2$	$PCyPh_2$	PCy_2Ph	$P(p\text{-tolyl})_3$
MeReO(mtp)Y*	1100	53	0.024	0.0002	0.05

Again, however, the overall chemistry is associative. This description describes **M–X** to **M–Y***; the second stage merely repeats the steps in the first.

An interesting correlation of the kinetic data has been realized against the stereoelectronic parameter χ_d parameter from the QALE method for phosphane ligands.[35] This parameter is a good measure of bonding ability. For a series of reactions in which the entering ligand Y was $PMePh_2$, a linear plot of log k vs. χ_d was obtained. Linear regression gives a slope of 0.19 ± 0.02 (Figure S–12). The same data show that bonding ability (measured by the pK_a of R_3PH^+) and steric considerations (from the cone angle θ) both play a role. With these parameters, the correlation of the rate constant is given by: $\chi_d = 27.79 -$

1.47 pK_a – 0.069 θ. A Hammett LFER correlation yields ρ = 1.3 (Figure S–13), suggesting that negative charge builds-up in the transition state.

MeReO(mtp)Py + PPh_3, a reinterpretation. The rate of replacement of Py by PPh_3 from MeReO(mtp)Py was previously reported to occur by parallel pathways, one involving MeReO(mtp)PPh_3*, the other "direct", represented by the rate constant k_6.[12] The reaction sequence is shown in Scheme 4.

Scheme 4. Originally-proposed route from pyridine to phosphine complex.

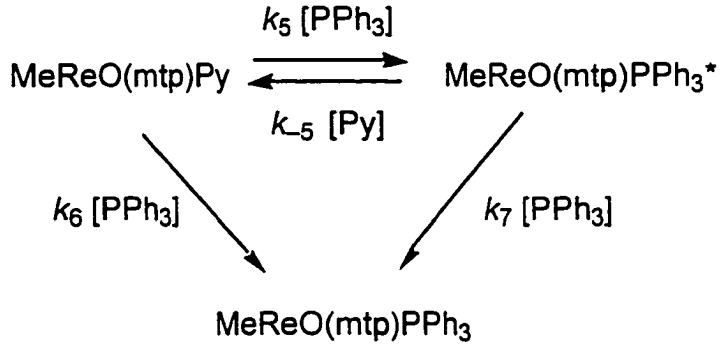

This model fits the data, with these values of k/L mol^{-1} s^{-1}: k_5 = 88.0, k_{-5}= 16.1, k_6 = 6.27, and k_7 = 0.2. Because $k_{-5}[Py] >> k_7[PPh_3]$, the rate expression is:

$$v = \left\{ k_6 + \frac{k_5 k_7 [PPh_3]}{k_{-5}[Py]} \right\} \times [\text{MeReO(mtp)Py}] \times [PPh_3] \qquad (12)$$

We now propose an alternative in which both pathways proceed by way of the **M–Y*** intermediate, and now claim that a direct pathway does not exist. The new reactions are shown in Scheme 5.

Scheme 5. Revised reactions for the conversion of a pyridine to a phosphine complex

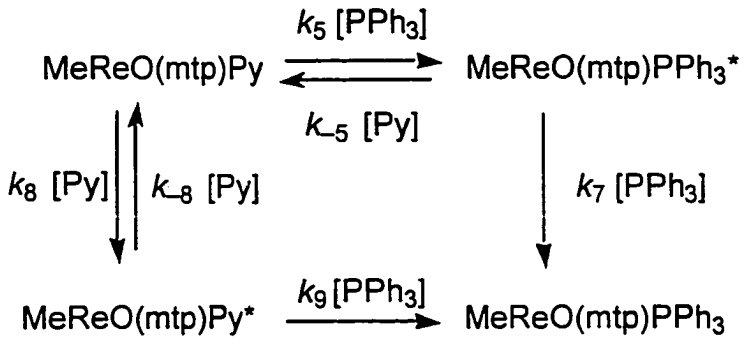

Provided $k_{-5}[Py] >> k_6[PPh_3]$ and $k_{-8}[Py] >> k_9[PPh_3]$ (both of which are valid since Py substitutions are so much faster than those of phosphines) the rate equation would be

$$v = \left\{ \frac{k_8 k_9}{k_{-8}} + \frac{k_5 k_7 [PPh_3]}{k_{-5}[Py]} \right\} \times [MeReO(mtp)Py] \times [PPh_3] \qquad (13)$$

Because the two isomers exist in a 9:1 equilibrium ratio, $k_8/k_{-8} = 0.1$. When the leading term was thought to be the value of k_6, its value was given as 6.27 L mol^{-1} s^{-1} . With these values we arrive at $k_9 = 63$ L mol^{-1} s^{-1}. This is quite comparable to the value of k_5; both rate constants represent the displacement of a pyridine complex with triphenylphosphine, and it is not unreasonable that they would be similar in value.

Recall earlier that the most reasonable interpretation of the 90/10 product ratio of the MeReO(mtp)(Me_2bpy) isomers was that the two pyridine isomers had the same reactivity. Our supposition that MeReO(mtp)(4-$Bu^tC_5H_4N$)* and MeReO(mtp)(4-$Bu^tC_5H_4N$) react with Me_2bpy at about the same rate is validated by reanalysis of the data given in the immediately preceding paragraphs.

Summary. A substantial family of the compounds MeReO(mtp)X (X = pyridine, phosphine) react with phosphines (Y) in two stages, via a reaction scheme in which an intermediate can be detected. It is a stereoisomer of the product. A turnstile mechanism has been proposed for each stage of the substitution process, because it accounts for isomer formation at each stage, while allowing for the principle of microscopic reversibility to be observed.

Acknowledgment. This research was supported by the U. S. Department of Energy, Office of Basic Energy Sciences, Division of Chemical Sciences under contract W-7405-Eng-82. The crystallographic analysis was done by Dr. Ilia Guzei. Helpful conversions with Prof. J. G. Verkade, Prof. L. K. Woo, and Mr. Gábor Lente are gratefully acknowledged.

Supporting Information Available: Complete tables of crystal data and refinement details, atomic coordinates, bond lengths and angles, and anisotropic displacement parameters; spectroscopic information, and graphs and plots of kinetic data (17 pages). This material is available gratis at http://pubs.acs.org

Supporting Information.

Table S–1. UV-visible spectra of MeReO(mtp)-L complexes

L	(ε) λ /nm	(ε) λ /nm	(ε) λ /nm
PPh_3	190 (606)	2700 (340)	
$PMePh_2$	189 (606)	3000 (341)	
PMe_2Ph	212 (594)	3000 (341)	
$PCyPh_2$	220 (600)	3000 (341)	
PCy_2Ph	133 (605)	1700 (347)	
PCy_3	175 (606)	2200 (347)	
PPh_3			1240 (410)
$PCyPh_2$*			2740 (410)
$PCyPh_2$			1140 (410)
PPh_3			1300 (400)
PCy_2Ph*			2050 (400)
PCy_2Ph			1150 (400)

Table S-2. The ^{1}H and ^{31}P NMR chemical shifts for selected MeReO(mtp)L compounds.

Compound	$-H_aH_b-S$[b]	$-H_aH_b-S$[b]	$Re-CH_3$[c]	CH_3[d]	CH_x[e]	^{31}P
$PCyPh_2$	4.90	3.13	2.89		3.3 (1H)	31.92
$PCyPh_2$*	5.10	4.80	2.99		3.4 (1H)	28.89
PCy_2Ph	5.05	3.39	2.95		2.8 (2H)	27.26
PCy_2Ph*	5.16	4.69	3.16		2.5 (1H) 3.1 (1H)	27.55
PCy_3	5.04	3.39	3.03		2.5 (3H)	
PPh_3	4.82	3.27	2.98			27.8
PPh_3*	5.10	4.89	3.08			25.92
P(*p*-tolyl)$_3$ [a]	4.88	3.33	3.06			26.50
P(*p*-tolyl)$_3$* [a]	5.14	4.90	3.16			
P(4-ClC_6H_4)$_3$	4.85	3.25	2.83			
P(4-FC_6H_4)$_3$	4.87	3.28	2.85			25.48
P(4-$MeOC_6H_4$)$_3$ [a]	4.94	3.39	3.10			
P(4-$MeOC_6H_4$)$_3$* [a]	5.19	4.92	3.20?			
$PMePh_2$	4.88	3.25	2.77	1.72		12.6
PMe_2Ph	4.89	3.21	2.69	1.38 1.44		-0.94
$P(MeO)Ph_2$	4.93	3.15	2.89	3.18		124.6
$P(MeO)_2Ph$	4.94	3.14	2.95	3.11 3.38		144.1
4-$^{t}BuC_6H_4N$	4.79	3.78	2.95			
4-$^{t}BuC_6H_4N$*	5.21	4.89	2.97			
C_6H_5N	4.70	3.67	2.77			

a) Lente, et al. Inorg. Chem., 2000, 39, 1311.
b) doublet (ca. 12 Hz)
c) doublets, except bottom three are singlets (not P containing ligands)
d) doublets (from methyl group of bound ligand)
e) broad multiplets (PCH_x group on bound ligand)

Table S-3. Crystal data and structure refinement for compound MeReO(mtp)PMePh$_2$.

Empirical formula	$C_{21}H_{22}OPReS_2$	
Formula weight	571.68	
Temperature	173(2) K	
Wavelength	0.71073 Å	
Crystal system	Monoclinic	
Space group	C2/c	
Unit cell dimensions	a = 27.9997(17) Å	α= 90°
	b = 11.1931(6) Å	β= 109.639(1)°
	c = 13.8873(8) Å	γ = 90°
Volume	4099.1(4) Å^3	
Z	8	
Density (calculated)	1.853 Mg/m^3	
Absorption coefficient	6.218 mm^{-1}	
F(000)	2224	
Crystal size	0.35 x 0.20 x 0.08 mm^3	
Theta range for data collection	1.98 to 26.37°.	
Index ranges	$-34 \le h \le 32, 0 \le k \le 13, 0 \le l \le 17$	
Reflections collected	18391	
Independent reflections	4178 [R(int) = 0.0333]	
Completeness to theta = 26.37°	100.0 %	
Absorption correction	Empirical with SADABS	
Transmission max/min	1.000 / 0.641	
Refinement method	Full-matrix least-squares on F^2	
Data / restraints / parameters	4178 / 0 / 237	
Goodness-of-fit on F^2	0.994	
Final R indices [I>2sigma(I)]	R1 = 0.0179, wR2 = 0.0373	
R indices (all data)	R1 = 0.0237, wR2 = 0.0384	
Largest diff. peak and hole	0.828 and -0.488 e.Å^{-3}	

Table S-4. Atomic coordinates (x 10^4) and equivalent isotropic displacement parameters ($Å^2$ x 10^3) for M-$PMePh_2$. U(eq) is defined as one third of the trace of the orthogonalized U^{ij} tensor.

	x	y	z	U(eq)
Re	3719(1)	8185(1)	1249(1)	20(1)
P	3465(1)	9996(1)	1946(1)	21(1)
S(1)	4335(1)	9418(1)	1089(1)	27(1)
S(2)	4218(1)	6514(1)	1299(1)	29(1)
O	3180(1)	7990(2)	253(2)	32(1)
C(1)	3729(1)	7426(3)	2664(2)	31(1)
C(2)	4897(1)	8574(3)	1052(2)	30(1)
C(3)	4790(1)	7616(3)	266(2)	27(1)
C(4)	5012(1)	7645(3)	-496(2)	36(1)
C(5)	4926(1)	6734(4)	-1202(3)	50(1)
C(6)	4610(1)	5794(4)	-1178(3)	47(1)
C(7)	4385(1)	5756(3)	-439(2)	38(1)
C(8)	4479(1)	6654(3)	297(2)	26(1)
C(9)	3903(1)	10437(3)	3187(2)	32(1)
C(10)	3396(1)	11295(2)	1127(2)	24(1)
C(11)	3700(1)	12298(3)	1433(3)	38(1)
C(12)	3632(2)	13259(3)	746(3)	47(1)
C(13)	3274(2)	13202(3)	-210(3)	45(1)
C(14)	2975(1)	12199(3)	-506(3)	40(1)
C(15)	3037(1)	11249(3)	157(2)	33(1)
C(16)	2851(1)	9831(2)	2129(2)	23(1)
C(17)	2488(1)	9030(3)	1542(2)	26(1)
C(18)	2024(1)	8919(3)	1690(2)	31(1)
C(19)	1919(1)	9597(3)	2428(2)	33(1)
C(20)	2275(1)	10393(3)	3008(2)	34(1)
C(21)	2736(1)	10524(3)	2858(2)	30(1)

Table S-5. Bond lengths [Å] and angles [°] for $MeReO(mtp)PMePh_2$.

Re-O	1.684(2)
Re-C(1)	2.132(3)
Re-S(1)	2.2759(7)
Re-S(2)	2.3213(7)
Re-P	2.4537(7)
P-C(9)	1.815(3)
P-C(10)	1.816(3)
P-C(16)	1.829(3)
S(1)-C(2)	1.849(3)
S(2)-C(8)	1.782(3)
C(2)-C(3)	1.488(4)
C(3)-C(8)	1.394(4)
C(3)-C(4)	1.396(4)
C(4)-C(5)	1.378(5)
C(5)-C(6)	1.383(5)
C(6)-C(7)	1.375(4)
C(7)-C(8)	1.394(4)
C(10)-C(15)	1.386(4)
C(10)-C(11)	1.387(4)
C(11)-C(12)	1.407(5)
C(12)-C(13)	1.371(5)
C(13)-C(14)	1.378(5)
C(14)-C(15)	1.379(4)
C(16)-C(17)	1.394(4)
C(16)-C(21)	1.396(4)
C(17)-C(18)	1.388(4)
C(18)-C(19)	1.384(4)
C(19)-C(20)	1.377(4)
C(20)-C(21)	1.383(4)
O-Re-C(1)	115.81(11)
O-Re-S(1)	119.88(8)

Table S-5 continued

C(1)-Re-S(1)	123.73(9)
O-Re-S(2)	106.51(7)
C(1)-Re-S(2)	80.22(8)
S(1)-Re-S(2)	91.37(3)
O-Re-P	97.60(7)
C(1)-Re-P	83.14(8)
S(1)-Re-P	82.39(3)
S(2)-Re-P	154.91(3)
C(9)-P-C(10)	105.80(14)
C(9)-P-C(16)	105.20(13)
C(10)-P-C(16)	105.12(13)
C(9)-P-Re	113.98(10)
C(10)-P-Re	113.43(9)
C(16)-P-Re	112.50(9)
C(2)-S(1)-Re	111.82(10)
C(8)-S(2)-Re	107.82(10)
C(3)-C(2)-S(1)	115.2(2)
C(8)-C(3)-C(4)	118.9(3)
C(8)-C(3)-C(2)	120.5(3)
C(4)-C(3)-C(2)	120.6(3)
C(5)-C(4)-C(3)	120.5(3)
C(4)-C(5)-C(6)	120.4(3)
C(7)-C(6)-C(5)	119.9(3)
C(6)-C(7)-C(8)	120.3(3)
C(7)-C(8)-C(3)	120.0(3)
C(7)-C(8)-S(2)	118.8(2)
C(3)-C(8)-S(2)	121.1(2)
C(15)-C(10)-C(11)	119.8(3)
C(15)-C(10)-P	118.0(2)
C(11)-C(10)-P	122.2(2)
C(10)-C(11)-C(12)	118.9(3)
C(13)-C(12)-C(11)	120.6(3)

Table S-5 continued

C(12)-C(13)-C(14)	120.0(3)
C(13)-C(14)-C(15)	120.1(3)
C(14)-C(15)-C(10)	120.6(3)
C(17)-C(16)-C(21)	118.7(3)
C(17)-C(16)-P	121.3(2)
C(21)-C(16)-P	120.0(2)
C(18)-C(17)-C(16)	120.5(3)
C(19)-C(18)-C(17)	120.2(3)
C(20)-C(19)-C(18)	119.7(3)
C(19)-C(20)-C(21)	120.6(3)
C(20)-C(21)-C(16)	120.3(3)

Symmetry transformations used to generate equivalent atoms:

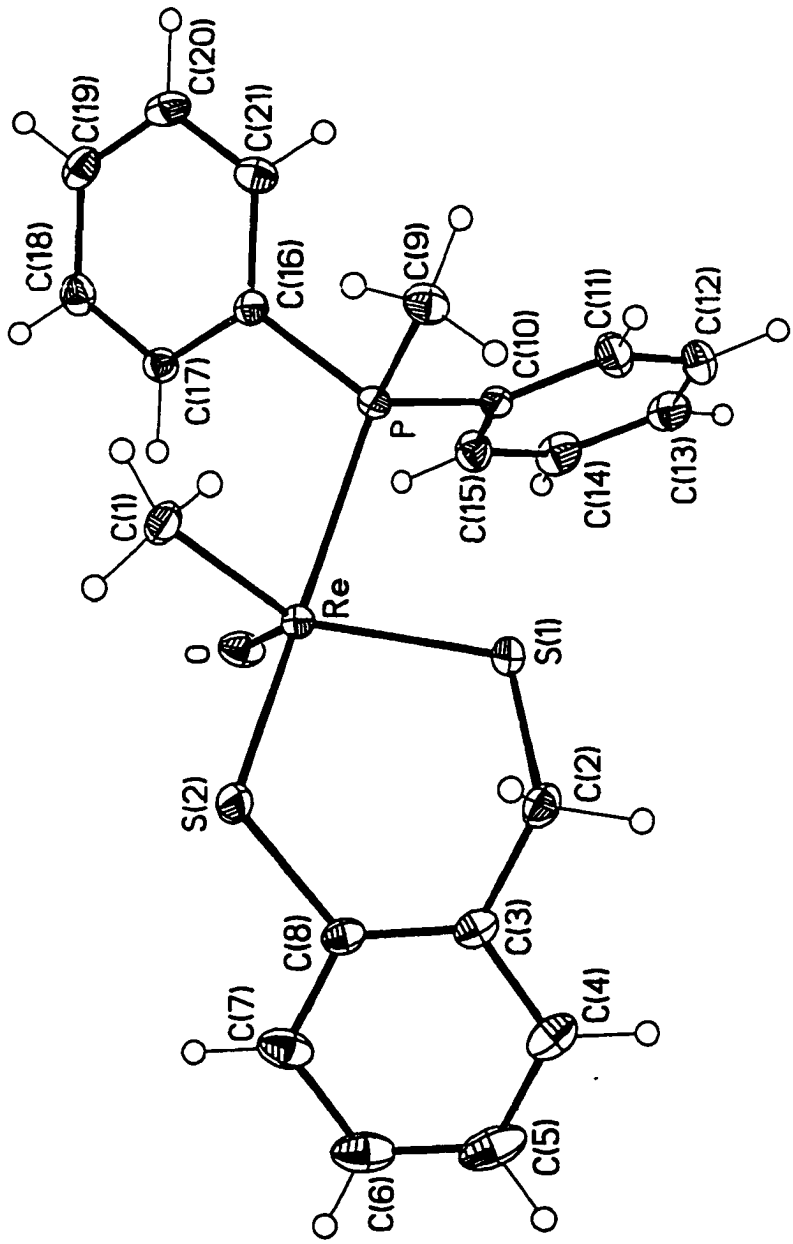

Figure S-1. The ORTEP of MeReO(mtp)$PMePh_2$ with 30% probability elipsoids. All hydrogen atoms were included in the structure factor calculation at idealized positions and were allowed to ride on the neighboring atoms with relative isotropic displacement coefficients.

Table S-6. Anisotropic displacement parameters ($Å^2 \times 10^3$) for M-$PMePh_2$. The anisotropic displacement factor exponent takes the form: $-2\pi^2[h^2 a^{*2} U^{11} + ... + 2 h k a^* b^* U^{12}]$

	U^{11}	U^{22}	U^{33}	U^{23}	U^{13}	U^{12}
Re	20(1)	19(1)	22(1)	-1(1)	8(1)	-1(1)
P	22(1)	21(1)	20(1)	-2(1)	6(1)	-1(1)
S(1)	30(1)	23(1)	30(1)	-1(1)	15(1)	-5(1)
S(2)	31(1)	22(1)	40(1)	5(1)	19(1)	3(1)
O	26(1)	37(1)	32(1)	-11(1)	6(1)	2(1)
C(1)	33(2)	31(2)	34(2)	7(1)	19(2)	0(1)
C(2)	23(2)	37(2)	33(2)	-2(1)	12(1)	-6(1)
C(3)	20(2)	38(2)	21(2)	3(1)	6(1)	6(1)
C(4)	30(2)	53(2)	29(2)	7(2)	13(2)	5(2)
C(5)	41(2)	88(3)	24(2)	1(2)	14(2)	19(2)
C(6)	37(2)	64(3)	35(2)	-18(2)	5(2)	13(2)
C(7)	29(2)	38(2)	43(2)	-9(2)	7(2)	8(2)
C(8)	19(2)	32(2)	26(2)	-1(1)	7(1)	5(1)
C(9)	30(2)	37(2)	24(2)	-8(1)	2(1)	-1(1)
C(10)	28(2)	19(1)	29(2)	1(1)	15(1)	2(1)
C(11)	45(2)	30(2)	39(2)	-3(2)	15(2)	-9(2)
C(12)	68(3)	25(2)	60(2)	-3(2)	37(2)	-10(2)
C(13)	68(3)	30(2)	48(2)	14(2)	37(2)	12(2)
C(14)	48(2)	44(2)	29(2)	13(2)	14(2)	7(2)
C(15)	37(2)	32(2)	30(2)	3(1)	10(2)	-3(2)
C(16)	27(2)	21(1)	21(1)	5(1)	9(1)	3(1)
C(17)	26(2)	25(2)	27(2)	0(1)	9(1)	3(1)
C(18)	25(2)	27(2)	40(2)	3(1)	11(1)	0(1)
C(19)	30(2)	35(2)	42(2)	13(2)	20(2)	8(1)
C(20)	36(2)	38(2)	32(2)	1(2)	17(2)	10(2)
C(21)	31(2)	29(2)	29(2)	-2(1)	8(1)	5(1)

Table S-7. Hydrogen coordinates (x 10^4) and isotropic displacement parameters ($Å^2$ x 10^3) for M-$PMePh_2$.

	x	y	z	U(eq)
H(1A)	3409	7607	2775	46
H(1B)	4012	7765	3223	46
H(1C)	3771	6558	2644	46
H(2A)	5140	9145	928	36
H(2B)	5063	8210	1732	36
H(4)	5223	8296	-529	44
H(5)	5085	6753	-1708	60
H(6)	4548	5174	-1673	56
H(7)	4164	5115	-429	46
H(9A)	4243	10531	3146	48
H(9B)	3909	9821	3693	48
H(9C)	3792	11197	3392	48
H(11)	3950	12337	2094	45
H(12)	3837	13954	947	57
H(13)	3232	13854	-670	53
H(14)	2726	12162	-1168	48
H(15)	2832	10558	-54	40
H(17)	2558	8558	1038	31
H(18)	1777	8376	1284	37
H(19)	1602	9514	2534	40
H(20)	2203	10856	3516	41
H(21)	2976	11088	3252	36

Table S-8. ^{1}H NMR Data for Reactions of MeReO(mtp)(4-Bu^{t}C$_5$H$_4$N) and 4,4-dimethyl-2,2'-bipyridine.

---

1. Pure Me_2bpy in C_6D_6.

8.70 (s, 2H), 8.52 (d, 2H, J = 4.8 Hz), 6.61 (d, 2H J = 4.8 Hz), 1.91, (s, 6H)

2. Pure 4-Bu^{t}C$_5$H$_4$N in C_6D_6.

8.55 (d, 2H, J = 1.6 Hz), 6.83 (d, 2H J = 6.0 Hz), 1.00, (s, 9H)

MeReO(mtp)(4-Bu^{t}C$_5$H$_4$N), isomer with Me trans to benzylic S:

(8 aromatic protons, 1 methyl group, 1 pair of methylene protons - non equiv., 1 tert-butyl group) -[all but two aromatic peaks identified for M-(4-Bu^{t}C$_5$H$_4$N)]

7.84‡ (d, 2H, J = 6.8 Hz), 7.76 (d, 1H, J = 8.4 Hz), 6.93 (m, 1H), 6.52‡ (d, 1H, J = 7.2 Hz), 4.83 (d, 1H, J = 12.8 Hz), 3.72 (d, 1H, J = 8.0 Hz), 2.89 (s, 3H), 0.78 (s, 9H)

‡ likely from the 4-*tert*-BuC$_5$H$_4$N ligand's protons

M-(4-tBuC$_5$H$_4$N)*; isomer with Me trans to phenolic S:

5.14 (d, 1H, J = 11.2 Hz), 4.83 (d, 1H, J = 12.8 Hz), 2.92 (s, 3H),

M-(Me_2bpy)* (formed in 90% yield, 9 of 10 aromatic peaks identified)

9.04 (d, 1H, J = 6.0 Hz), 8.15 (d, 1H, J = 5.6 Hz), 7.66 (m, 1H), 7.32 (m, 1H), 7.08 (s, 1H), 7.01 (m, 2H), 6.27 (d, 1H, J = 6.0 Hz), 5.75 (d, 1H, J = 6.0 Hz), 5.45 (d, 1H, J = 11.6 Hz), 4.72 (d, 1H, J = 11.6 Hz), 3.47 (s, 3H), 1.98 (s, 3H), 1.55 (s, 3H)

M--(Me_2bpy) (formed in 10% yield; 7 aromatic resonance identified)

8.92 (d, 1H, J = 6.0 Hz), 8.41 (d, 1H, J = 5.6 Hz), 8.14 (d, 1H), 7.35 (d, 1H, J), 7.32 (m, 1H), 6.26 (d, 1H, J = 4.4 Hz), 5.66 (d, 1H, J = 5.2 Hz), 5.28 (d, 1H, J = 12.8 Hz), 4.16 (d, 1H, J = 12.4 Hz), 3.16 (s, 3H)

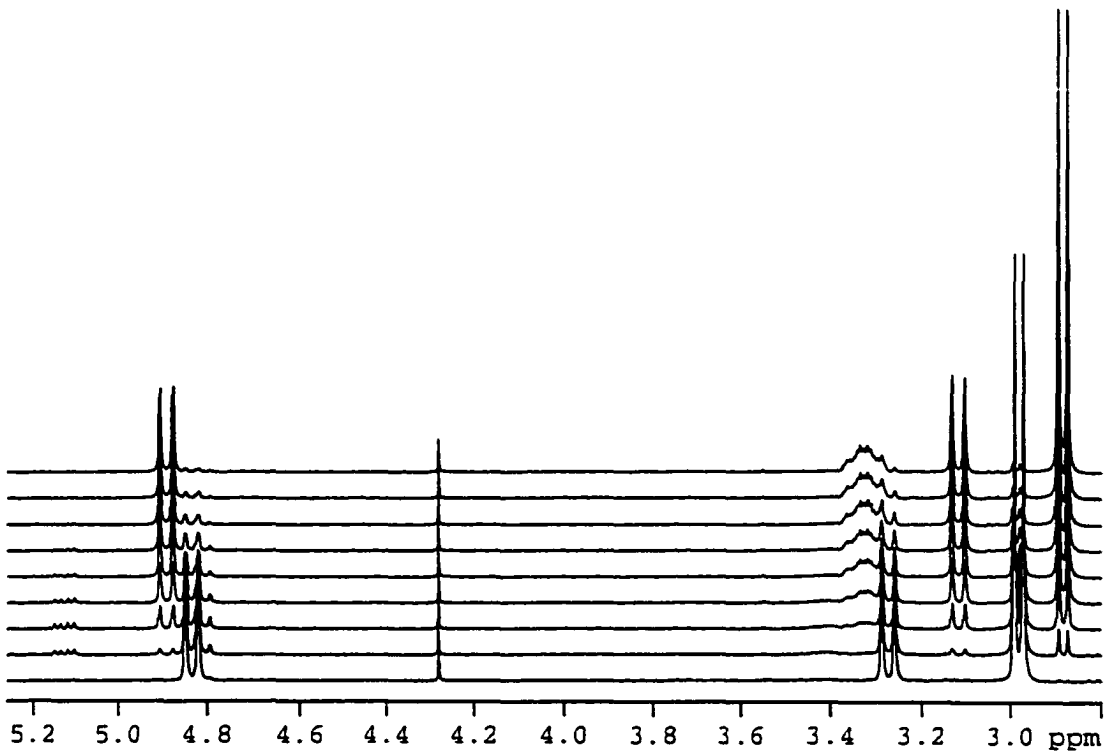

Figure S-2. Stacked ^{1}H NMR spectra showing the time evolution of the reaction between 10 mM MeReO(mtp)PPh_3 and 37 mM $PCyPh_2$. The intermediate does not rise to high concentrations, but its resonance can be seen at 5.11 ppm.

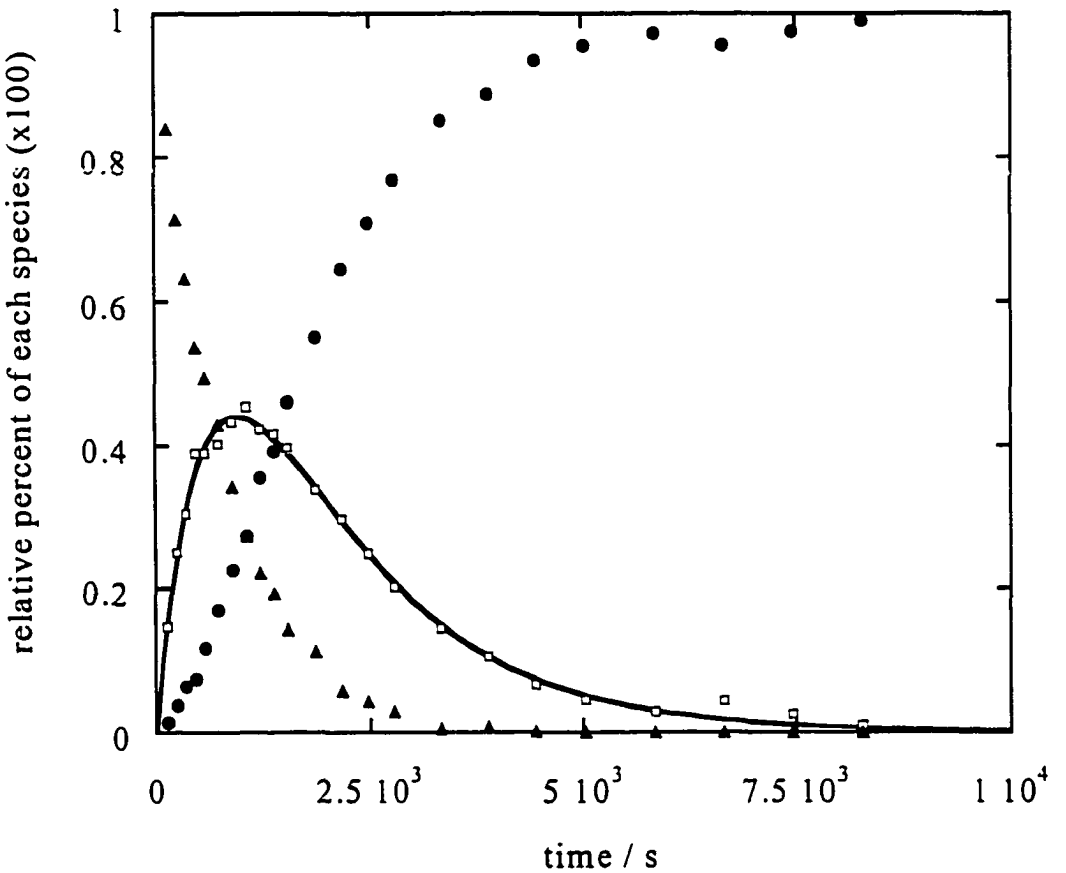

Figure S-3. A plot showing the time evolution of the intensities (from integrating all of the spectra like the few shown in Figure 5, main text) for the reaction between 3.5 mM $MeReO(mtp)P(4\text{-}ClC_6H_4)_3$ and 36 mM $PCyPh_2$ in C_6D_6 at 25 °C; $MeReO(mtp)PCyPh_2$ (circles), $MeReO(mtp)PCyPh_2$* (open squares) $MeReO(mtp)P(4\text{-}ClC_6H_4)_3$ (triangles). The smooth curves represent the fitting to bi-exponential kinetics.

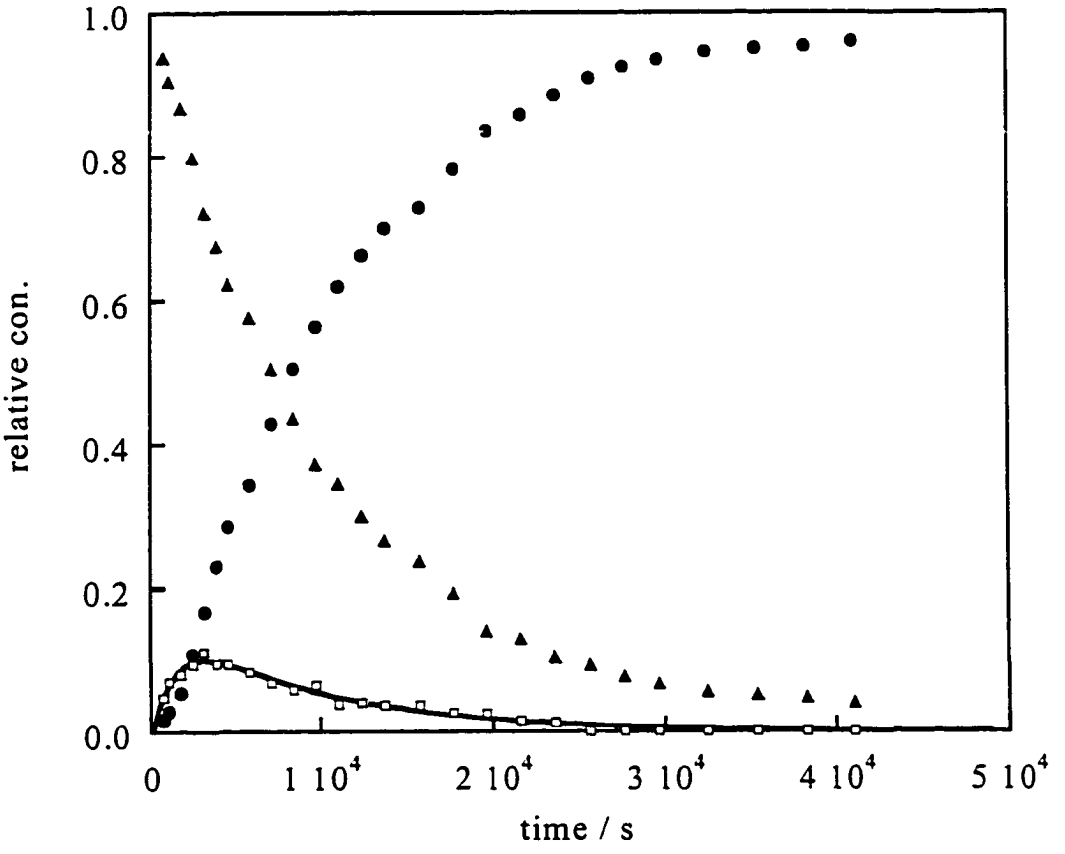

Figure S-4. A plot showing the time evolution of the intensities (from integrating all of the spectra like the few shown in Figure S–3) for $MeReO(mtp)PPh_3$ reacting with $PCyPh_2$; $MeReO(mtp)PCyPh_2$ (circles), $MeReO(mtp)PCyPh_2$* (open squares) $MeReO(mtp)PPh_3$ (triangles). The smooth curves represent the fitting to bi-exponential kinetics.

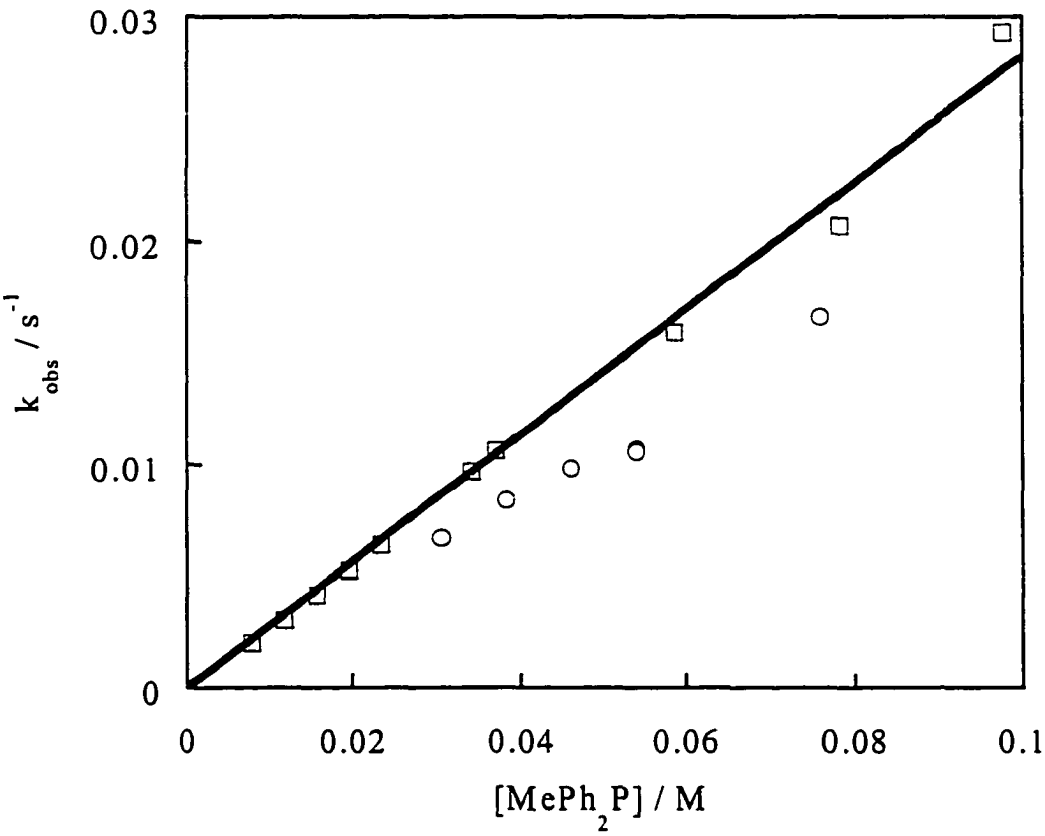

Figure S-5. A plot of k_{obs} versus [$PMePh_2$], comparing UV (open squares) and ^1H NMR (circles). The NMR data are relatively imprecise because the reaction time is short compared to the time for acquiring the data. The spectrophotometric data give k = 0.28 L mol^{-1} s^{-1} at 25.0 °C.

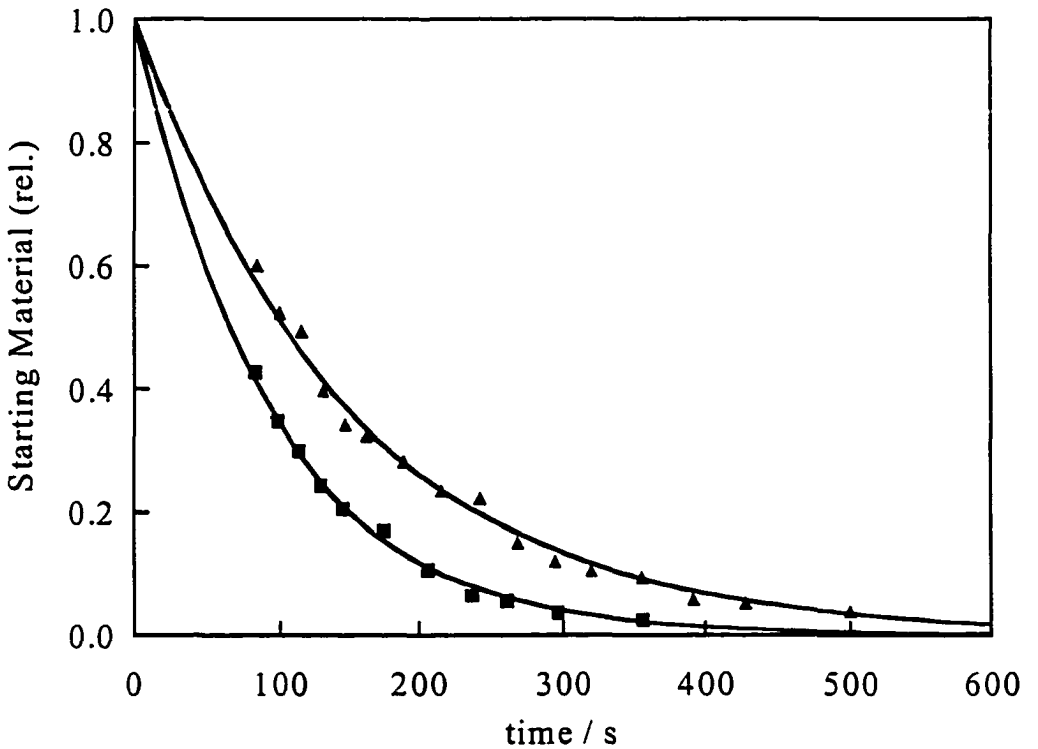

Figure S-6. Two reaction-time profiles from ^{1}H NMR kinetics for the between M-PPh_3 and $MePh_2P$ in C_6D_6. The data has been fit to a single exponential equation which yields the first order rate constants of 1.07 $\times 10^{-2}$ s^{-1} (squares) and 6.7 $\times 10^{-3}$ s^{-1} (triangles). The conditions are, respectively: [Re-PPh_3] = 7.8 mM, [$MePh_2P$] = 54 mM; [Re-PPh_3] = 2.0 mM, [$MePh_2P$] = 30.6 mM and temperature = 298 K.

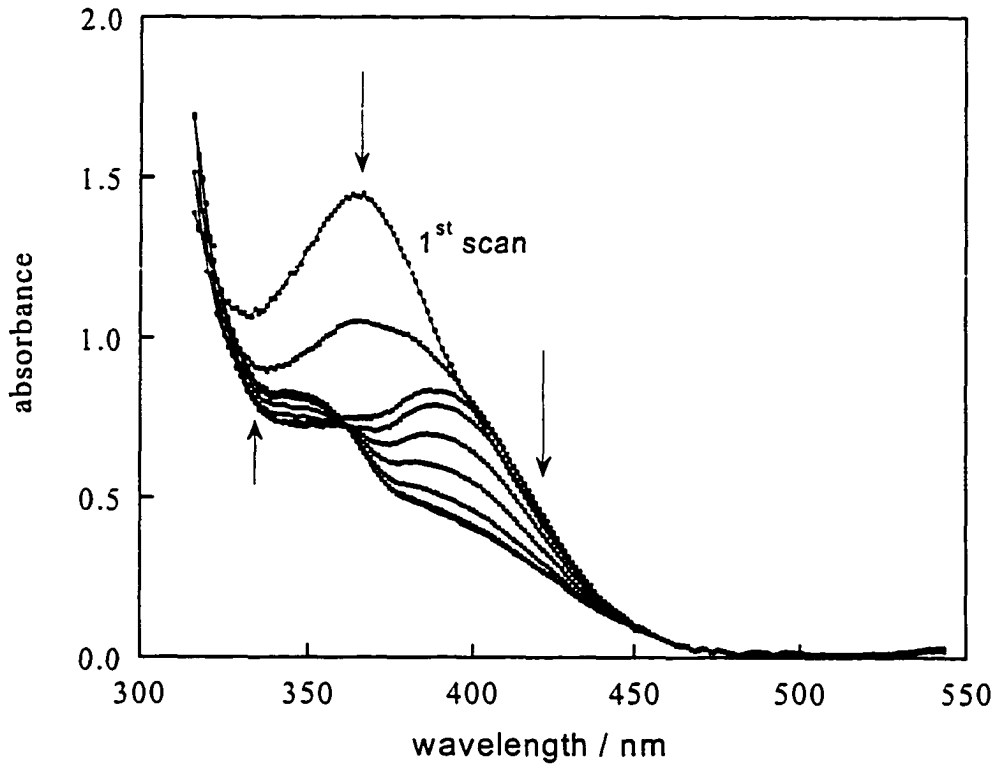

Figure S-7. A series of stacked scans from RSM stopped-flow experiments done on the reaction of MeReO(mtp)(4-Bu^{t}C$_5$H$_4$N) and MePh$_2$P. The scans are 1.1 sec apart, although many more were collected.

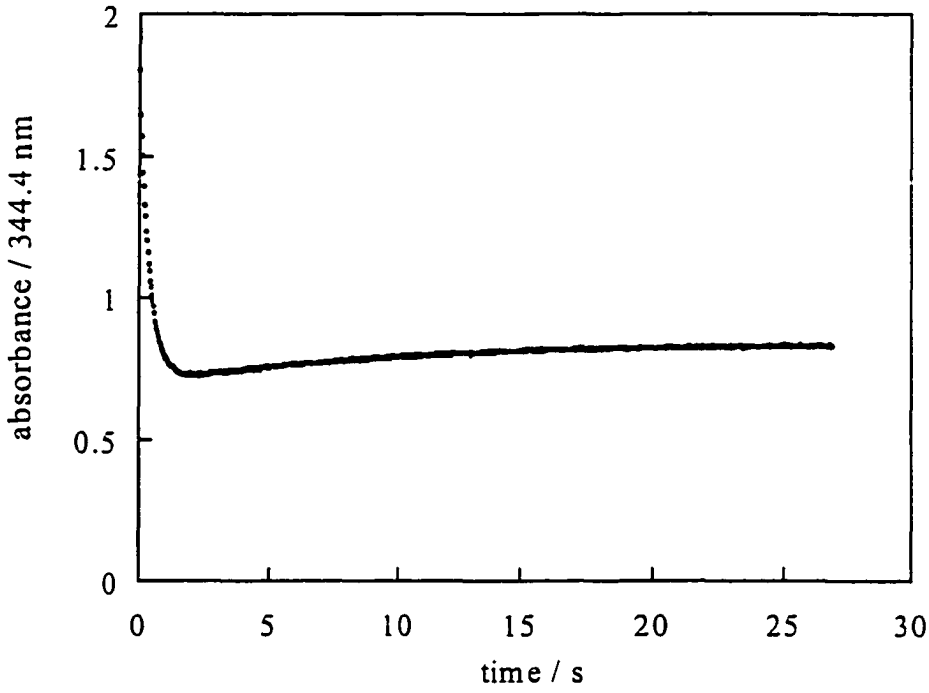

Figure S-8. A stopped-flow kinetic trace extracted at 344.4 nm for the reaction between 0.24 mM MeReO(mtp)(4-Bu^{t}C$_5$H$_4$N) and 2.7 mM PMePh$_2$, in benzene. There is also 3.3 mM NC$_5$H$_4$-4-Bu^t present.

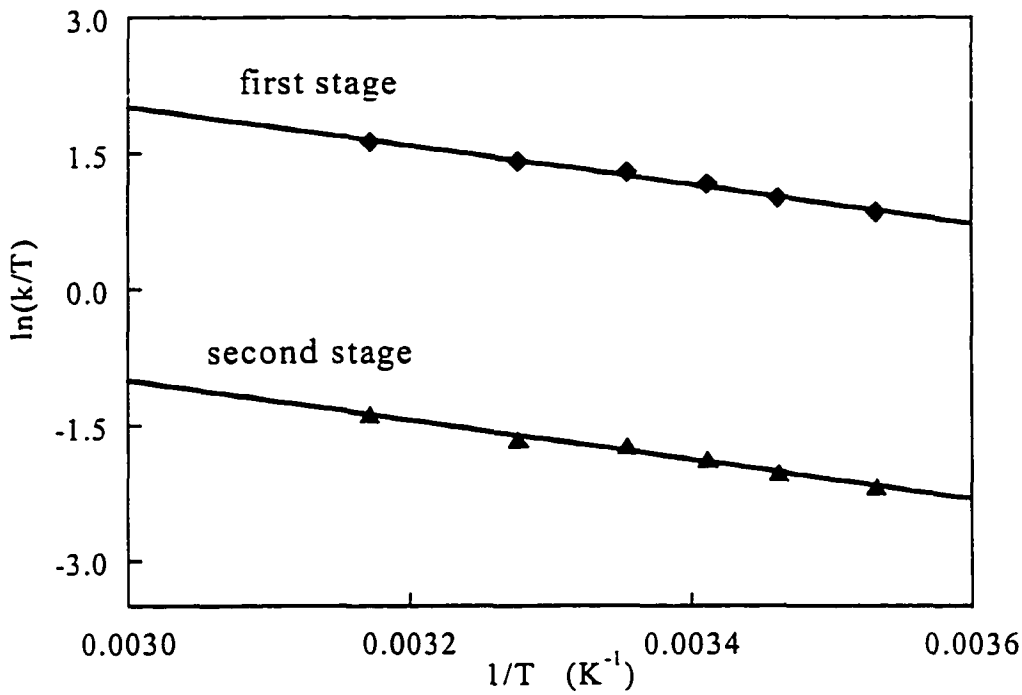

Figure S-9. Eyring plots for successive reactions, MeReO(mtp)(4-Bu^{t}C$_5$H$_4$N) and PMePh$_2$ (first stage) and MeReO(mtp)PMePh$_2$* and PMePh$_2$. The values of $\Delta H^{\ddagger}$ are 17.7 and 18.2 kJ mol^{-1}; of $\Delta S^{\ddagger}$, –127 and –151 J K^{-1} mol^{-1}.

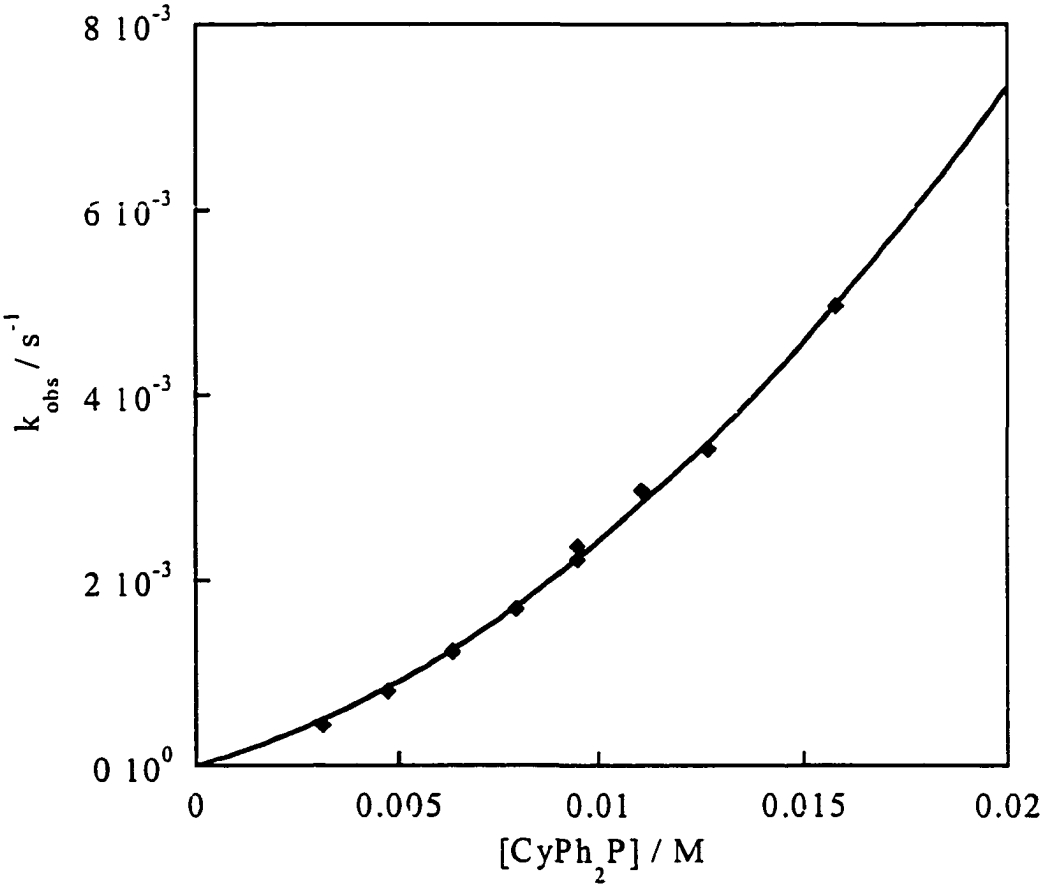

Figure S-10. The observed rate constant, k_{obs}, versus [$CyPh_2P$] for the reaction of monomerization of the dimer. The line was generated for the equation $k_a[CyPh_2P] + k_b[CyPh_2P]^2$.

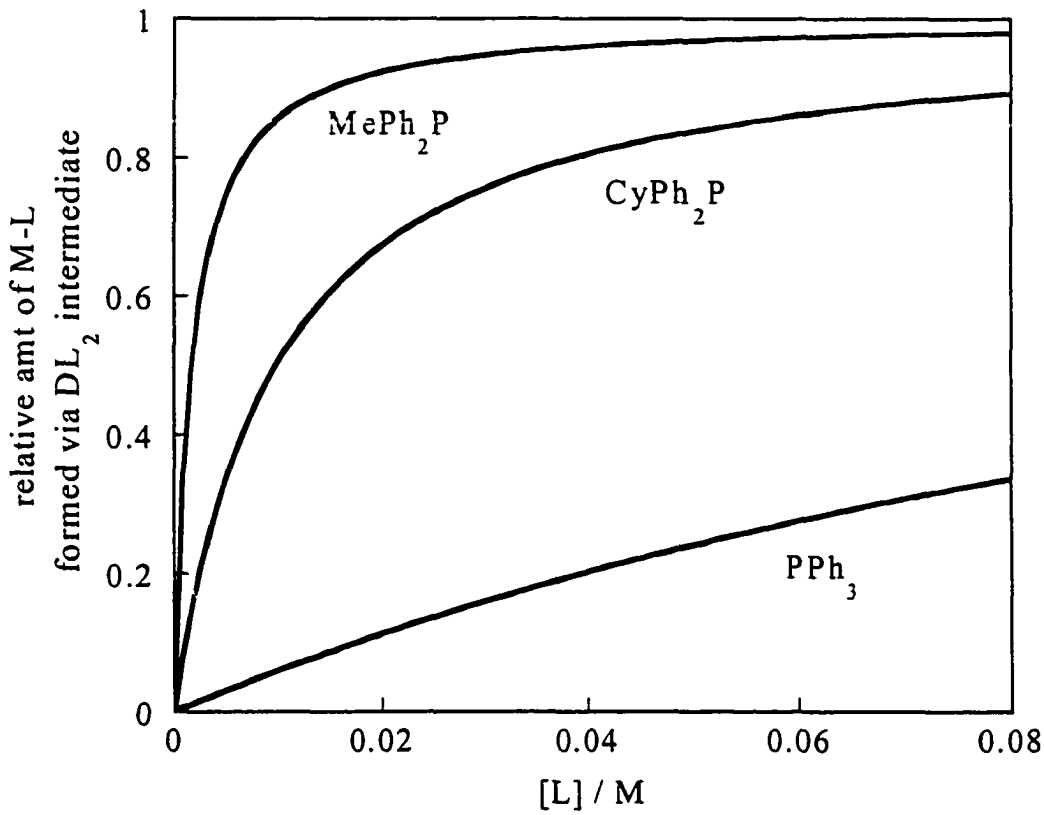

Figure S-11. The figure displays, as a function of ligand concentration, the calculated amount of total monomer (**M-L**) that is formed via the $\mathbf{DL_2}$ pathway.

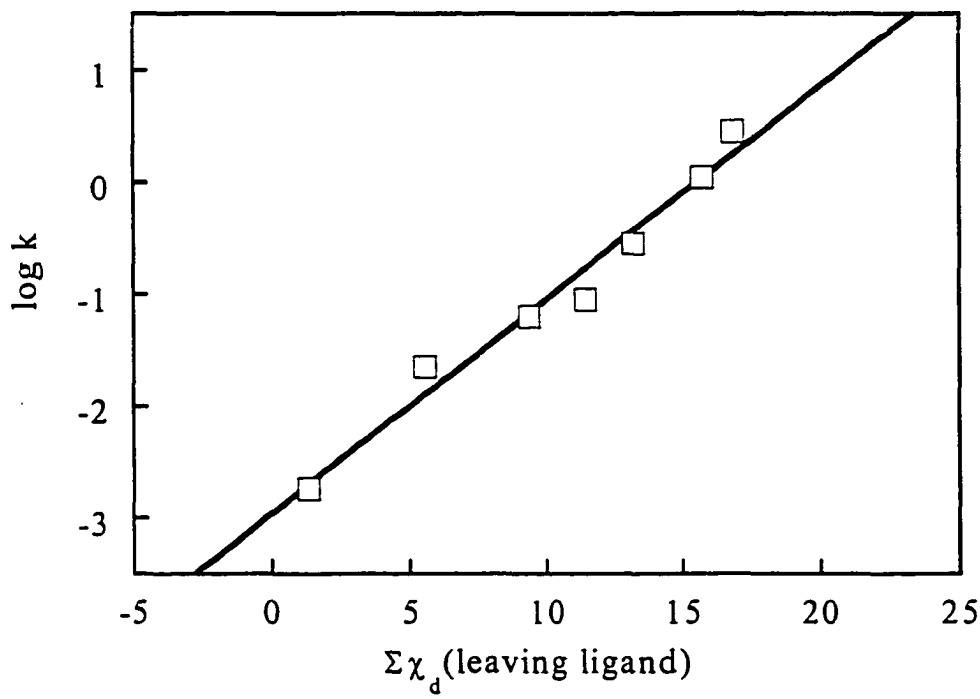

Figure S-12. A plot of log k vs the stereoelectronic parameter χ_d for the phosphines, for reactions with various phosphines as the leaving group X upon reaction the the entering ligand PMe_2Ph. the slope of the linear correlation, showing that the X groups that are the weaker Lewis bases are the best leaving groups.

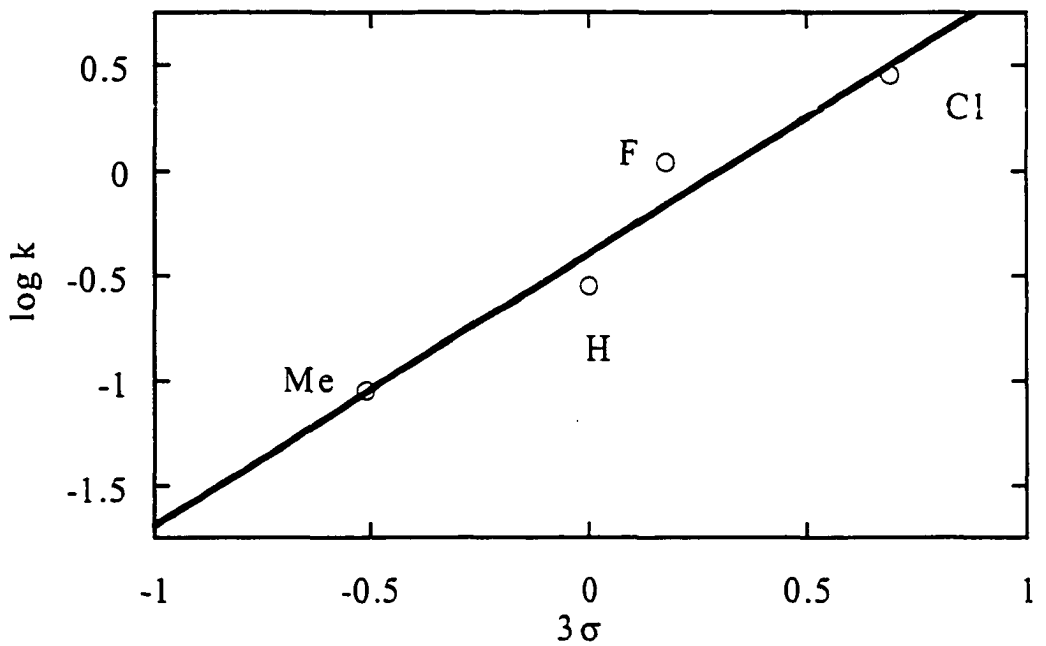

Figure S-13. A Hammett plot (log k) against substituent constant (σ) multiplied by three, for the reactions of MeRe)(mtp)(P(4-$XC_6H_4)_3$) and $MePh_2P$. Rate constants were determined in benzene at 25 °C. The slope and reaction constant (ρ) is 1.3.

References

(1) Espenson, J. H. *Chem. Commun* **1999,** 479-488.

(2) Herrmann, W. A.; Kühn, F. E. *Acc. Chem. Res.* **1997,** *30,* 169-180.

(3) Gable, K. P. *Adv. Organomet. Chem.* **1997,** *41,* 127-161.

(4) Vassell, K. A.; Espenson, J. H. *Inorg. Chem.* **1994,** *33,* 5491-5498.

(5) Abu-Omar, M. M.; Espenson, J. H. *J. Am. Chem. Soc.* **1995,** *117,* 272.

(6) Abu-Omar, M. M.; Espenson, J. H. *Inorg. Chem.* **1995,** *34,* 6239-6240.

(7) Abu-Omar, M. M.; Appleman, E. H.; Espenson, J. H. *Inorg. Chem.* **1996,** *35,* 7751-7757.

(8) Jung, J.-H.; Albright, T. A.; Hoffman, D. M.; Lee, T. R. *J. Chem. Soc., Dalton Trans.* **1999,** 4487-4494.

(9) Lahti, D. W.; Espenson, J. H. *Inorg. Chem.* **2000,** *39,* 2164-2167.

(10) Wang, Y.; Espenson, J. H. *Org. Lett.* **2000,** *2,* 3525-3526.

(11) Jacob, J.; Guzei, I. A.; Espenson, J. H. *Inorg. Chem.* **1999,** *38,* 1040-1041.

(12) Lente, G.; Guzei, I. A.; Espenson, J. H. *Inorg. Chem.* **2000,** *39,* 1311-1319.

(13) Lente, G.; Jacob, J.; Guzei, I. A.; Espenson, J. H. *Inorg. React. Mech. (Amsterdam)* **2000,** *2,* 169-177.

(14) Mayer, J. M.; Tulip, T. H.; Calabrese, J. C.; Valencia, E. *J. Am. Chem. Soc.* **1987,** *109,* 157-163.

(15) Ramirez, F.; Ugi, I. *Advan. Phys. Org. Chem.* **1971,** *9,* 25-126.

(16) Gillespie, P.; Hoffman, P.; Klusacek, H.; Marquarding, D.; Pfohl, S.; Ramirez, F.; Tsolis, E. A.; Ugi, I. *Angew. Chem., Int. Ed. Engl.* **1971,** *10,* 687-715.

(17) Ugi, I.; Marquarding, D.; Klusacek, H.; Gillespie, P.; Ramirez, F. *Accounts Chem. Res.* **1971**, *4*, 288-296.

(18) Casares, J. A.; Espinet, P. *Inorg. Chem.* **1997**, *36*, 5428-5431.

(19) Casares, J. A.; Espinet, P.; Soulantica, K.; Pascual, I.; Orpen, A. G. *Inorg. Chem.* **1997**, *36*, 5251-5256.

(20a) Jacob, J.; Lente, G.; Guzei, I. A.; Espenson, J. H. *Inorg. Chem.* **1999**, *38*, 3762-3763.

(20b) Herrmann, W. A.; Kratzer, R. M.; Fischer, R. W. *Angew. Chem., Int. Ed. Eng.* **1997**, *36*, 2652-2654.

(21) Sheldrick, G. **1997**, Bruker Analytical X–Ray Systems, Siemens: Madison, WI.

(22) Blessing, R. H. *Acta Cryst.* **1995**, *A51*, 33-38.

(23) Concerning these descriptors: "...the difference between an 'approximate trigonal bipyramid' and an 'approximate square pyramid' may be vanishingly small." [Langford, C. H.; Gray, H. B. "Ligand Substitution Processes" W. A. Benjamin, Inc. New York, 1965, p 1918]. The second designation is used here in the interest of providing a pictorial frame of reference, not to exclude the alternative.

(24) Cremer, S. E.; Chorvat, R. J. *J. Org. Chem.* **1967**, *32*, 4066.

(25) Griffin, C. E.; Kundu, S. K. *J. Org. Chem.* **1969**, *34*, 1532.

(26) Ross, J. A.; Martz, M. D. *J. Org. Chem.* **1969**, *34*, 399-404.

(27) Ma, E. S. F.; Rettig, S. J.; James, B. R. *Chem. Commun* **1999**, 2463-2464.

(28) Blower, P. J.; Dilworth, J. R.; Hutchinson, J. P.; Nicholson, T.; Zubieta, J. *J. Chem. Soc., Dalton Trans.* **1986**, 1339-1345.

(29) Eisenberg, R.; Gray, H. B. *Inorg. Chem.* **1967**, *6*, 1844-1849.

(30) Stiefel, E. I.; Eisenberg, R.; Rosenberg, R. C.; Gray, H. B. *J. Am. Chem. Soc.* **1966,** *88,* 2956.

(31) Danopoulos, A. A.; Wong, A. A. C.; Wilkinson, G.; Hursthouse, M. B.; Hussain, B. *J. Chem. Soc., Dalton Trans.* **1990,** 315-331.

(32) Saha, B.; Espenson, J. H. unpublished observations.

(33) Rockey, T. R.; Espenson, J. H. unpublished results.

(34) Shan, X.; Espenson, J. H. unpublished results.

(35) Dias, P. B.; Minas de Piedade, M. E.; Martinho Simoes, J. A. *Coord. Chem. Rev.* **1994,** *135,* 737-807.

CHAPTER II. SYNTHESIS AND CHARACTERIZATION OF A COMPOUND CONTAINING THE NOVEL $(O{=}Re)_2(\mu\text{-}OH)$ UNIT

A paper to be submitted *Inorganic Chemistry*.

David W. Lahti, Ilia Guzei, and James H. Espenson

Abstract

Treatment of $\{CH_3Re(O)(mtp)\}_2$ ($mtpH_2$ = 2-(mercaptomethyl)thiophenol) with tetra-n-butylammonium chloride in benzene which has been layered over water results in the formation of $[Bu^n{}_4N][\{MeReO(mtp)\}_2(\mu\text{-}OH)]$, which was characterized crystallographically. The hydroxo group is shared equally between the two rhenium atoms, with ∠ Re-O(H)-Re = 99.2(2)°. The product is dark pink in color and is insoluble in water and sparingly soluble in benzene. Bond distances are Re=O 168.0(4) pm and Re-(μ-OH), 218.5(3) pm.

Introduction

A dithiolato(oxo)rhenium(V) dimer, $\{MeReO(mtp)\}_2$, **1**, was recently prepared and contains a Re_2S_2 core, is a starting point for this work.[1] Figure 1 shows its structural formula, along with formulas for several of its derivatives. Formally each of these sulfur atoms bridges one rhenium and forms a covalent bond to the other, but the four Re–S bond distances are hardly different: $d(Re{-}S)_{cov}$ = 236.1, 236.6 pm as compared to $d(Re{-}S)_{br}$ = 238.8, 239.4 pm. Also, **1** retains its structural integrity in non-coordinating solvents (benzene, toluene, chloroform, etc.). The two monomeric units are held together by the coordinate bridge bonds, which are present presumably to satisfy the requirement of the

coordination number and electron density. Indeed, the reaction of **1** with a Lewis base L, such as pyridine or a phosphine, gives rise to mononuclear compounds MeReO(mtp)L.[2,3]

We have shown that **1** and its monomeric forms catalyze oxygen-transfer reactions, e.g., from pyridine-N-oxides to phosphines.[4] With an eye toward developing this catalytic chemistry in semi-aqueous media, we explored certain combinations that resulted in the synthesis of a new compound, described herein. Compounds of rhenium that contain a bridging hydroxide ligand are rare. If a molecule can be characterized with a ligand on each rhenium atom of **1**, while not causing cleavage of the Re–S coordinate bonds, it helps support one of the intermediate that has been prosposed for the monomerization of **1**.[3,5]

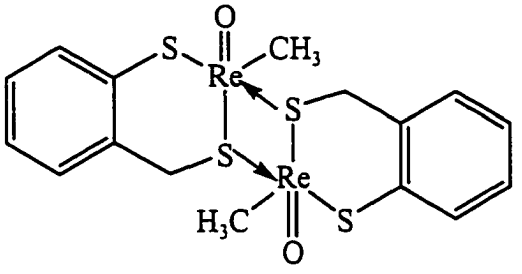

{MeReO(mtp)}$_2$ **1**

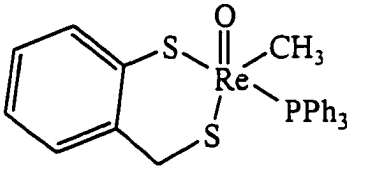

MeReO(mtp)PPh$_3$

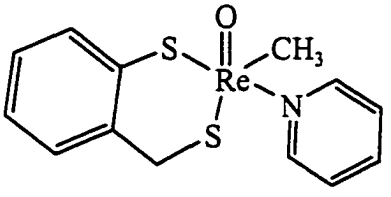

MeReO(mtp)Py

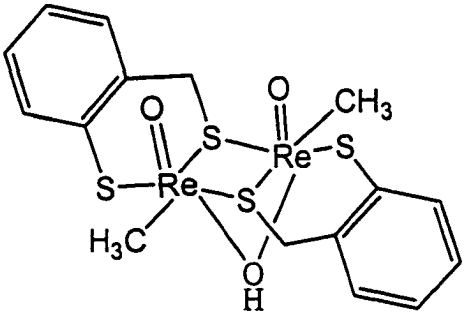

[{MeReO(mtp)}$_2$(μ-OH)]$^-$ **2**

Figure 1. Selected dithiolato based rhenium compounds.

Experimental

Methyltrioxorhenium(VII), MTO, was prepared from sodium perrhenate according to a published procedure.[6] The dimeric complex $\{MeReO(mtp)\}_2$ as described previously from methyltrioxorhenium(VII) and 2-mercaptomethylthiolphenol ($mtpH_2$), reported earlier.[1] Solvents and reagents were purchased, and used as received. Typically 4 mg of **1** dissolved was dissolved in 5-10 ml of benzene has about and 20-40 mg of tetra-n-butylammonium chloride was added, and then the solution was layered over 8-12 ml water.

Results and Discussion

A benzene solution of yellow-brown **1** containing excess tetra-n-butylammonium chloride was layered over water. A solid formed and dichroic red-green crystals suitable for X-ray diffraction grew at the interface over two days. The diffraction study showed that an ionic compound had formed, $[Bu^n_4N][\{MeReO(mtp)\}_2(\mu\text{-}OH)]$, **2**, shown in figure 2, along with selected bond lengths and angles. Full details of the X-ray refinement of **2** are given in the Supporting Information. Figure S-1 includes the counter cation in the structure. The chemical equation is shown, eq 1. The crystallographic information is summarized in tables S–1-to-5.

$$\mathbf{1} + Bu^n_4NCl + H_2O \xrightarrow[C_6H_6/H_2O]{} \mathbf{2} + HCl \qquad (1)$$

No structure of this type $(O{=}M)_2(\mu\text{-}OH)$ type appears to have been reported. This new complex has a C_2 symmetric axis down the bridging hydroxo ligand; the Re–O bond lengths are 218.4 pm whereas the terminal rhenium-oxo bonds are 168.0 pm in length. The presence of the cation, tetra-n-butylammonium, in the structure further confirms the need for

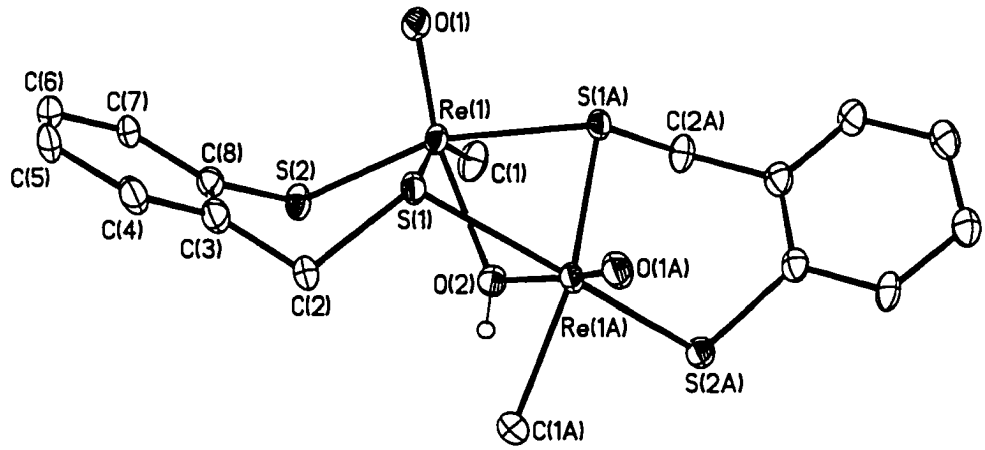

Figure 2. Perspective view of the rhenium compound **2** with themal ellipsoids at the 40% probablity level. Selected bond lengths (pm) and angles (deg): Re(1)–O(1), 168.0(4); Re(1)–C(1), 215.3(5); Re(1) –O(2), 218.5(3); Re(1) –S(1), 243.30(13); Re(1)–S(2), 233.69(13); S(1) –C(2), 183.9(5); S(2)–C(8), 178.7(5); O(1)–Re–C(1), 97.3(2); O(1)–Re–O(2), 168.75(12); C(1)–Re–O(2), 80.81(19); O(1) –Re–S(2), 102.35(12); C(1) –Re–S(2), 84.40(17); S(1)–Re–S(1A), 77.63(5); Re(1)–S(1)–Re(1A), 86.36(4); Re(1) –O(2)–Re(1A), 99.89(17); C(8)–S(2)–Re(1A), 107.36(16).

an anion; hydroxide. Table 1 shows bond lengths and related bond angles for some multinuclear rhenium compounds that contain either a bridging hydroxide or oxo ligand, as well as other useful information. The bridging hydroxo bond length range from 200–230 pm, while bridging oxo groups have bond lengths of 190 pm or less. This data further supports a bridging hydroxide unit in compound **2**.

The Re=O distance in **2** was 168.0 pm, essentially the same as in **1** (167.4 pm) and in other mononuclear rhenium compounds.[1,3,5,7] The Re–S(1) bond lengths in the four membered ring have grown to 2.45 Å from 2.38 Å in **1**. The most striking change that occurs

Table 1. Various rhenium compounds that contain a bridging oxo or hydroxo ligand(s).

Compounds	Re-O (pm)	Re-OH (pm)	Re-Re (pm) a bond ?[a]	reference and ox. state
$[Re_4(C_6H_5NCOCH_3)_6(Cl)(\mu\text{-}O)(\mu\text{-}OH)\text{-}(MeOH)_3][ReO_4]_2$				8
Re(3) – O(6) – Re(1) angle 136(1)	194(2) 188(2)		no	Re(III)
Re(4) – O(10) – Re(1) angle 123(1)		206(3) 229(2)	no	
$[(\mu\text{-}O)\{CH_3Re(O)_2(8\text{-oxyquinoline})\}_2]$				9
Re – O(1) – Re angle 180	187.1(1)		no	Re(VII)
$[Re_2(\mu\text{-}O)O_4(CH_2CMe_3)_4]$				10
Re(1) – O(5) – Re(2) angle 166.3(5)	194.0(11) 189.6(11)		no	Re(VII)
$[Re_2(\mu\text{-}O)_2O_2(CH_2CMe_3)_4]$				11
Re(1) – O(6) – Re(2) angle 85.8(7)	196.7(17) 186.1(18)		260.6(1) yes	Re(V)
Re(1) – O(5) – Re(2) angle 83.3(7)	194.6(18) 197.7(18)			
$[Re_2(\mu\text{-}CH_2)(\mu\text{-}O)(O)_2Me_4(PMe_3)_2]$				11
Re – O – Re	197.1(14) 187.8(14)		254.8(2) yes	Re(VI)
$[Re_2(\mu\text{-}CH_2)(\mu\text{-}O)(O)_2Me_4]$				12
Re – O – Re	190.2(16) 193.9(17)		265.2(2) yes	Re(VI)
$[(\mu\text{-}OH)\{MeRe(O)(SCH_2C_6H_4S)\}_2]$				b
Re – O – Re angle 99.89(17)		218.5(3)	337 no	Re(V)

a) stating whether a bond between two rhenium atoms exists
b) this paper

upon coordination of the hydroxide ligand is the collapsing of the Re---Re distance which becomes 334 pm from 368 pm in **1**. To achieve this, the Re–S–Re angle has collapsed to 86° from 101° while the S---S distance actually grows to 3.063 Å from 2.896 Å in **1**. However, the Re---Re distance remains too long to be considered to have a bonding interaction between the rhenium atoms.[13] The hydroxide ligand binds *trans* to the terminal rhenium–oxo bonds, giving an "A" frame type structure consisting of Re_2O_3. Further, **2** features distorted octahedral symmetry around the rhenium with ∠ Re-O(H)-Re = 99.2(2)°. The dihedral angle of the Re_2S_2 core goes from 19.2° in **1** to 41.2° in **2**.

Chloride ions are in fact known to monomerize **1** into $[Bu^n_4N][MeReO(mtp)Cl]$. In the presence of water, however, the dimeric structure of **1** is not disrupted. Curiously, **1** does not react with Bu^n_4NOH in benzene, suggesting a role for chloride in the process. We note that partially-opened dimeric structures have been found[2] and postulated;[14] ligated but unopened derivatives of **1** lie on the pathway to monomer formation.[3,5] An attempt was made to prepare a compound analogous to **2**, but with a μ-SH group. No reaction analogous to eq 1 occured, however, on substituting H_2S for water.

Mechanistic studies of monomerization of **1** with numerous Lewis bases support the existence of two intermediates (designated: **DL**-dimer with one ligand, $\mathbf{DL_2}$-dimer with two ligands) on the pathway toward monomerization. Kinetic evidence aside, the $[\{MeReO(mtp)\}_2(DMSO)]$ adduct, which has been previous reported,[2] supports the **DL** type intermediate inferred from kinetics studies. Compound **2** now has a structure that is reminiscent of $\mathbf{DL_2}$, while not stoichometrically achieved, it shows that each Re atom can bind to a ligand simultaneously: in this case, it just happens to be the same ligand.

Acknowledgment

This research was supported by a grant from the National Science Foundation. Some experiments were conducted with the facilities of the Ames Lab.

Supporting Information

Complete tables of the crystal data and refinement details, atomic coordinates, molecular structure with the cation, synthetic procedure, bond lengths and angles, and anisotropic displacement parameters.

Supporting Information

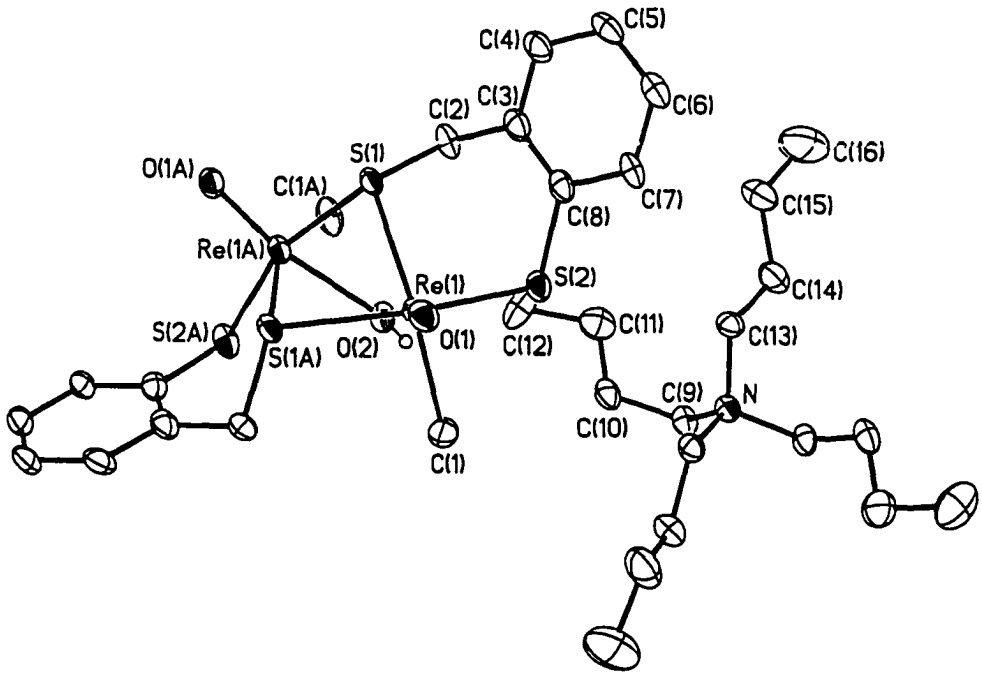

Figure S-1. Perspective view of the rhenium compound **2** with themal ellipsoids at the 40% probablity level. The tetra-n-butyl ammonium cation is also shown.

Table S-1. Crystal data and structure refinement for **2**.

Empirical formula	$C_{32} H_{55} N O_3 Re_2 S_4$	
Formula weight	1002.41	
Temperature	173(2) K	
Wavelength	0.71073 Å	
Crystal system	Monoclinic	
Space group	P2/c	
Unit cell dimensions	a = 10.8441(8) Å	α= 90°
	b = 9.2669(6) Å	β= 117.528(10)°
	c = 20.9735(13) Å	γ = 90°
Volume	1869.0(2) $Å^3$	
Z	2	
Density (calculated)	1.781 Mg/m^3	
Absorption coefficient	6.725 mm^{-1}	
F(000)	984	
Crystal size	0.40 x 0.40 x 0.20 mm^3	
Theta range for data collection	2.12 to 26.37°	
Index ranges	$-13 \le h \le 12, 0 \le k \le 11, 0 \le l \le 26$	
Reflections collected	16529	
Independent reflections	3830 [R(int) = 0.0354]	
Completeness to theta = 26.37°	100.0 %	
Absorption correction	Empirical with SADABS	
Max. and min. transmission	0.3465 and 0.1739	
Refinement method	Full-matrix least-squares on F^2	
Data / restraints / parameters	3830 / 0 / 194	
Goodness-of-fit on F^2	1.005	
Final R indices [I>2sigma(I)]	R1 = 0.0293, wR2 = 0.0855	
R indices (all data)	R1 = 0.0354, wR2 = 0.0887	
Largest diff. peak and hole	1.836 and -1.653 $e.Å^{-3}$	

Table S-2. Atomic coordinates (x 10^4) and equivalent isotropic displacement parameters ($Å^2$ x 10^3) for **2**. U(eq) is defined as one third of the trace of the orthogonalized U^{ij} tensor.

	x	y	z	U(eq)
Re(1)	6732(1)	5808(1)	7841(1)	27(1)
S(1)	4871(1)	6791(1)	6741(1)	28(1)
S(2)	7613(2)	4420(1)	7214(1)	36(1)
O(1)	7955(4)	7088(4)	8218(2)	35(1)
O(2)	5000	4291(4)	7500	32(1)
N	10000	447(6)	7500	27(1)
C(1)	7688(7)	4202(6)	8668(3)	44(2)
C(2)	4864(6)	5728(6)	5999(3)	36(1)
C(3)	6184(6)	5993(5)	5944(3)	35(1)
C(4)	6148(6)	6813(6)	5379(3)	37(1)
C(5)	7345(6)	7062(6)	5320(3)	40(1)
C(6)	8610(6)	6517(6)	5833(3)	36(1)
C(7)	8668(6)	5735(5)	6405(3)	34(1)
C(8)	7445(6)	5462(5)	6462(3)	32(1)
C(9)	8802(6)	-538(5)	7410(3)	33(1)
C(10)	7446(6)	181(6)	7297(3)	38(1)
C(11)	6352(7)	315(7)	6538(3)	50(2)
C(12)	4983(7)	850(7)	6493(5)	65(2)
C(13)	9568(5)	1451(5)	6853(2)	30(1)
C(14)	9318(7)	752(6)	6152(3)	45(2)
C(15)	8665(8)	1888(8)	5548(3)	62(2)
C(16)	8497(11)	1404(12)	4845(4)	99(3)

Table S-3. Bond lengths [Å] and angles [°] for **2**.

Re(1)-O(1)	1.680(4)
Re(1)-C(1)	2.153(5)
Re(1)-O(2)	2.185(3)
Re(1)-S(2)	2.3369(13)
Re(1)-S(1)	2.4330(13)
Re(1)-S(1)#1	2.4541(12)
S(1)-C(2)	1.839(5)
S(1)-Re(1)#1	2.4541(12)
S(2)-C(8)	1.787(5)
O(2)-Re(1)#1	2.185(3)
N-C(9)	1.526(6)
N-C(9)#2	1.526(6)
N-C(13)#2	1.530(6)
N-C(13)	1.530(6)
C(2)-C(3)	1.507(8)
C(3)-C(8)	1.385(8)
C(3)-C(4)	1.393(7)
C(4)-C(5)	1.381(7)
C(5)-C(6)	1.390(8)
C(6)-C(7)	1.378(8)
C(7)-C(8)	1.408(7)
C(9)-C(10)	1.530(7)
C(10)-C(11)	1.486(8)
C(11)-C(12)	1.525(9)
C(13)-C(14)	1.511(7)
C(14)-C(15)	1.545(9)
C(15)-C(16)	1.470(10)
O(1)-Re(1)-C(1)	97.3(2)
O(1)-Re(1)-O(2)	168.75(12)
C(1)-Re(1)-O(2)	80.81(19)
O(1)-Re(1)-S(2)	102.35(12)
C(1)-Re(1)-S(2)	84.40(17)
O(2)-Re(1)-S(2)	88.55(7)
O(1)-Re(1)-S(1)	108.07(12)
C(1)-Re(1)-S(1)	154.44(18)
O(2)-Re(1)-S(1)	73.72(7)
S(2)-Re(1)-S(1)	92.76(5)
O(1)-Re(1)-S(1)#1	96.06(12)
C(1)-Re(1)-S(1)#1	97.26(16)
O(2)-Re(1)-S(1)#1	73.29(7)
S(2)-Re(1)-S(1)#1	161.17(5)

Table S-3 continued

S(1)-Re(1)-S(1)#1	77.63(5)
C(2)-S(1)-Re(1)	106.22(19)
C(2)-S(1)-Re(1)#1	112.16(18)
Re(1)-S(1)-Re(1)#1	86.36(4)
C(8)-S(2)-Re(1)	107.36(16)
Re(1)-O(2)-Re(1)#1	99.89(17)
C(9)-N-C(9)#2	106.6(5)
C(9)-N-C(13)#2	111.6(3)
C(9)#2-N-C(13)#2	111.1(3)
C(9)-N-C(13)	111.1(3)
C(9)#2-N-C(13)	111.6(3)
C(13)#2-N-C(13)	105.1(5)
C(3)-C(2)-S(1)	110.2(4)
C(8)-C(3)-C(4)	119.3(5)
C(8)-C(3)-C(2)	120.8(5)
C(4)-C(3)-C(2)	119.9(5)
C(5)-C(4)-C(3)	120.7(5)
C(4)-C(5)-C(6)	120.1(5)
C(7)-C(6)-C(5)	119.8(5)
C(6)-C(7)-C(8)	120.1(6)
C(3)-C(8)-C(7)	119.9(5)
C(3)-C(8)-S(2)	123.0(4)
C(7)-C(8)-S(2)	117.1(4)
N-C(9)-C(10)	117.4(4)
C(11)-C(10)-C(9)	115.9(5)
C(10)-C(11)-C(12)	111.5(6)
C(14)-C(13)-N	116.5(4)
C(13)-C(14)-C(15)	108.3(5)
C(16)-C(15)-C(14)	114.4(7)

Symmetry transformations used to generate equivalent atoms:
#1 -x+1,y,-z+3/2 #2 -x+2,y,-z+3/2

Table S-4. Anisotropic displacement parameters ($Å^2 \times 10^3$) for **2**. The anisotropic displacement factor exponent takes the form: $-2\pi^2 [h^2 a^{*2} U^{11} + ... + 2 h k a^* b^* U^{12}]$

	U^{11}	U^{22}	U^{33}	U^{23}	U^{13}	U^{12}
Re(1)	34(1)	24(1)	31(1)	4(1)	22(1)	1(1)
S(1)	36(1)	26(1)	30(1)	0(1)	23(1)	1(1)
S(2)	49(1)	26(1)	48(1)	6(1)	35(1)	9(1)
O(1)	40(2)	34(2)	36(2)	3(2)	23(2)	-2(2)
O(2)	41(3)	21(2)	44(3)	0	28(3)	0
N	35(3)	18(2)	32(3)	0	20(3)	0
C(1)	46(3)	45(3)	50(4)	22(3)	30(3)	12(3)
C(2)	39(3)	44(3)	35(3)	-11(2)	26(3)	-6(2)
C(3)	48(3)	31(3)	39(3)	-5(2)	30(3)	0(2)
C(4)	42(3)	46(3)	26(3)	-6(2)	20(2)	1(2)
C(5)	54(3)	47(3)	29(3)	-3(2)	29(3)	-3(3)
C(6)	45(3)	37(3)	40(3)	-6(2)	30(3)	-6(2)
C(7)	39(3)	37(3)	38(3)	-10(2)	30(3)	-4(2)
C(8)	43(3)	23(2)	41(3)	-5(2)	30(3)	-1(2)
C(9)	41(3)	22(2)	46(3)	0(2)	28(3)	-5(2)
C(10)	48(3)	33(3)	49(3)	3(3)	36(3)	-2(2)
C(11)	53(4)	47(3)	52(4)	2(3)	27(3)	-12(3)
C(12)	35(4)	56(4)	87(6)	-1(4)	14(4)	11(3)
C(13)	35(3)	27(2)	30(3)	4(2)	18(2)	0(2)
C(14)	51(4)	53(4)	38(3)	0(3)	27(3)	-1(3)
C(15)	65(4)	84(5)	46(4)	16(3)	33(3)	4(4)
C(16)	119(8)	123(8)	50(5)	17(5)	34(5)	14(7)

Table S-5. Hydrogen coordinates (x 10^4) and isotropic displacement parameters ($Å^2$x 10^3) for **2**.

	x	y	z	U(eq)
H(2)	5000	3266	7500	39
H(1A)	8631	4512	9006	66
H(1B)	7733	3282	8448	66
H(1C)	7137	4080	8925	66
H(2A)	4785	4689	6083	43
H(2B)	4052	6003	5542	43
H(4)	5290	7206	5031	44
H(5)	7305	7607	4927	47
H(6)	9433	6683	5790	44
H(7)	9535	5379	6762	40
H(9A)	9130	-1158	7842	39
H(9B)	8588	-1180	6994	39
H(10A)	7059	-377	7566	46
H(10B)	7667	1160	7510	46
H(11A)	6202	-637	6299	60
H(11B)	6668	996	6280	60
H(12A)	4743	267	6809	97
H(12B)	4245	766	5996	97
H(12C)	5081	1863	6643	97
H(13A)	8705	1955	6775	36
H(13B)	10300	2193	6975	36
H(14A)	8683	-82	6048	54
H(14B)	10208	401	6185	54
H(15A)	7742	2162	5497	74
H(15B)	9256	2763	5693	74
H(16A)	9413	1209	4878	149
H(16B)	8029	2159	4486	149
H(16C)	7936	521	4702	149

References

(1) Jacob, J.; Guzei, I. A.; Espenson, J. H. *Inorg. Chem.* **1999**, *38*, 1040-1041.

(2) Jacob, J.; Lente, G.; Guzei, I. A.; Espenson, J. H. *Inorg. Chem.* **1999**, *38*, 3762-3763.

(3) Lente, G.; Guzei, I. A.; Espenson, J. H. *Inorg. Chem.* **2000**, *39*, 1311-1319.

(4) Wang, Y.; Espenson, J. H. *Organic Letters* **2000**, *2*, 3525.

(5) Lahti, D. W.; Espenson, J. H. *submitted for publication.*

(6) Herrmann, W. A.; Kratzer, R. M.; Fischer, R. W. *Angew. Chem., Int. Ed. Eng.* **1997**, *36*, 2652-2654.

(7) Mayer, J. M.; Tulip, T. H.; Calabrese, J. C.; Valencia, E. *J. Am. Chem. Soc.* **1987**, *109*, 157.

(8) Cotton, F. A.; Lu, J.; Huang, Y. *Inorg. Chem.* **1996**, 1839.

(9) Takacs, J.; Cook, M. R.; Kiprof, P.; Kuchler, J. G.; Herrmann, W. A. *Organometallics* **1991**, *10*, 316-320.

(10) Blackbourn, R. B.; Hupp, J. T. *Inorg. Chem.* **1989**, *28*, 3786.

(11) Cai, S.; Hoffman, D. M.; Huffman, J. C.; Wierda, D. A.; Woo, H.-G. *Inorg. Chem.* **1987**, *26*, 3693.

(12) Hoffman, D. M.; Wierda, D. A. *J. Am. Chem. Soc.* **1990**, *112*, 7056.

(13) Schmidt, -. B., B.; Abram, U. *Z. Anorg. Allg. Chem.* **2000**, *626*, 951.

(14) Huang, R.; Espenson, J. H. *submitted for publication.*

CHAPTER III. THE CHEMISTRY OF CHELATING PHOSPHORUS LIGANDS TO Re(V)

A paper to be published in *Inorganic Chemistry*

David W. Lahti and James H. Espenson

Introduction

Molecules containing two phosphorus atoms are of interest since they can often act as chelating ligands or as bridging ligands, which can link two metal centers so as to form binuclear complexes.[1,2] The ligands $Ph_2PCH_2PPh_2$ [bis(diphenylphosphino)methane] (or dppm) and $Ph_2P(CH_2)_2PPh_2$ [bis(diphenylphosphino)ethane] (or dppe) are two very popular bidentate ligands. Two similar derivatives, with less steric demands,[3] have the phenyl groups (Ph) replaced with methyl groups (Me) to form $Me_2PCH_2PMe_2$, dmpm, and $Me_2P(CH_2)_2PMe_2$, dmpe. Advantages of the dppm and dppe ligands is their low unit cost and less sensitivity to oxygen. These ligands are shown below.

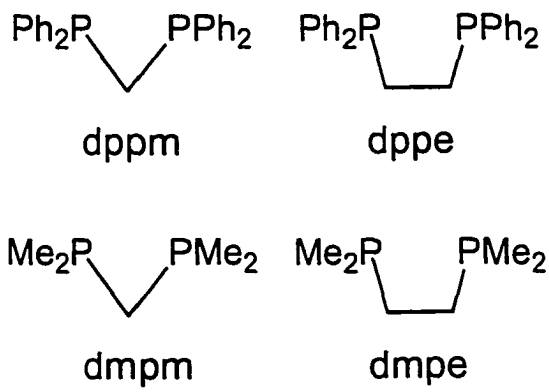

Actually, dppm is well known for bridging two metals in a complex, in fact often a pair of them will bridge two metals together, eq 1.[4] Also, dppe and dppm can act as monodentate ligands with one phosphorus bound to a metal, leaving one uncoordinated. An

example is shown, eq 2, along with the synthetic route, of monodentate binding.[5] These molecules can also chelate to a single metal center, to form a ring, a 4-membered one for dppm[6] and a 5-membered one for dppe.[7]

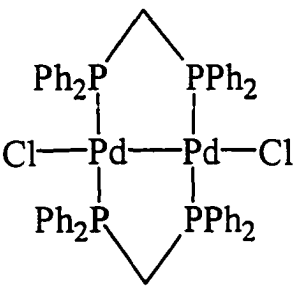

(1)

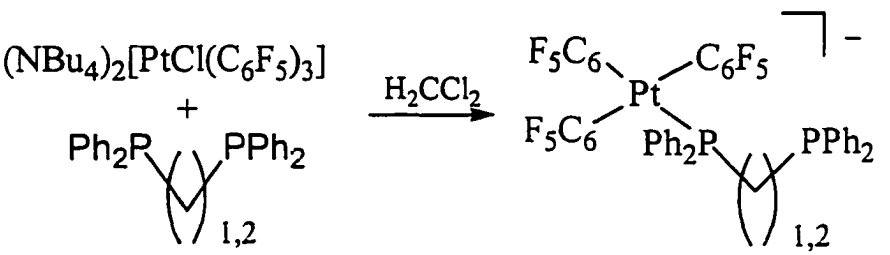

(2)

Given the 5-coordinate and dimeric structure of $\{CH_3(O)Re(mtp)\}_2$, **D**, where mtp is the dianion of 2-methylmercaptothiolphenol (H_2mtp), it is feasible to add a bidentate ligand to bridge these rhenium atoms together; each rhenium would become 6-coordinate. Typically, when **D** reacts with Lewis base ligands (L), such as phosphines or pyridines, to form two mononuclear $CH_3(O)Re(mtp)L$ or M–L complexes, the final product remains 5-coordinate. The reaction of **D** and PPh_3 is shown, eq 3. For monomerization not to occur,

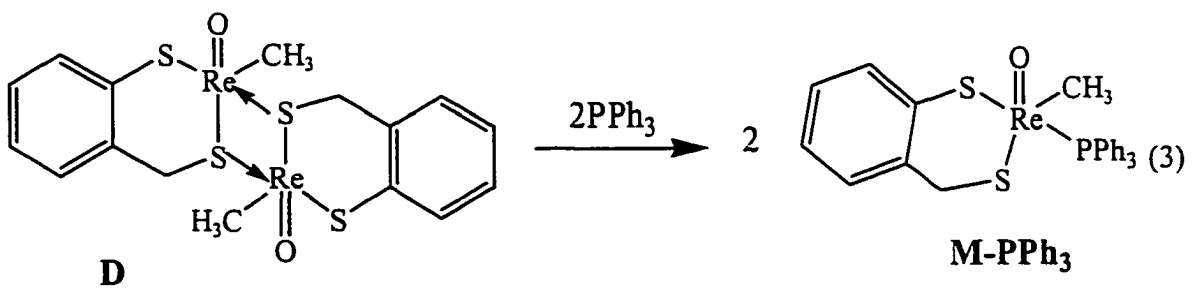

(3)

D **M-PPh$_3$**

the pair of Re–S must remain in tact. Reactions were performed with **D** and dppe and dppm, and also between the monomeric form, $CH_3ReO(mtp)(4\text{-}Bu^tC_5H_4N)$, formed from **D** and 4-*tert*-butylpyridine. These compounds are shown below.

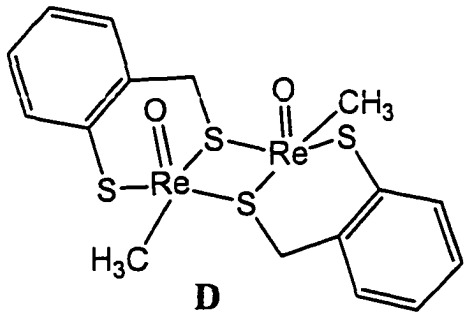

D

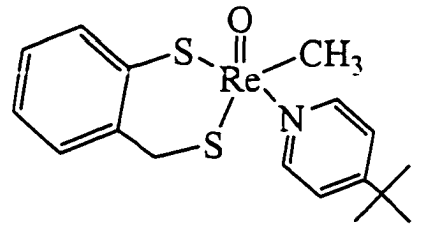

$MeReO(mtp)(4\text{-}Bu^tC_5H_4N)$

Experimental

Methyltrioxorhenium(VII), MTO, was prepared from sodium perrhenate according to a published procedure.[8] The dimeric complex $\{MeReO(mtp)\}_2$ as described previously from methyltrioxorhenium(VII) and 2-mercaptomethylthiolphenol ($mtpH_2$), reported earlier.[9] It was treated with ca. 10 fold excess pyridine to produce monomeric pyridine adducts. Solvents and reagents were purchased, and used as received. A Bruker DRX–400 spectrometer was used to record NMR spectra. Shimadzu 3101 and 2501 spectrophotometers were used for optical spectra. Most reactions were performed in C_6D_6.

Results

General Observations. When dppm and dppe are treated with yellow **D**, the solution rapidly turns green. Virtually the same green color formed when monodentate phosphines, such as PPh_3, reacts with **D**, see eq 3. These reactions are quite rapid, as the green color forms on mixing. Clearly, Re–P bonds are formed in both case, just as with PPh_3, the structure of which has been previously reported.[10]

Monomeric pyridine complexes, like $CH_3Re(O)(mtp)(4\text{-}tBuC_5H_4N)$, (M–tBuPy), can be treated with dppm and dppe as well. It has been shown that phosphorus donating ligands readily displace pyridine ligands.[10,11] The reactions with dppm give a single product, althought when **D** is used, there is evidence for an intermediate, but that species has not be identified. For dppe, the results are not completely clear, however, similarities exist in the spectra of the product whether **D** or M–tBuPy were used.

Reaction Stoichiometry. The reaction stoichiometry of **D** with these bidentate ligands is different. Each **D** reacts with two dppm molecules and just one dppe molecule, for a complete reaction. This was confirmed with ^1H NMR for dppm. For dppe the stoichiometry of the reaction was determined using Job's method of analysis.[12] This ratio of one dppe for every **D** molecule is confirmed by figure S-1. This plot shows a maximum value of absorbance at 1 mM **D**. Since the total concentration of dppe and **D** must always sum to 2 mM, [**D**] and [dppe] are equal at this point. This confirms the stoichiometry of 1:1, as under these conditions a maximum amount of product is formed, which absorbs more at this wavelength. Thus, each phosphorus from dppe binds to a rhenium atom; ^{31}P NMR studies show no chemical shifts that correspond to uncoordinated phosphorus atoms. Further, no evidence exists to support rhenium remaining 4-coordinate in these dithiolatorhenium(V) compounds, an ancillary ligand seems to always be necessary. For dppm, each takes one rhenium center and thus two binding modes are possible, η^1 or η^2.

NMR Studies. The ^1H & ^{31}P NMR studies for the dppm reactions are quite straight forward. The dppm ligand reacts with **D** to yield only one product, by ^1H NMR, whether **D** or M-tBuPy is used. The adduct formed $CH_3Re(O)(mtp)$dppm or M–dppm is similar to the $CH_3Re(O)(mtp)L$ or M–L type complexes that have been described in detail elsewhere,

especially when L = $MePh_2P$.[11] This is notable from the ^1H NMR data in table 1, for these complexes. The ^1H NMR is shown in figure 1.

This product, M-dppm, is found to have five NMR signals, accounting for seven protons, in the range from 2.8 - 5 ppm: two doublets from the methylene protons of the dithiolato ligand, one doublet peak attributable to the Re–Me resonance (split once by phosphorus - with three times the integration) and an A B quartet. The A B quartet signals can be assigned to the protons of the methylene bridge of dppm. Table 1 lists the ^1H NMR peaks along with coupling constants for M-dppm in C_6D_6 and in D_8C_7 and for M–$PMePh_2$ (in C_6D_6).

The ^{31}P NMR spectrum of M–dppm is shown in figure S-2. It is quite noticeable that the peaks are sharp, despite the fact that some excess free dppm is present. This data is

Table 1. ^1H NMR of dithiolato rhenium(V) complexes of dppm and $PMePh_2$.

	Compound (solvent)							
Group	M-dppm (C_6D_6)			M-dppm (C_7D_8)			M-$PMePh_2$ (C_6D_6)	
	δ	^1J (Hz)		δ	^1J (Hz)		δ	^1J (Hz)
		(H-H)	(P-H)		(H-H)	(P-H)		(H-H)
SCH_aH_bC[a]	4.86	11.2		4.80	11.2		4.88	11.6
SCH_aH_bC[a]	3.17	11.6		3.08	11.6		3.25	11.2
Re-CH_3[b]	2.92	8.4		2.81	8.4		2.77	8.8
PCH_cH_dP[c]	3.83	15.0	9	3.80	14.4	9		
PCH_cH_dP[c]	3.59	14.8	9	3.55	14.6	9		

a) doublet from diastereotopic hydrogen on a methylene group
b) doublet from phosphorus
c) one part of an A B quartet

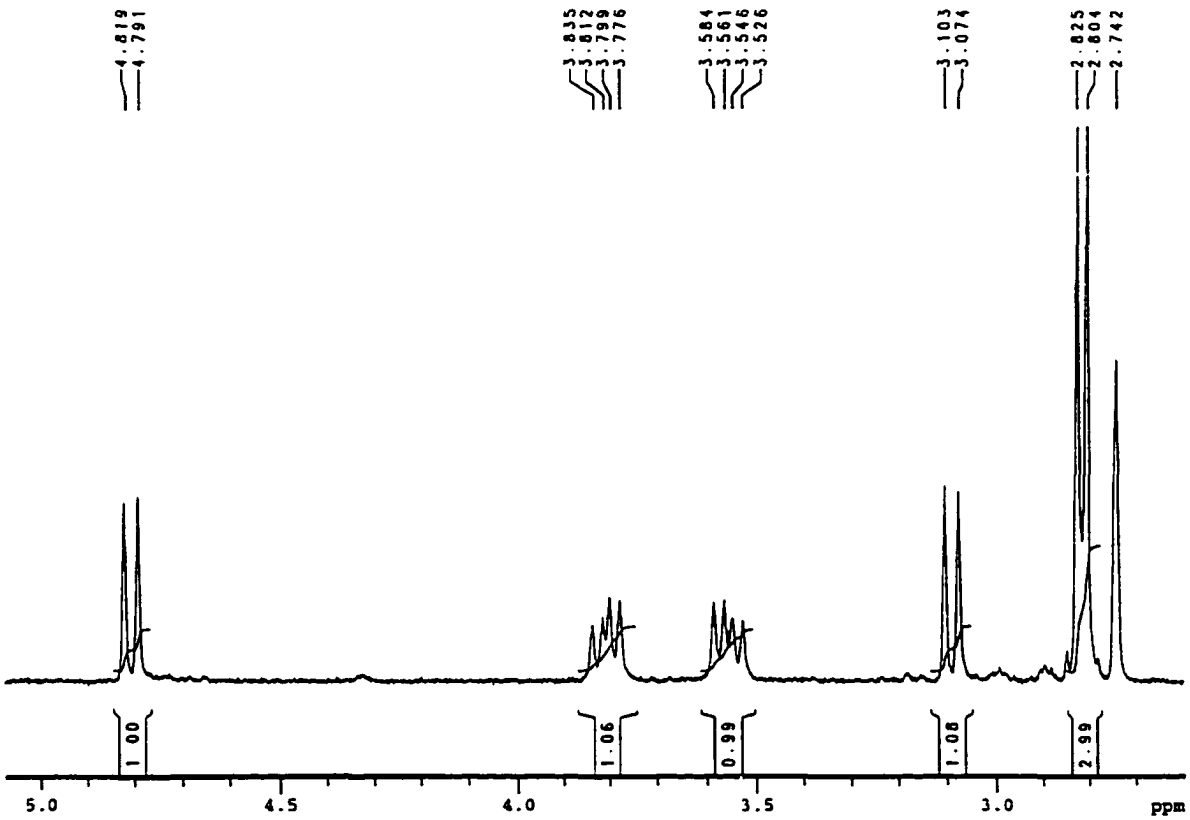

Figure 1. The ^{1}H NMR spectrum of M–(η^{1}–dppm) in C_7D_8 over the range from 2.6 to 5.1 ppm. The peaks are listed in table 1. The A B quartet is between 3.5 and 3.9 ppm and the peaks are described in table 1. The integration markers confirm seven protons, three of which are from a methyl group, and four from distinctly different single protons.

shown in table 2, for this compounds, as well as for some compounds with phoshorus ligands, most with dppm. The complex, M–dppm, has two doublets that are about 45 ppm apart; one for a free phosphorus and one for a bound phosphorus atom. A ^{31}P NMR spectrum without proton decoupling causes the doublet at -25 ppm (assigned to the uncoordinated phosphorus) to appear as a doublet of triplets. This shows that the protons of the dppm methylene protons are quite similar to each other, while curiously they don't cause noticeable coupling to the signal from the phosphorus atom bound to rhenium, at ca. 20 ppm.

To confirm which couplings originate from phosphorus, especially of the A B quartet, phosphorus decoupled ^{1}H NMR (^{1}H NMR $\{^{31}P\}$) was done. These experiments caused changes in the spectra, especially when the 20 ppm peak was decoupled, (the ^{31}P NMR signal assigned the coordinated phosphorus of dppm). Figure S-3 shows the result from this ^{1}H $\{^{31}P\}$ NMR experiment, and it is clear the A B quartet has less coupling, and the doublet of the Re-CH_3 resonance is now a singlet, further confirming that the methyl group on rhenium is a doublet from a bound phosphorus atom. When the peak at -25 ppm is decoupled, the signal from the dppm protons, while broader now, still shows the same coupling features, figure S-4. This indicates that the uncoordinated phosphorus is not causing coupling. Moving the decoupling further upfield to -150 ppm, figure S-5, yields ^{1}H NMR spectra quite similar to that of figure 1, the one with no decoupling at all.

Isomerization. When M–tBuPy is used as a source of rhenium, there are actually two isomers present, as determined by ^{1}H NMR; one form is quite minor (about 10%). However, when these react with dppm, only one product is formed. Thus, despite lack of mechanistic and kinetics studies, there is likely an intermediate at work here, given the

Table 2. ^{31}P NMR shifts for various phosphorus containing species.

Complex	^{31}P NMR ppm	^{1}J(P-P) Hz	reference
Me(O)Re(mtp)(dppm)[a]	19.99 -25.26	64 65	this report
Me(O)Re(mtp)(dppm)[b]	19.93 -25.12	66 66	this report
Me(O)Re(mtp)($PMePh_2$)	12.6[c]	0	#8
$[(F_5C_6)_3Pt(\eta^1$-dppm)]$^-$	6.60 -28.83	47 47	#5
$[(F_5C_6)_3Pt(\eta^1$-dppe)]$^-$	8.58 -12.89	35 35	#5
dppm (free)[a]	-21.5		this report

a) C_6D_6
b) D_8C_7
c) singlet (no coupling)

results found previously for ligand exchange reaction with these dithiolatorhenium(V) compounds.[11]

A bridging adduct, with dppe. The results from ^{1}H NMR experiments of the dppe reactions, while not difficult to explain, do not offer as much help in assigning a firm structure to the product, figure S-6. The ^{1}H NMR shows two sets of peaks that can be assigned to the Re–CH_3 group and two sets of doublets, one around 5 ppm and one around 3.3 ppm, figure S-5. The peaks assigned to the Re–CH_3 have an unusual triplet type shape, and are considered to be "virtually coupled" with the phosphorus atoms of dppe bridging the rhenium centers.[13] These peaks are often variable as to which peak is larger. The peaks at 3.0 and 4.7 ppm each look like two doublet that are nearly similar in chemical shift value,

albeit the one at 3.0 ppm is superimposed on many multiplets that could originate from the carbon backbone (C_2H_4) of dppe.

Iron containing phosphorus chelate. During this work, another ligand 1,1' -bis(diphenylphosphino)-ferrocene, **1**, was reacted with **D** as well. In this reaction, too, there was a bright green color formed. The material was difficult to isolate in crystalline form. However, a molecular structure of this iron containing ligand was determined. This information can be found in the supplemental material. Tables of crystal data and structure refinement, atomic coordinates, bond lengths and angles, anisotopic displacement factors and hydrogen coordinates are given in tables S–1-to-5, respectively, in the supplemental material.

Discussion

All evidence from the reactions involving dppm suggests that it binds to [Me(O)Re(mtp)] in a monodentate fashion, eq 4, regardless of whether rhenium is initially in a dimeric form, **D**, or monomeric, M–tBuPy. The spectroscopic feartures of the sole product do not depend on which source of rhenium is used. The ^{31}P NMR spectra shows two doublet peaks that are about 45 ppm apart, one of which is quite close to the chemical shift of the free ligand. This is the case with other monodentate complexes of dppm, table 2, and thus strengthens our interpretation. The ^{1}H NMR spectrum has features like other five-coordinate complexes, based on Me(O)Re(mtp) like M–$PMePh_2$, table 1. Thus the best way to represent this product is Me(O)Re(mtp)(η^1–dppm) or M–(η^1–dppm). The M–$PMePh_2$ compound was found to have the ancillary ligand trans to the phenolic sulfur, and since its chemical shift is similar to M–(η^1–dppm), that structure is reasonable.

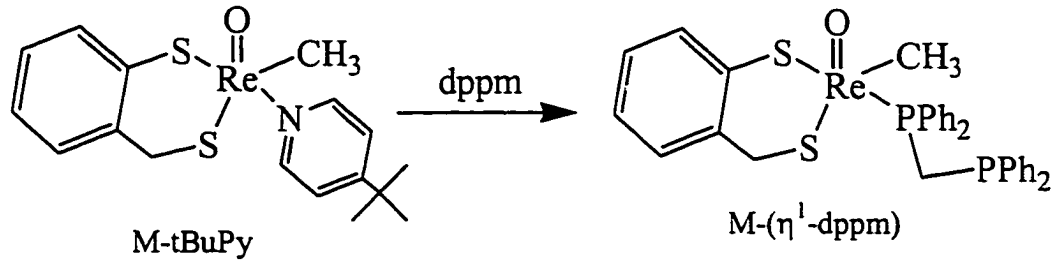

(4)

While the reaction above is shown without an intermediate, that can not be assumed. In fact, an intermediate is likely, given the information collection of ligand exchange reactions on these complexes.[11] The minor form, M–tBuPy*, likely directly gives M–(η¹–dppm), whereas the major form, M–tBuPy may first yield the intermediate species, M–(η¹–dppm)*, eq 5. Then M–(η¹–dppm)* would have to rearrange to form M–(η¹–dppm), eq 6. However, this is curious since when M–tBuPy solutions (containing both isomers) are treated with bipyridines, two products are formed, and their ratio appears static.[11] In this case, the product ratio happens to match that of the starting materials, M–tBuPy and M–tBuPy*.

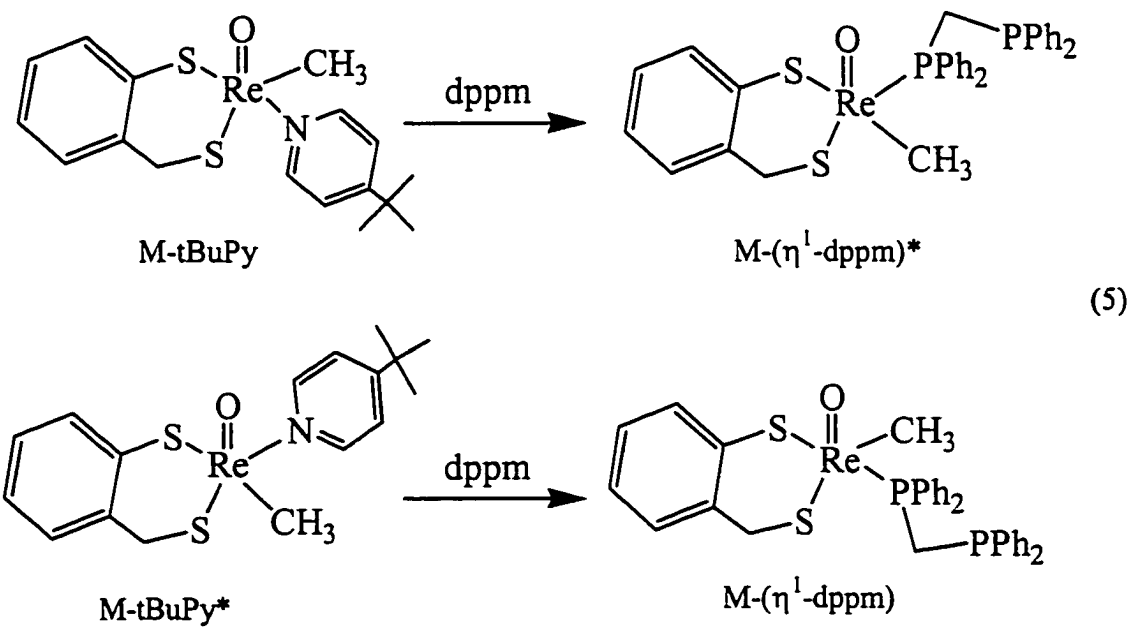

(5)

The peaks from the methylene unit of dppm, of the M–(η^1–dppm) product, are interesting in that only the coordinated phosphorus causes spliting to these protons. It is possible that the other phosphorus couples only very weakly and its coupling is not observed. Figure S-3 shows more clearly the A B quartet, which now solely has coupling attributed to the hydrogen atoms, as the coupling from phosphorus is gone. Since the decoupling window is not so wide, going further upfield for selected decoupling frequencies, revealed a pair of a spectra where the coupling from the bound phosphorus still appeared, figures S-3 and S-4. This shows that the uncoordinated phosphorus does not significantly couple anything.

The results for the **D** and dppe reaction show that each phosphorus atom has a rhenium atom bound to it; there are two Re–P bonds created. Indeed, a bridging molecule is supported with the results from Job's method of analysis. Again, one dimer (with two Re atoms) reacts with one dppe molecule. The structure however cannot be reasonably be interpreted from the ^{1}H NMR for two reasons. The first reason is that the pair of chemical shifts assigned to methyl groups suggests two inequivalent structure around rhenium, perhaps the M–L / M–L* configuration could be important; one rhenium taking each form. However, when M–L / M–L* type configurations are observed, the chemical shift from the methylene protons, from the mtp ligand, are greatly different than that of the M–L complex, table 3.[11] The fact that at about 4.7 and 3.0 ppm two pair of doublets appear with nearly the same chemical shift does not work to strengthen this argument. The multiplet peaks at about 3 ppm are attributable to the C_2H_4 backbone of dppe. Certainly, the most unusual feature is the shape of the methyl resonances, they look something like a triplet. They are considered to be "virtually coupled," something reasonably attributable to a bridging dppe complex.[13]

Table 3. The chemical shift of the methylene protons on the mtp ligand of MeReO(mtp)L compounds.

Chemical shifts (ppm) for CH_2 of mtp				
ligand (L)	M-L		M-L*	
$PCyPh_2$	4.90	3.13	5.10[a]	4.80
4-$Bu^tC_5H_4N$	4.79	3.78	5.21	4.89
dppe	4.75 4.78	3.02 3.05		

a) doublet of doublets, all other peaks doublets

The structure of the iron containing phosphorus complex was found to have the cyclopentadienyl rings in a position such that the phosphorus units are 180 degrees apart. When 1 was treated with **D**, there was a bright green color formed. Clearly, Re–P bonds are made. The structure however, is not known.

Overall, the results from this work is interesting, with some of the results more difficult to interpret than others, there remains opportunity here to study these systems more, especially in light of the new mechanism proposed involving a 'turnstile' type movement of ligands.[11] Kinetics and mechanistic studies may reveal how these reaction procede, and how the following reaction, eq 6, occurs. It would be important to know whether this reaction occurs via an *intra* or *inter* molecular rearrangement.

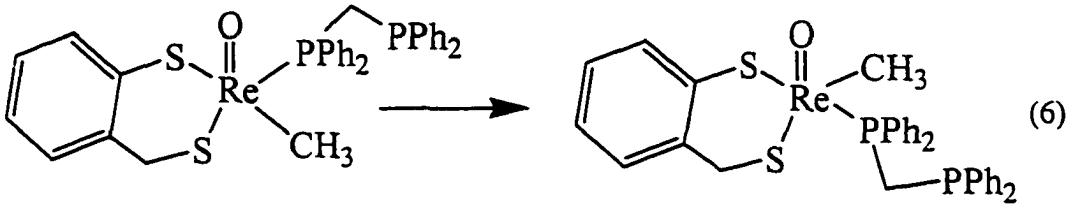

(6)

Acknowledgment

This research was supported by a grant from the National Science Foundation. Some experiments were conducted with the facilities of the Ames Lab.

Supporting Information

Complete tables of the crystal data and refinement details, atomic coordinates, molecular structure with the cation, bond lengths and angles, and anisotropic displacement parameters.

Supporting Information

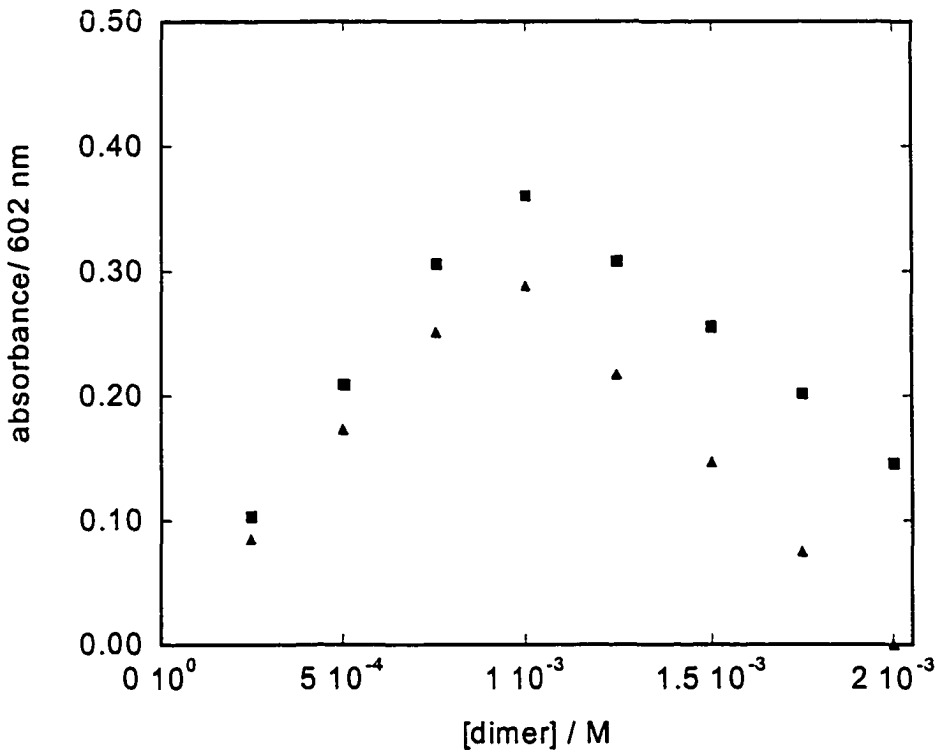

Figure S-1. A Job's method plot for the reaction of **D** and dppe. The absorbance at 602 nm versus the concentration of the dimer, **D**, where the sum of the concentration of the **D** and the ligand is 2 mM. The actual absorbance values, squares, and the corrected values, triangles, both show the peak to be at 1 mM.

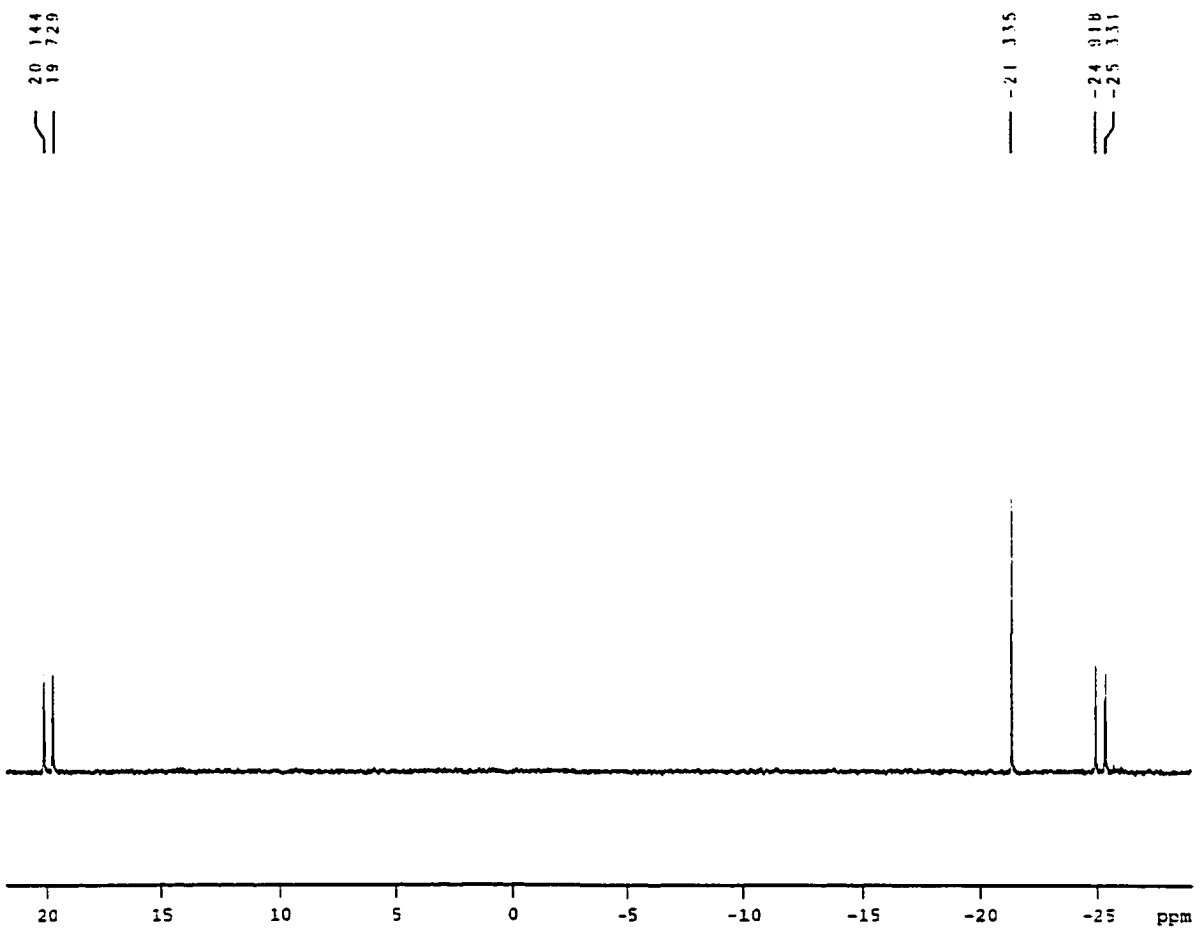

Figure S-2. The ^{31}P NMR spectrum of M–(η^1–dppm) in C_7D_8. The pair of doublets are assigned to each P of dppm, one bound and one free. The singlet for some excess free dppm. All of the peaks are sharp.

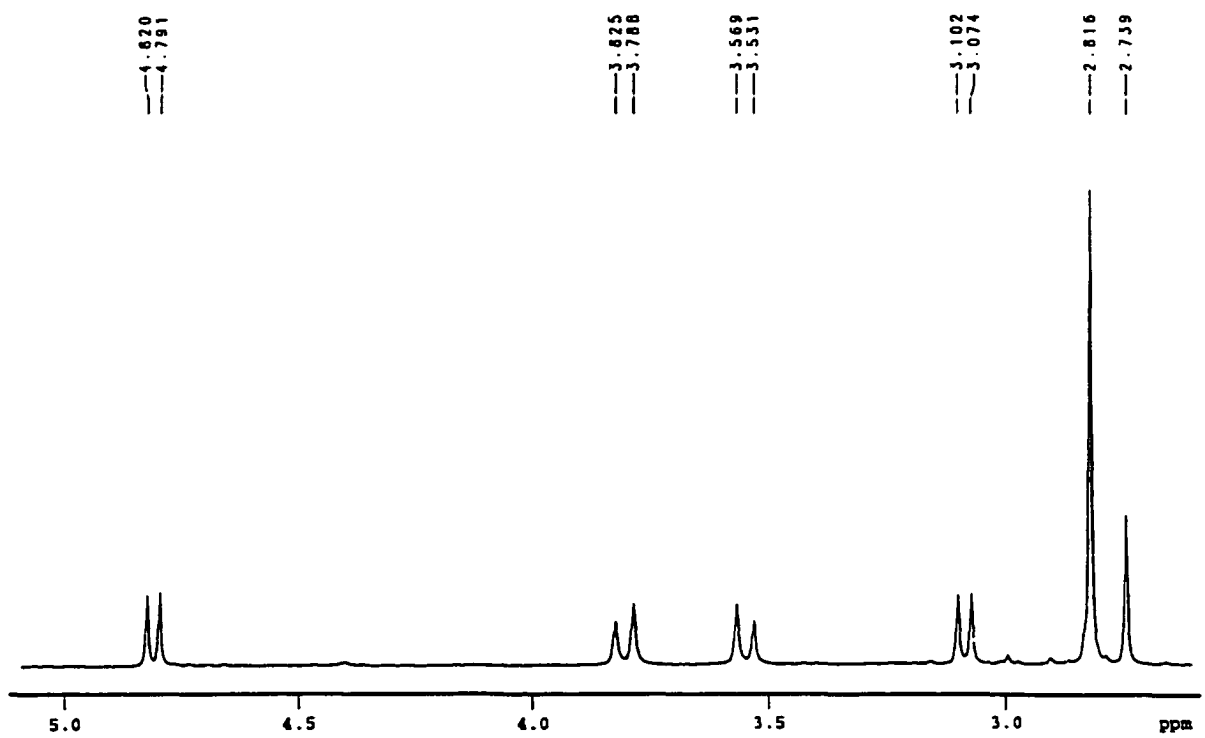

Figure S-3. The ^{1}H NMR $\{^{31}P\}$ spectrum of M–(η^{1}–dppm) in C_7D_8 over the range of about 2.6 to 5.1 ppm. The peaks are described in table 1, and the decoupling is now set at 20 ppm. It is of particular interest that the coupling to the phosphorus at 20 ppm, in ^{31}P NMR, causes certain couplings to disappear.

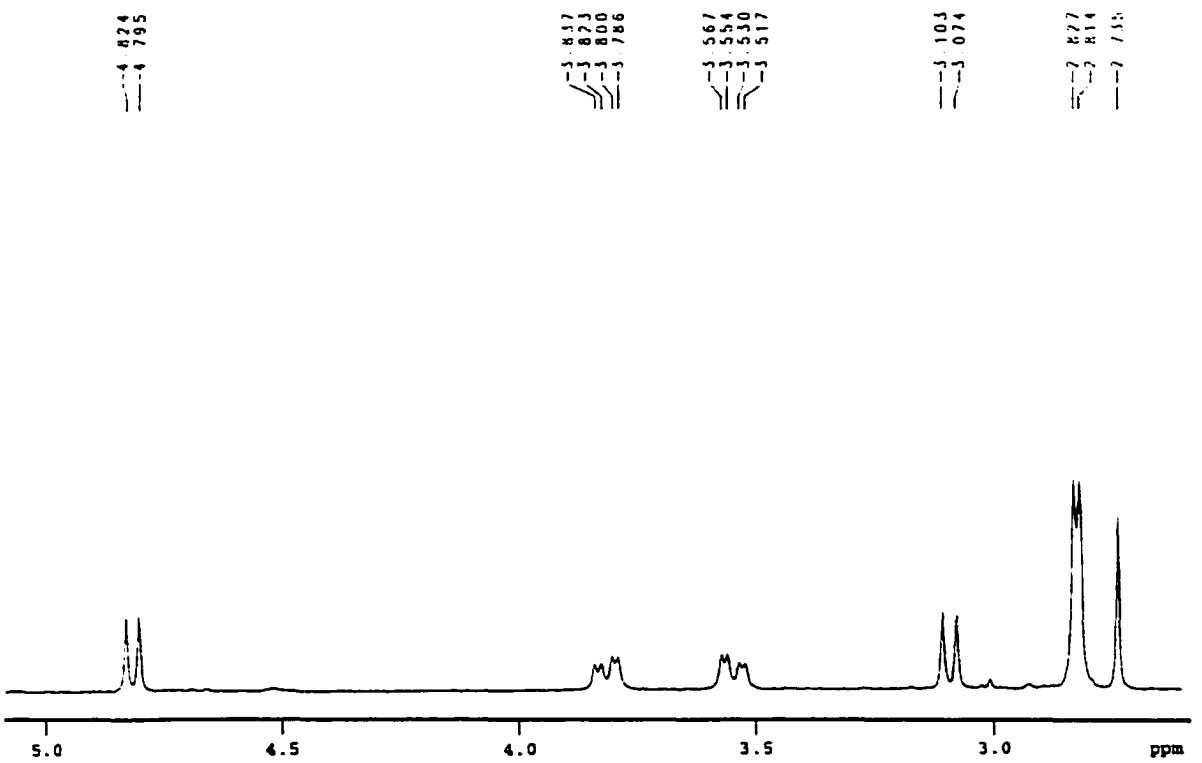

Figure S-4. The ^{1}H NMR $\{^{31}P\}$ spectrum of M–(η^{1}–dppm) in C_7D_8 over the range of about 2.6 to 5.1 ppm. The decoupling is now set at -25 ppm, the chemical shift corresponding to the free phosphorus atom of dppm.

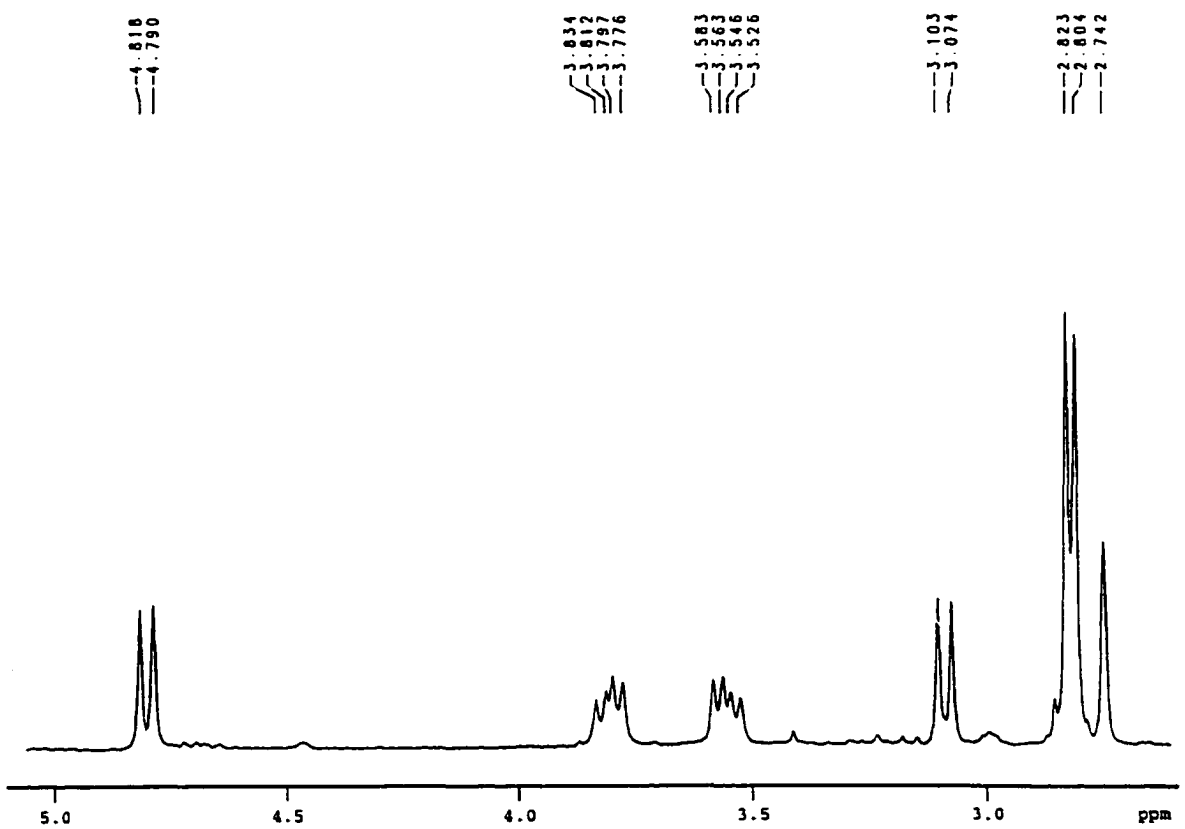

Figure S-5. The ^{1}H NMR $\{^{31}P\}$ spectrum of M–(η^{1}–dppm) in C_7D_8 over the range of about 2.6 to 5.1 ppm. The decoupling is now set at -150 ppm. This spectrum looks similar to figure 1, where there has been no decoupling at all.

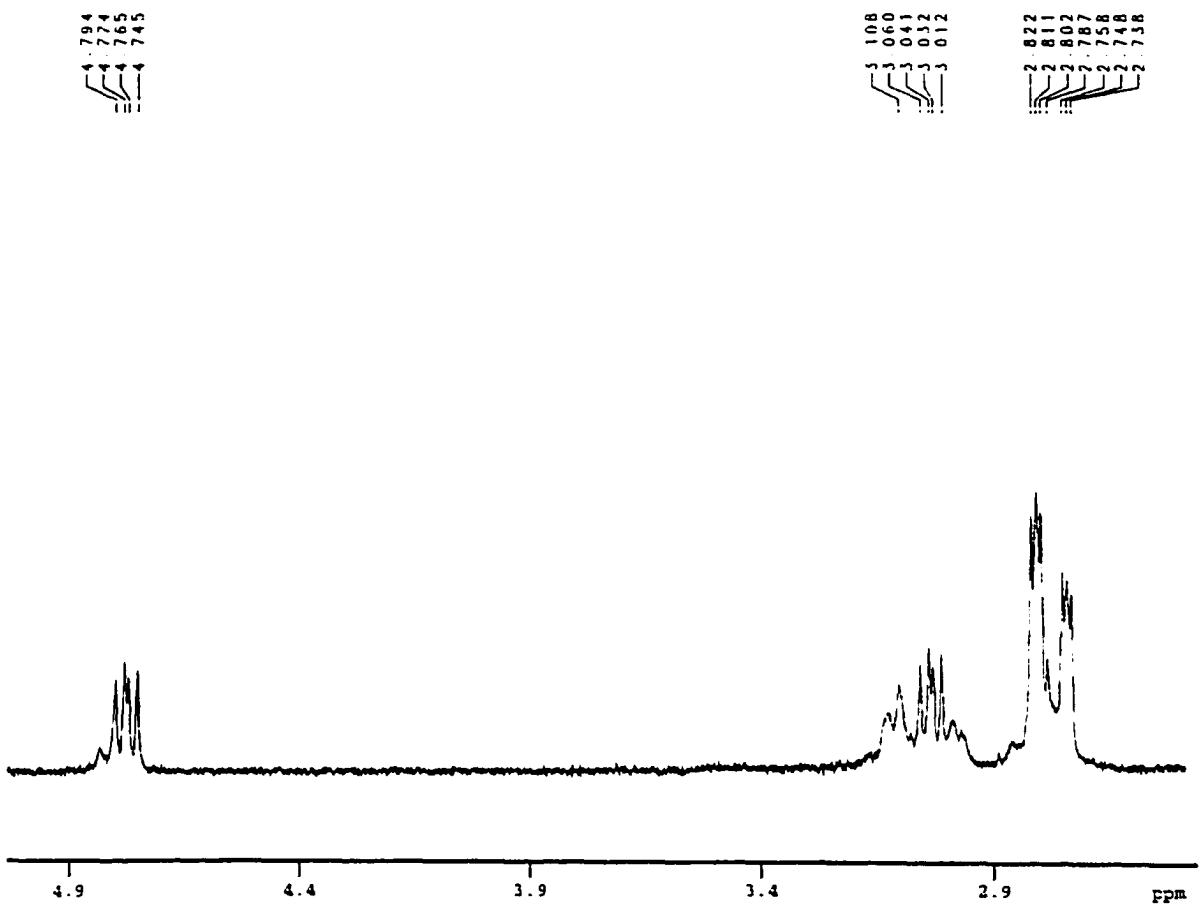

Figure S-6. The ^{1}H NMR $\{^{31}P\}$ spectrum of the result of M-tBuPy and dppe mixed in C_7D_8, over the range of about 2.5 to 5.0 ppm.

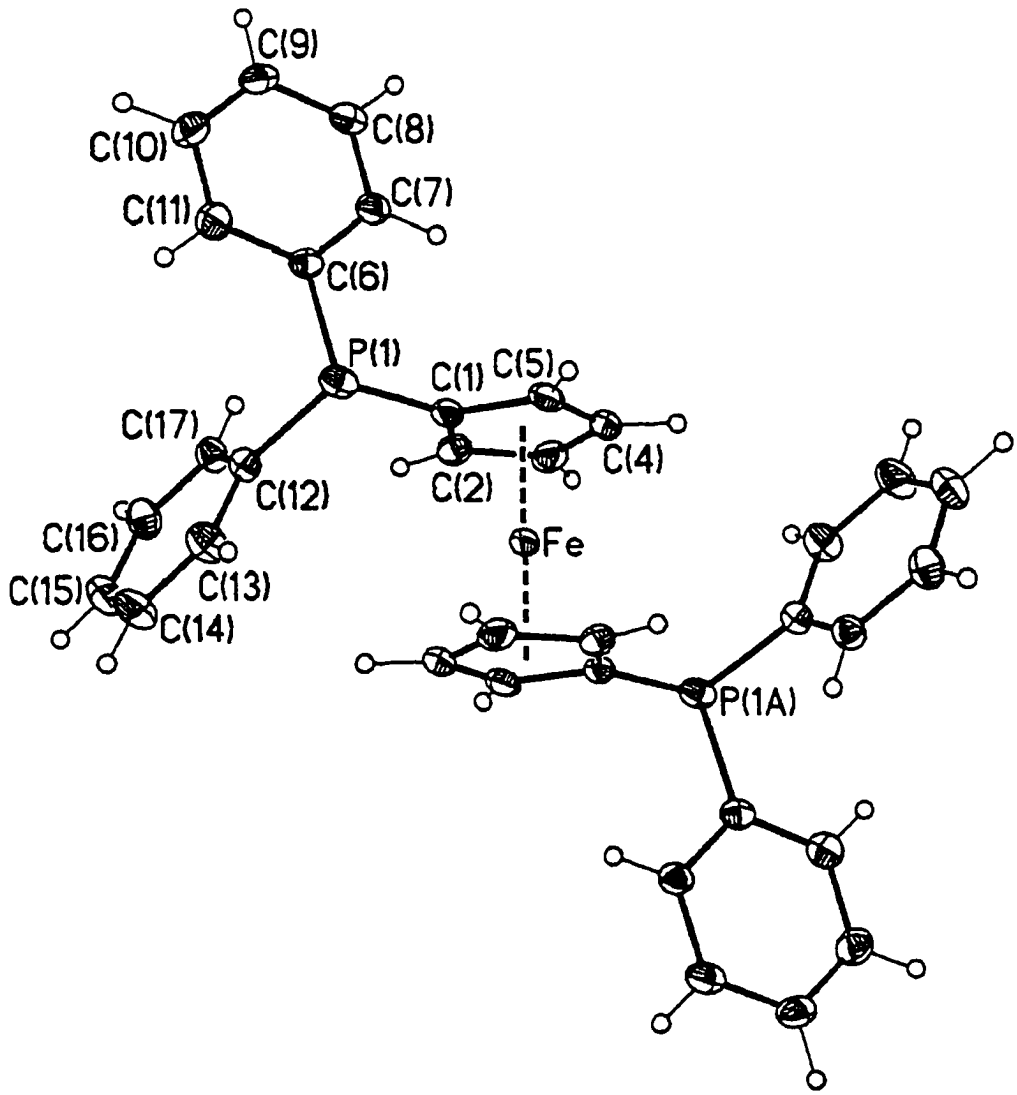

Figure S-7. The molecular structure of 1 drawn with 30% probability elipsoids.

Table S-1. Crystal data and structure refinement for 1.

Empirical formula	$C_{34}H_{28}FeP_2$	
Formula weight	554.35	
Temperature	173(2) K	
Wavelength	0.71073 Å	
Crystal system	Monoclinic	
Space group	$P2_1/c$	
Unit cell dimensions	a = 8.6260(8) Å	α= 90°
	b = 18.4753(17) Å	β= 101.448(2)°
	c = 8.6909(8) Å	γ = 90°
Volume	1357.5(2) $Å^3$	
Z	2	
Density (calculated)	1.356 Mg/m^3	
Absorption coefficient	0.695 mm^{-1}	
F(000)	576	
Crystal size	0.35 x 0.30 x 0.30 mm^3	
Theta range for data collection	2.20 to 26.37°.	
Index ranges	-10<=h<=10, 0<=k<=23, 0<=l<=10	
Reflections collected	8070	
Independent reflections	2767 [R(int) = 0.0247]	
Completeness to theta = 26.37°	99.9 %	
Absorption correction	Empirical with SADABS	
Max. and min. transmission	0.8186 and 0.7929	
Refinement method	Full-matrix least-squares on F^2	
Data / restraints / parameters	2767 / 0 / 169	
Goodness-of-fit on F^2	1.024	
Final R indices [I>2sigma(I)]	R1 = 0.0348, wR2 = 0.0940	
R indices (all data)	R1 = 0.0516, wR2 = 0.0999	
Largest diff. peak and hole	0.538 and -0.239 $e.Å^{-3}$	

Table S-2. Atomic coordinates (x 10^4) and equivalent isotropic displacement parameters ($Å^2$x 10^3) for 1. U(eq) is defined as one third of the trace of the orthogonalized U^{ij} tensor.

	x	y	z	U(eq)
Fe	0	5000	5000	36(1)
P(1)	1137(1)	3643(1)	7726(1)	35(1)
C(1)	1122(2)	4576(1)	7088(2)	34(1)
C(2)	166(3)	5179(1)	7343(2)	37(1)
C(3)	688(3)	5801(1)	6631(3)	48(1)
C(4)	1966(3)	5589(2)	5938(3)	54(1)
C(5)	2248(3)	4843(2)	6197(3)	47(1)
C(6)	2152(2)	3746(1)	9784(2)	31(1)
C(7)	3107(2)	4336(1)	10312(3)	34(1)
C(8)	3951(2)	4373(1)	11840(3)	41(1)
C(9)	3861(3)	3818(1)	12874(3)	45(1)
C(10)	2905(3)	3228(1)	12372(3)	46(1)
C(11)	2077(3)	3186(1)	10846(3)	42(1)
C(12)	-906(2)	3478(1)	7930(2)	33(1)
C(13)	-1818(3)	2998(1)	6899(3)	45(1)
C(14)	-3391(3)	2869(1)	6969(3)	53(1)
C(15)	-4062(3)	3214(1)	8081(3)	48(1)
C(16)	-3156(3)	3676(1)	9138(3)	43(1)
C(17)	-1597(3)	3810(1)	9067(3)	36(1)

Table S-3. Bond lengths [Å] and angles [°] for 1.

Fe-C(5)	2.031(2)
Fe-C(5)#1	2.031(2)
Fe-C(1)#1	2.036(2)
Fe-C(1)	2.036(2)
Fe-C(2)#1	2.040(2)
Fe-C(2)	2.040(2)
Fe-C(4)	2.044(2)
Fe-C(4)#1	2.044(2)
Fe-C(3)	2.053(2)
Fe-C(3)#1	2.053(2)
P(1)-C(1)	1.811(2)
P(1)-C(12)	1.831(2)
P(1)-C(6)	1.839(2)
C(1)-C(2)	1.429(3)
C(1)-C(5)	1.444(3)
C(2)-C(3)	1.419(3)
C(3)-C(4)	1.412(4)
C(4)-C(5)	1.411(4)
C(6)-C(7)	1.388(3)
C(6)-C(11)	1.397(3)
C(7)-C(8)	1.384(3)
C(8)-C(9)	1.375(3)
C(9)-C(10)	1.385(3)
C(10)-C(11)	1.378(3)
C(12)-C(13)	1.389(3)
C(12)-C(17)	1.393(3)
C(13)-C(14)	1.391(3)
C(14)-C(15)	1.378(4)
C(15)-C(16)	1.377(3)
C(16)-C(17)	1.381(3)
C(5)-Fe-C(5)#1	180.0
C(5)-Fe-C(1)#1	138.41(9)
C(5)#1-Fe-C(1)#1	41.59(9)
C(5)-Fe-C(1)	41.59(9)
C(5)#1-Fe-C(1)	138.41(9)
C(1)#1-Fe-C(1)	180.0
C(5)-Fe-C(2)#1	111.03(10)
C(5)#1-Fe-C(2)#1	68.97(10)
C(1)#1-Fe-C(2)#1	41.05(9)
C(1)-Fe-C(2)#1	138.95(9)

Table S-3 continued

C(5)-Fe-C(2)	68.97(10)
C(5)#1-Fe-C(2)	111.03(10)
C(1)#1-Fe-C(2)	138.95(9)
C(1)-Fe-C(2)	41.05(9)
C(2)#1-Fe-C(2)	180.000(1)
C(5)-Fe-C(4)	40.50(10)
C(5)#1-Fe-C(4)	139.50(10)
C(1)#1-Fe-C(4)	111.13(9)
C(1)-Fe-C(4)	68.87(9)
C(2)#1-Fe-C(4)	111.90(10)
C(2)-Fe-C(4)	68.10(10)
C(5)-Fe-C(4)#1	139.50(10)
C(5)#1-Fe-C(4)#1	40.50(10)
C(1)#1-Fe-C(4)#1	68.87(9)
C(1)-Fe-C(4)#1	111.13(9)
C(2)#1-Fe-C(4)#1	68.10(10)
C(2)-Fe-C(4)#1	111.90(10)
C(4)-Fe-C(4)#1	180.00(14)
C(5)-Fe-C(3)	68.50(11)
C(5)#1-Fe-C(3)	111.50(11)
C(1)#1-Fe-C(3)	111.08(9)
C(1)-Fe-C(3)	68.92(9)
C(2)#1-Fe-C(3)	139.43(9)
C(2)-Fe-C(3)	40.57(9)
C(4)-Fe-C(3)	40.32(11)
C(4)#1-Fe-C(3)	139.68(11)
C(5)-Fe-C(3)#1	111.50(11)
C(5)#1-Fe-C(3)#1	68.50(11)
C(1)#1-Fe-C(3)#1	68.92(9)
C(1)-Fe-C(3)#1	111.08(9)
C(2)#1-Fe-C(3)#1	40.57(9)
C(2)-Fe-C(3)#1	139.43(9)
C(4)-Fe-C(3)#1	139.68(11)
C(4)#1-Fe-C(3)#1	40.32(11)
C(3)-Fe-C(3)#1	180.00(10)
C(1)-P(1)-C(12)	103.85(10)
C(1)-P(1)-C(6)	99.90(9)
C(12)-P(1)-C(6)	101.80(10)
C(2)-C(1)-C(5)	106.7(2)
C(2)-C(1)-P(1)	131.63(17)
C(5)-C(1)-P(1)	121.63(19)

Table S-3 continued

C(2)-C(1)-Fe	69.62(12)
C(5)-C(1)-Fe	69.03(12)
P(1)-C(1)-Fe	127.75(11)
C(3)-C(2)-C(1)	108.7(2)
C(3)-C(2)-Fe	70.22(13)
C(1)-C(2)-Fe	69.33(12)
C(4)-C(3)-C(2)	107.7(2)
C(4)-C(3)-Fe	69.49(15)
C(2)-C(3)-Fe	69.21(13)
C(5)-C(4)-C(3)	109.1(2)
C(5)-C(4)-Fe	69.26(13)
C(3)-C(4)-Fe	70.19(13)
C(4)-C(5)-C(1)	107.8(2)
C(4)-C(5)-Fe	70.23(13)
C(1)-C(5)-Fe	69.38(12)
C(7)-C(6)-C(11)	117.7(2)
C(7)-C(6)-P(1)	122.69(17)
C(11)-C(6)-P(1)	119.39(16)
C(8)-C(7)-C(6)	121.4(2)
C(9)-C(8)-C(7)	120.2(2)
C(8)-C(9)-C(10)	119.3(2)
C(11)-C(10)-C(9)	120.6(2)
C(10)-C(11)-C(6)	120.8(2)
C(13)-C(12)-C(17)	118.1(2)
C(13)-C(12)-P(1)	118.45(17)
C(17)-C(12)-P(1)	123.42(16)
C(12)-C(13)-C(14)	120.9(2)
C(15)-C(14)-C(13)	120.0(2)
C(16)-C(15)-C(14)	119.5(2)
C(15)-C(16)-C(17)	120.6(2)
C(16)-C(17)-C(12)	120.7(2)

Symmetry transformations used to generate equivalent atoms:
#1 -x,-y+1,-z+1

Table S-4. Anisotropic displacement parameters ($Å^2 x\ 10^3$) for **1**. The anisotropic displacement factor exponent takes the form: $-2\pi^2[\ h^2\ a^{*2}U^{11} + ... + 2\ h\ k\ a^*\ b^*\ U^{12}\ ]$

	U^{11}	U^{22}	U^{33}	U^{23}	U^{13}	U^{12}
Fe	29(1)	53(1)	23(1)	1(1)	0(1)	-14(1)
P(1)	30(1)	40(1)	34(1)	-10(1)	6(1)	0(1)
C(1)	28(1)	48(1)	23(1)	-2(1)	1(1)	-7(1)
C(2)	41(1)	45(1)	23(1)	-4(1)	2(1)	-4(1)
C(3)	57(2)	46(2)	33(1)	3(1)	-11(1)	-15(1)
C(4)	44(1)	74(2)	37(1)	13(1)	-10(1)	-33(1)
C(5)	26(1)	80(2)	32(1)	0(1)	0(1)	-13(1)
C(6)	26(1)	34(1)	34(1)	-2(1)	4(1)	7(1)
C(7)	28(1)	39(1)	36(1)	0(1)	5(1)	2(1)
C(8)	30(1)	49(2)	41(1)	-3(1)	1(1)	-1(1)
C(9)	36(1)	57(2)	37(1)	4(1)	-2(1)	9(1)
C(10)	44(1)	47(2)	45(1)	14(1)	4(1)	9(1)
C(11)	40(1)	35(1)	49(1)	0(1)	5(1)	2(1)
C(12)	31(1)	32(1)	36(1)	-2(1)	6(1)	0(1)
C(13)	45(1)	45(1)	46(1)	-16(1)	11(1)	-5(1)
C(14)	44(1)	52(2)	60(2)	-13(1)	5(1)	-18(1)
C(15)	34(1)	43(2)	67(2)	0(1)	12(1)	-8(1)
C(16)	41(1)	41(1)	51(1)	-2(1)	19(1)	-1(1)
C(17)	36(1)	37(1)	36(1)	-5(1)	8(1)	-5(1)

Table S-5. Hydrogen coordinates (x 10^4) and isotropic displacement parameters ($Å^2$ x 10^3) for **1**.

	x	y	z	U(eq)
H(2)	-732	5164	7914	44
H(3)	225	6297	6612	58
H(4)	2558	5914	5336	65
H(5)	3083	4551	5833	56
H(7)	3183	4722	9610	41
H(8)	4595	4783	12175	49
H(9)	4448	3840	13921	53
H(10)	2819	2848	13087	55
H(11)	1448	2771	10513	50
H(13)	-1361	2754	6135	54
H(14)	-4003	2543	6249	63
H(15)	-5142	3134	8119	57
H(16)	-3609	3905	9924	52
H(17)	-988	4131	9801	43

References

(1) Cotton, F. A.; Wilkinson, G. *Advanced Inorganic Chemistry*; 5th ed., 1988.

(2) Fujita, K.-i.; Hamada, T.; Yamaguchi, R. *J. Chem. Soc., Dalton Trans.* **2000**, 1931.

(3) Kullberg, M. L.; Lemke, F. R.; Powell, D. R.; Kubiak, C. P. *Inorg. Chem.* **1985**, *24*, 3589.

(4) Brown, M. P.; Puddephatt, R. J.; Rashidi, M.; Seddon, K. R. *J. Chem. Soc., Dalton Trans.* **1977**, 951.

(5) Uson, R.; Fornies, J.; Tomas, M.; Fandos, R. *Journal of Organometallic Chemistry* **1984**, *262*, 253-260.

(6) Winter, R. F.; Hornung, F. M. *Organometallics* **1999**, *18*, 4005.

(7) Wicht, D. K.; Kourkine, I. V.; Kovacik, I.; Glueck, D. S.; Concolino, T. E.; Yap, G. P. A.; Incarvito, C. D.; Rheingold, A. L. *Organometallics* **1999**, *18*, 5381-5394.

(8) Herrmann, W. A.; Kratzer, R. M.; Fischer, R. W. *Angew. Chem., Int. Ed. Eng.* **1997**, *36*, 2652-2654.

(9) Jacob, J.; Guzei, I. A.; Espenson, J. H. *Inorg. Chem.* **1999**, *38*, 1040-1041.

(10) Lente, G.; Guzei, I. A.; Espenson, J. H. *Inorg. Chem.* **2000**, *39*, 1311-1319.

(11) Lahti, D. W.; Espenson, J. H. *submitted for publication.*

(12) Jones, M. M. *Elementary Coordination Chemistry*; Prentice-Hall, Inc.:, 1964.

(13) Verkade, J. G. *Private Communication.*

CHAPTER IV. THE OXIDATION OF SULFOXIDES BY HYDROGEN PEROXIDE, CATALYZED BY METHYLTRIOXORHENIUM(VII)

A paper published in *Inorganic Chemistry*

David W. Lahti and James H. Espenson*

Abstract

Dialkyl- and diarylsulfoxides are oxidized to sulfones by hydrogen peroxide using methyltrioxorhenium as the catalyst. The reaction rate is negligible without a catalyst. The kinetics study was performed in CH_3CN–H_2O (4:1 v/v) at 298 K with $[H^+]$ at 0.1 M, conditions which make the equilibration between MTO and its peroxo complexes more rapid than the oxygen-transfer step. The values for the rate constant for the oxygen-transfer step lie in the range 0.1-3 $L\ mol^{-1}\ s^{-1}$. The rate constants were significantly smaller than for the oxidation of sulfides to sulfoxides. A study of ring-substituted diaryl sulfoxides yielded kinetics results that are consistent with nucleophilic attack of the sulfur atom on the peroxide oxygen group since $\rho = -0.65$. The results cited refer to the reactions of the diperoxo from of the catalyst, $CH_3Re(O)(\eta^2\text{-}O_2)_2H_2O$. The monoperoxo complex showed no measurable reactivity towards sulfoxides, in contrast with the situation for nearly every other substrate.

That unusual finding suggests a hydrogen-bonded interaction between the substrate and the diperoxorhenium compound which cannot exist with the monoperoxo compound.

Introduction

Methyltrioxorhenium (CH_3ReO_3, abbreviated as MTO) is an effective catalyst for reactions in which a substrate X, usually an electron-rich species, is oxidized to XO by hydrogen peroxide:

$$X + H_2O_2 \rightarrow XO + H_2O \qquad (1)$$

In these reactions an oxygen atom is transferred from peroxide to the substrate. The important place of O-atom transfer in industry and biology has been documented,[1] and a common mechanism suggested for inorganic and organic peroxides.[2] The particular place of MTO in this arena has been reviewed.[3-6] In brief, two peroxorhenium compounds play catalytic roles, *usually about equally*; they have been designated **A** and **B**, as shown in **Scheme 1**. The species **A** and **B** attain their equilibrium concentrations rapidly but not instantaneously; during the operation of the catalytic cycle the improved steady-state method[7] approximates their concentrations to good accuracy.

In studying the oxidation of alkyl and aryl sulfides (X = R_2S, ArSR, Ar_2S) to sulfoxides, it was noted that further oxidation to sulfones ensued over longer times.[8] We were motivated to examine this second oxidation step, not only by its fundamental interest and utility in organic synthesis,[9] but also by certain recent findings with diaryl sulfines, X = Ar_2CSO. These compounds show a remarkable U-shaped Hammett plot when aromatic subtituents are changed; thioketones, Ar_2CS, presented a regular progression of rates.[10] Since this phenomenon could in part be attributed to the presence of an electronegative

oxygen atom on the sulfines, we undertook a study of the kinetics of oxidation of diaryl sulfoxides. The sulfoxides are related to diaryl sulfides as sulfines are to thioketones, whose reactions feature a steady (ordinary) increase in rate as substituents on the aromatic ring are made more electron-donating.[8] A series of substrates Ar_2SO was therefore examined as a part of this study.

Scheme 1

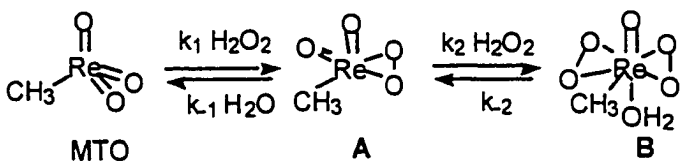

Experimental Section

Materials. Reagent grade acetonitrile was used; laboratory distilled water was purified by a Milli-Q water system. To maintain homogeneity and afford reasonable solubility for these reagents, particularly the less soluble diaryl sulfoxides, 4:1 acetonitrile-water was used as the solvent. MTO was purchased or prepared from sodium perrhenate.[11] Most sulfoxides were obtained commercially.

Bis(4-dinitrophenyl)sulfoxide was prepared from the sulfide by MTO-catalyzed oxidation. The sulfide (2.5 mmol in 25 mL acetonitrile) was treated with 1.0 equiv. hydrogen peroxide and 4% MTO. The product was isolated after a 24 h reaction time by filtration after overnight cooling at ~10 °C. Elem. anal. ($C_{12}H_8SN_2O_5$) found (calcd.): C, 49.09 (49.31); H, 2.61 (2.76); N, 9.48 (9.58).

Kinetics. The progress of most reactions was monitored spectrophotometrically, with NMR used occasionally. The reactions were carried out at 25.0 °C in quartz NMR tubes.

The solutions contained 0.10 M trifluoromethanesulfonic acid to stabilize MTO-peroxide against deactivation.[12]

Owing to the high molar absorptivities, short-path (0.02–0.1 cm) UV cuvettes were used. Typical reaction conditions were 1 mM sulfoxide, 100 mM hydrogen peroxide, and 0.5 mM MTO. These conditions offer accurate absorbance changes. The recorded absorbance amplitudes agreed with those calculated from the molar absorptivities for the conversion of sulfoxide to sulfone. The NMR method was mandatory for Me_2SO, given the lack of suitable absorptions. The CH_3–S(O)R resonance was monitored with time. Both UV and NMR methods were used for **3** as a double-check. Typical NMR concentrations were 10 mM sulfoxide, 1 M hydrogen peroxide and 1.0 mM MTO.

Results

Values for equilibrium and rate constants for **Scheme 1** pertinent to the interpretation of the data have been determined: $K_1 = k_1/k_{-1} = 347$ L mol^{-1}, $K_2 = 91$ L mol^{-1}; $k_1 = 15.5$ L mol^{-1} s^{-1}, and $k_2 = 0.17$ L mol^{-1} s^{-1}.[10] Most kinetics experiments were carried out with a hydrogen peroxide concentration sufficiently high that essentially all of the rhenium was present as the diperoxo compound **B**. Under such conditions, the contribution of **A** to the kinetics can be entirely ignored. The data consist of absorbance-time (UV) or intensity-time (NMR) values, such as those displayed in **Figure 1**. Each experiment was fit very well by a first-order rate equation, establishing a first-order dependence on the sulfoxide concentration. As shown in **Figure 2** for PhS(O)Me and $(4\text{-}NO_2C_6H_4)_2SO$, the plot of k_{obs} against $[Re]_T$ is linear. This pattern affirms this rate law:

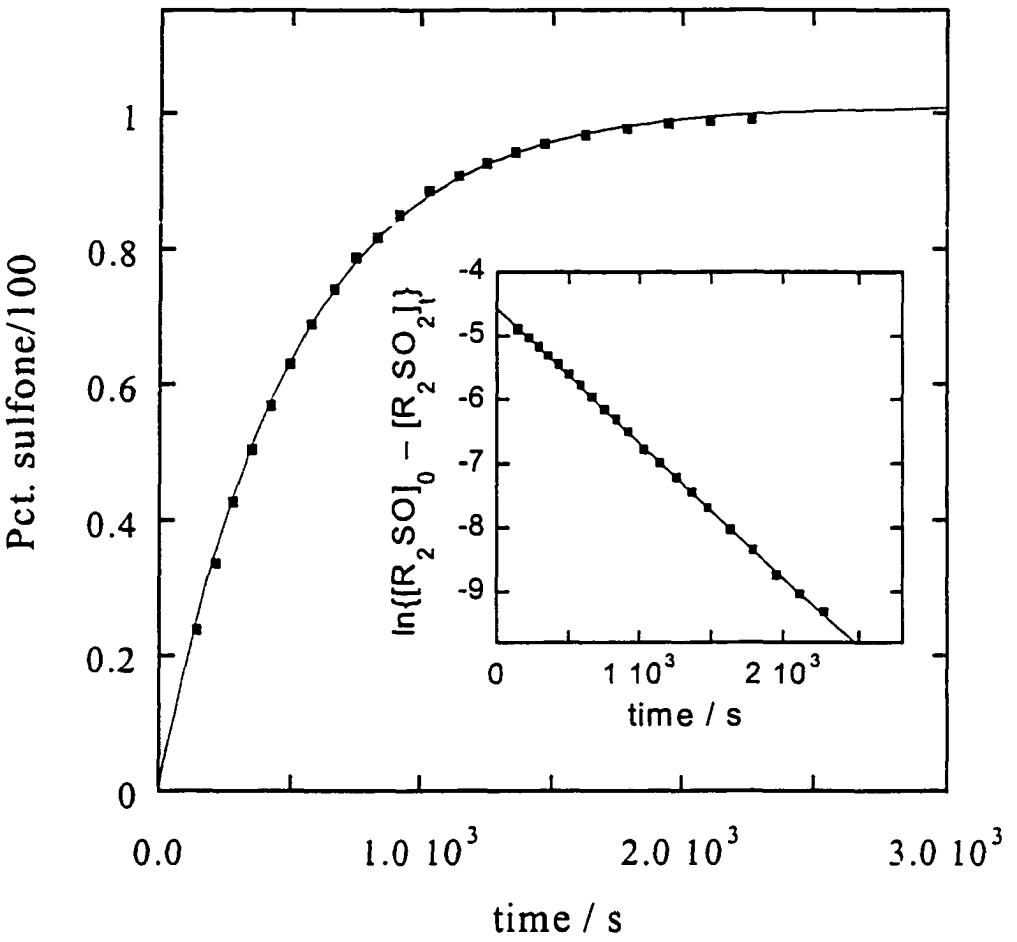

Figure 1. The buildup of bis(dimethyl)sulfone as determined from the integrated intensity of its ^{1}H resonance. The inset shows that fit to first-order kinetics through the linearity of the plot of $\ln\{[Me_2SO]_0 - [Me_2SO_2]_t\}$ with time which gave $k = 2.07 \times 10^{-3}$ s^{-1}. Initial concentrations were 1.3 mM MTO, 9.9 mM dmso, 1.0 M H_2O_2 in 4:1 acetonitrile-water containing 0.1 M HOTf.

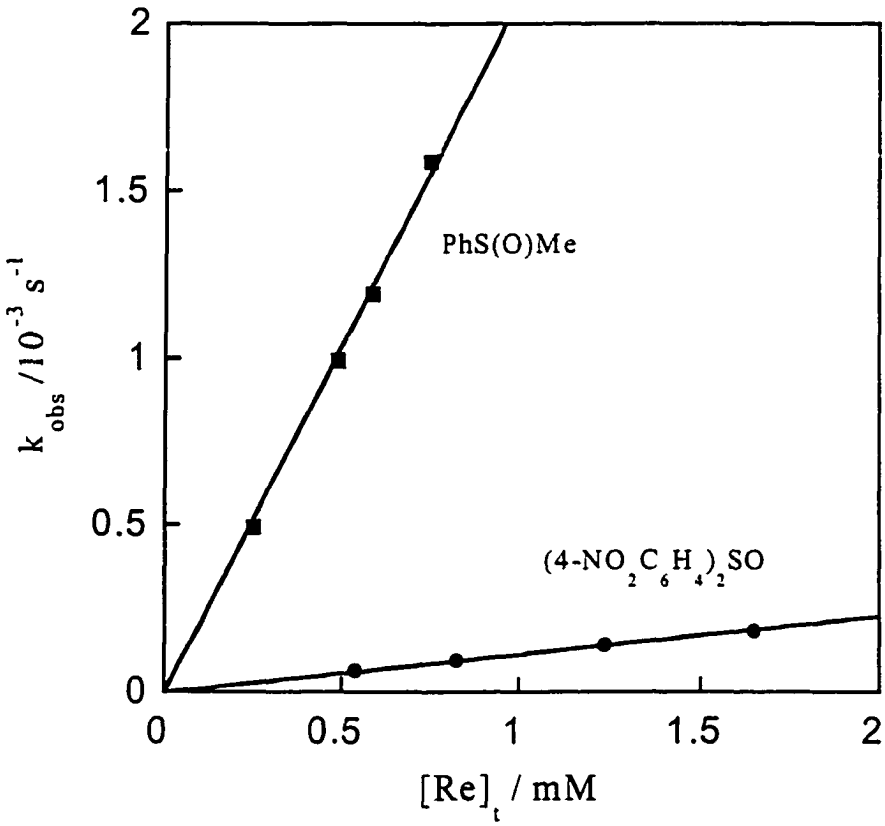

Figure 2. The pseudo-first-order rate constants (k_{obs}) for bis(4-nitrophenyl) sulfoxide (circles) and PhS(O)Me (squares) versus the total initial MTO concentration. The slopes, which represent k_4, are 2.08 and 0.113 L mol^{-1} s^{-1}, respectively.

$$d[R_2SO_2] / dt = k_4[R_2SO][Re]_T \qquad (2)$$

The rate constant proved independent of the hydrogen peroxide concentration in the range 0.1–1.0 mol/L. These concentration dependences show that the slope of the lines in **Figure 2** afford the values of k_4, the rate constant for the reaction between **B** and R_2SO. The values of k_4 for the various sulfoxides studied are presented in **Table 1**. For entry **3**, data from NMR and spectrophotometry were used to confirm agreement between the two techniques. Thus, the value of k_4 for Me_2SO, (which seemed low, given the trends in **Table 1**) can be trusted. Further, it was redetermined multiple times.

Kinetics experiments were also carried out at much lower concentrations of hydrogen peroxide. These are the conditions under which k_3 for the reaction between **A** and sulfoxides could be determined. With no immediate success in determining k_3 under the selected conditions, the kinetics simulation program KinSim[13-15] was used to select the optimum conditions, especially the peroxide concentration, that would best elicit the reactivity of **A**. Regardless of any reasonable assumption as to the relative values of k_3 and k_4, no contribution from the k_3 term could be detected experimentally. To ensure that the procedure was sound, experiments were carried out on thioanisole, for which the k_3 step provides the major pathway, as once again confirmed. Then, to be certain that the sulfoxide does not interact with catalytic intermediate **A**, measurements were carried out on a mixture of diphenyl sulfoxide and thioanisole. The results obtained were as if thioanisol alone had

Table 1. Rate Constants for the Oxidation of Sulfoxides with Hydrogen Peroxide Catalyzed by Methyltrioxorhenium

Entry	Substrate	k_4 / L mol^{-1} s^{-1}
1	Me_2SO	1.5 ± 0.1*
2	PhS(O)Me	2.08 ± 0.03
3	4-$MeC_6H_4S(O)Me$	2.83 ± 0.07
		2.9 ± 0.1*
4	$PhCH_2S(O)Me$	2.87 ± 0.05
5	$(PhCH_2)_2SO$	2.02 ± 0.02
6	$(4\text{-}MeOC_6H_4)_2SO$	3.10 ± 0.02
7	$(4\text{-}MeC_6H_4)_2SO$	1.72 ± 0.01
8	Ph_2SO	0.91 ± 0.02
9	$(4\text{-}FC_6H_4)_2SO$	0.68 ± 0.02
10	$(4\text{-}ClC_6H_4)_2SO$	0.54 ± 0.02
11	$(4\text{-}NO_2C_6H_4)_2SO$	0.113 ± 0.001

* Determined from NMR; others determined from UV-Vis measurements

been used; the sulfoxide did not alter the rate and in the time allotted it was itself not oxidized. We thus conclude $k_4/k_3 \geq 250$ for diphenyl sulfoxide: the k_3 path does not enter.

Sulfoxides are much less reactive towards **A** than **B** and they do not coordinate to MTO (or **A**) to any detectable extent. Thus, they do not affect the oxidation of sulfides by MTO-H_2O_2. These points are not out of the ordinary, in that sulfoxides are not strong Lewis bases and sulfides are oxidized more rapidly than sulfoxides. The relative reactivities of **A** and **B** are striking; only for allylic alcohols has such an effect been noted, $k_3 << k_4$,[16] which was reasonably ascribed to special hydrogen bonding.

Discussion

Large kinetic differences are found between sulfides and sulfoxides, favoring the sulfides by some 10^3; which has been noted for these species before.[17-20] The inductive effect of the oxo group on the sulfoxide must greatly lower the nucleophilicity of the sulfur atom. It is important to contrast kinetics against thermodynamics. For that purpose we use values for thermodynamic functions of the sulfur compounds given.[21] For these two reactions the values of the molar Gibbs energies at 298 K are as shown:

$$Me_2S + H_2O_2 \rightarrow Me_2SO + H_2O \qquad -206 \text{ kJ}$$

$$Me_2SO + H_2O_2 \rightarrow Me_2SO_2 + H_2O \qquad -307 \text{ kJ}$$

These data apply to $Me_2S(O)_n$ in the gas phase, but the same picture emerges when data are referenced to the condensed state.[22] This trend is more or less independent of the R-group on the sulfur atom; for Ph_2S analogues, for which $\Delta H°$ but not $\Delta G°$ values are known,[21] the ΔH_i values are –221 and –324 kJ, respectively. Thus, it is clear that the thermodynamic trends lie in opposite order to the kinetic trends.

The rate constants for the series $(X\text{-}C_6H_4)_2SO$ were analyzed by the linear-free-energy correlation method described by Hammett. For this purpose the x-axis is given by 2σ, where σ is the Hammett substituent constant. Twice the value of sigma was taken, since two equivalent groups are present in these compounds. The resulting correlation is displayed in **Figure 3**. The slope of the line gives the reaction constant as $\rho = -0.65$. The linearity of the plot indicates that a common mechanism, and a common rate-controlling step, operates throughout the series.[18] The negative value of ρ shows that the reaction center (the sulfur atom) becomes more positive in the transition state than in the reagent, consistent with a mechanism in which the peroxide group has become electrophically activated by coordination to the heptavalent rhenium of **B**. In that sense, then, the electron pair of the sulfoxide has it acting as a nucleophile attacking the peroxo oxygen of **B**. This mechanism has been assigned to nearly all reactions in which substrate X is oxidized by hydrogen peroxide under the catalytic influence of MTO.[3,4] (The notable exception is the case of the sulfines, $X = Ar_2CSO$.[10])

We can make certain comparisons between the diaryl sulfoxides reported here with rate constants for diarylthioketones,[10] and aryl sulfides.[8] In that case, the available data refer not to Ar_2S but to ArSMe.[8] The Hammett reaction constants are given here:

Ar_2SO	Ar_2CS	ArSMe	Ar_2CSO
2σ	2σ	σ	2σ
$\rho = -0.65$	~ -1.1	-0.98	U-shaped

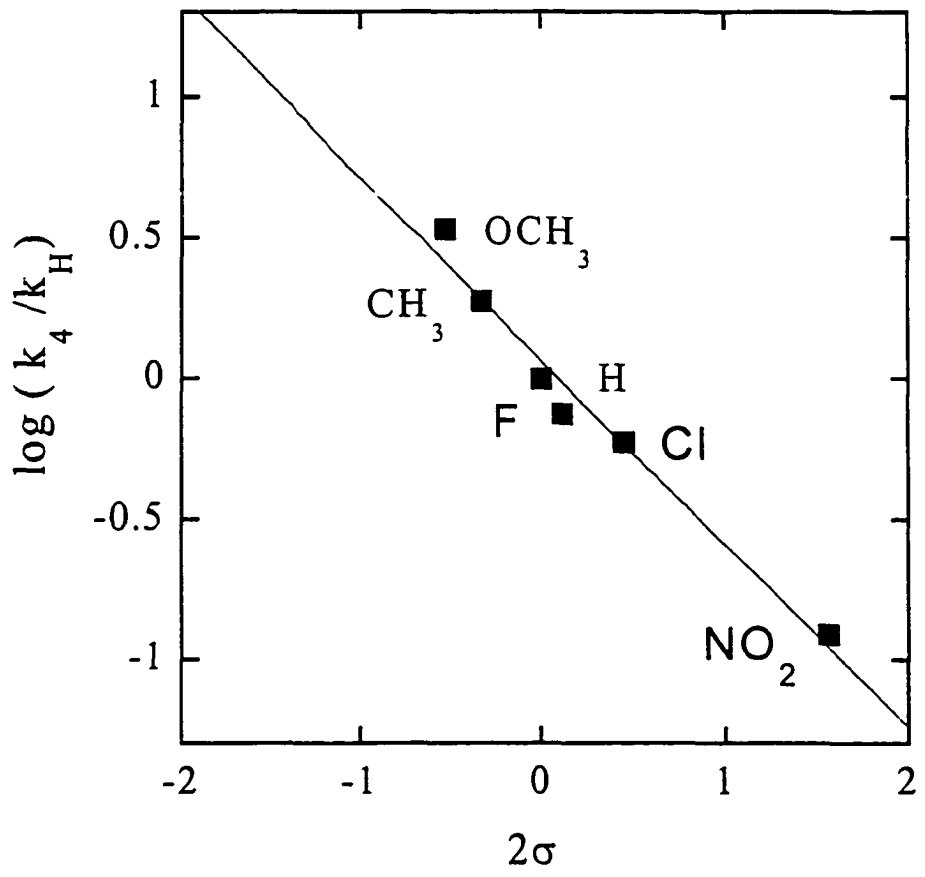

Figure 3. A Hammett plot for the oxidation of substituted diarylsulfoxides by hydrogen peroxide with MTO as a catalyst. The slope of the line gives $\rho = -0.65$.

Clearly the same effects operate along each series, save for the thioketones. The fact that the sulfoxides have a smaller ρ-value compared to the sulfides is consistent with the electronegative oxygen atom muting the kinetic effects of the ring substituent, owing to its polarizing effects in the transition state. Much more dominant than those trends, however, are the large changes (~10^3) in reactivity of sulfides to sulfoxides.[19]

Another means of exploring these effects is by means of a linear-free-energy correlation between parallel sets of compounds, sulfides and sulfoxides. This method allows the inclusion of sets of compounds that cannot be accommodated in a single Hammett correlation. **Figure 4** presents a plot of the rate constant k_4 for sulfoxides, ArS(O)Me and Ar_2SO, against the rate constant (k_3 or k_4, as available) for ArSMe and Ar_2S. The number of data points is limited, and the correlation far from perfect. Nonetheless, these results suggest that the same electronic factors are, by-and-large, applicable to all the rate constants for the parallel reactions of sulfoxides and sulfides. The slope of that imperfect correlation is about 0.4 ± 0.1, again showing that the electronic effects of the additional oxygen atom on the reaction center. The matter under discussion is not simply that sulfoxides are much less reactive than the sulfides, which was dealt with in the opening part of the Discussion. Rather, this point concerns the *relative* rates along the series, sulfoxide compared to sulfide. Put another way, each sulfoxide is less reactive than its sulfide, but along a series in which the sulfide rate constants rise a given amount, those for the sulfoxide rise less. This effect signals a lessening of the effect of the oxygen atom for the more reactive compounds.

The most notable feature of the kinetic data for the sulfoxides is the lack of a detectable contribution for the k_3 pathway. In other words, oxidation proceeds entirely

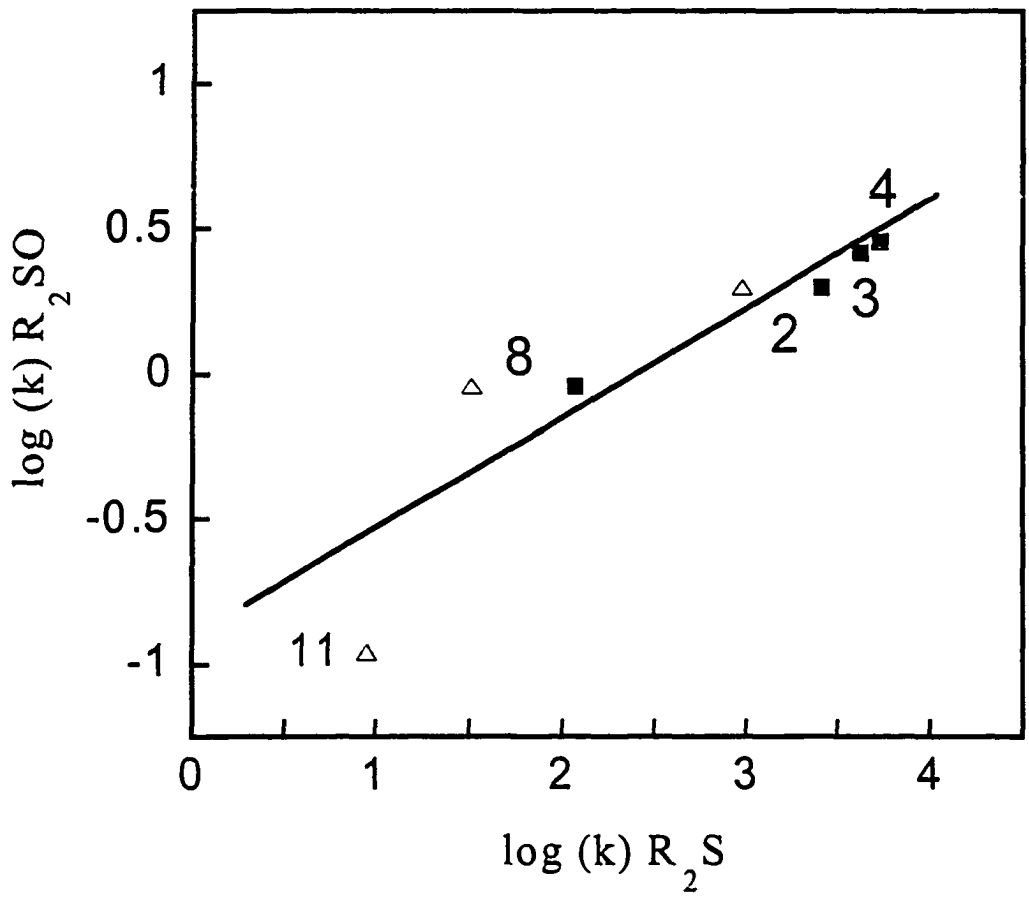

Figure 4. Values of log (k_4) for selected sulfoxides versus log (k_x) for the parent sulfide compounds (ref. 12). Compounds are numbered according to Table 1. A general linear correlation with a slope of about 0.4, can be seen. Values for the sulfides are k_3 (filled squares) and k_4 (open triangles).

through the diperoxorhenium compound **B**, and not at all with **A**. This contrasts with the usual trend for many substrates, where **A** and **B** react at comparable rates ($k_3 \sim k_4$).[3,4] Indeed, in most of those cases **A** carries the much larger portion of the reaction, owing to a rate of regeneration of **B** from **A** that makes the more probable fate of **A** oxygen atom transfer; namely (often) this inequality holds: $k_3[X] >> k_2[H_2O_2]$. The single exception to these general statements to date has been the oxidation of allylic alcohols,[16] a reaction that has also been examined by others.[23,24] That unusual finding was interpreted to suggest a hydrogen-bonded interaction between the substrate and the diperoxorhenium compound **B**, which cannot exist with **A**, as conveyed by the structure shown (see reference 15).

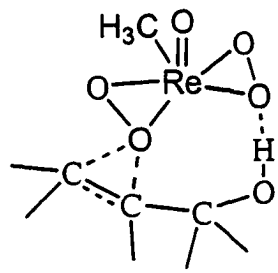

Sulfoxides do not offer a parallel pathway. It is however known that **B** has a water molecule bonded to rhenium and **A** does not. Thus, the Re atom in **B** is seven-coordinate structure,[25] and in **A** five-coordinate.[11] The water molecule can allow for hydrogen bonding in the transition state of the oxidation. The oxo group on the sulfoxide can hydrogen-bond with this water molecule and make a six membered ring:

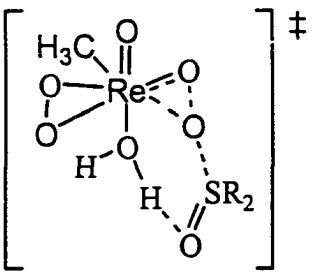

In support of this suggestion it should be noted that sulfones are formed to a greater extent during sulfide oxidation by MTO–H_2O_2 as the water concentration increases.[17]

Acknowledgment. This research was supported by a grant from the National Science Foundation (CHE–9625349). Some experiments were conducted with the use of the facilities of the Ames Laboratory. We are grateful for a reviewer's suggestion concerning the structure of the transition state with the special role for water.

References

(1) Holm, R. H. *Chem. Rev.* **1987**, *87*, 1401-1449.

(2) Mimoun, H. *Angew. Chem., Int. Ed. Engl.* **1982**, *21*, 734-750.

(3) Espenson, J. H.; Abu-Omar, M. M. *Adv. Chem. Ser.* **1997**, *253*, 99-134.

(4) Espenson, J. H. *Chem. Commum* **1999**, 479-488.

(5) Rom‹o, C. C.; KŸhn, F. E.; Herrmann, W. A. *Chem. Rev.* **1997**, *97*, 3197.

(6) Herrmann, W. A.; KŸhn, F. E. *Acc. Chem. Res.* **1997**, *30*, 169.

(7) Espenson, J. H. *Chemical Kinetics and Reaction Mechanisms*; 2 ed.; McGraw-Hill, Inc.: New York, 1995, 86-90.

(8) Vassell, K. A.; Espenson, J. H. *J. Am. Chem. Soc.* **1994**, *33*, 5491.

(9) Tanaka, K.; Kaji, A. in *The chemistry of sulphones and sulphoxides*; Patai, S., Rappoport, Z., Stirling, C. J. M., Eds.; John Wiley & Sons, Ltd: London, 1988, p 759.

(10) Huang, R.; Espenson, J. H. *J. Org. Chem.* **1999**, *64*, 6374.

(11) Herrmann, W. A.; Kratzer, R. M.; Fischer, R. W. *Angew. Chem., Int. Ed. Engl.* **1997**, *36*, 2652-2654.

(12) Abu-Omar, M.; Hansen, P. J.; Espenson, J. H. *J. Am. Chem. Soc.* **1996**, *118*, 4966-4974.

(13) Barshop, B. A.; Wrenn, C. F.; Frieden, C. *Anal. Biochem.* **1983**, *130*, 134.

(14) Frieden, C. *Trends Biochem Sci.* **1993**, *18*, 58-60.

(15) Frieden, C. *Methods in Enzymology* **1994**, *240*, 311-322.

(16) Tetzlaff, H. A. R.; Espenson, J. H. *Inorg. Chem.* **1999**, *38*, 881-885.

(17) Adam, W.; Mitchell, C. M.; Saha-Moller, C. R. *Tetrahedron* **1994**, *50*, 13121.

(18) Ballistreri, F. P.; Tomaselli, G. A.; Toscano, R. M.; Bonchio, M.; Conte, V.; Di Furia, F. *Tetrahedron Lett.* **1994**, *35*, 8041.

(19) Di Furia, F.; Modena, G. *Pure Appl. Chem.* **1982**, *54*, 1853.

(20) Yamazaki, S. *Bull. Chem. Soc. Jpn.* **1996**, *69*, 2955.

(21) Benson, S. W. *Chem. Rev.* **1978**, *78*, 23-35.

(22) *Thermochemistry of sulfoxides and sulfones*; Herron, J. T., Eds.; John Wiley & Sons: New York, 1988.

(23) Adam, W.; Wirth, T. *Acc. Chem. Res.* **1999**, *32*.

(24) Adam, W.; Mitchell, C.; Saha-Moller, C. *J. Org. Chem.* **1999**, *64*, 3699.

(25) Herrmann, W. A.; Fischer, R. W.; Scherer, W.; Rauch, M. U. *Angew. Chem., Int. Ed. Engl.* **1993**, *32*, 1157.

GENERAL CONCLUSION

The family of MeReO(mtp)L compounds, which are showing promising catalytic behavior, have proved to be an interesting class of compounds to study, given their unusual method of ligand exchange. All of these processes involve an intermediate species, which curiously is a stereoisomer of the product. The intermediate and product do not undergo unimolecular rearrangement, another ligand is needed. The 'turnstile' mechanism has been proposed to describe how the ligands exchange, and why and intermediate forms at all. That said, we have proposed that the entering and leaving ligands must do so from the same position, if the principle of microscopic reversibility is to hold, and the turnstile mechanism can explain this. It is of course important to understand how ligands substitute on these compounds, since that is an important part the catalytic process.

The intermediate interestingly shows an unusual long range (four-bond) coupling, which may occur when a W-configuration exists. Such an arrangement can be drawn here, involving H_aH_b–C–S–Re–P. Certainly this coupling only happens when a phosphorus donor ligand is used, and decoupling experiments have shown that ^{31}P to be the origin of the 'extra' splitting. Thus, a lot more is now known about the intermediate, often denoted M–L*, which had been previously observed but not well studied. Unfortunately, no x-ray structures, of compounds with the intermediate configuration, are known. However, the intermediate is believed to have the ancillary ligand and the methyl group in opposite positions.

The preparation of the hydroxide bridging dimer adduct, is important since it further supports the intermediates that have been proposed during kinetics studies of monomerization of $\{MeReO(mtp)\}_2$, or **D**. This, is especially nice since an adduct that

supports the other intermediate in the scheme as been previously prepared, namely the dimethylsulfoxide adduct of **D**.

The work with chelating ligands was interesting, the results were unfortunately not without some conundrums. It does seem certain that the stoichiometry is different for dppm and dppe, and that for dppm yields two MeRe(mtp)(η^1-dppm) compounds for every **D** that reacts. The results with dppe were not so clear. Certainly Re–P bonds are made, but the absolute structure of the product is not known.

The oxidation of sulfoxides proved to be quite unique in that only **B** can oxidize them. Only one other case of such unusual reactivity was reported. This fact has been attributed to hydrogen bonding of a coordinated water molecule of **B** hydrogen-bonding to the sulfoxide substrate in the transition state of the oxygen transfer reaction.

ACKNOWLEDGMENTS

I would like thank Dr. James H. Espenson for guidance over my graduate career. Further, I am also very thankful for support, friendship and scientific assistance from Dr. Andreja Bakac, Dr. Weidong Wang, and the other members of the Espenson research group, past and present. Indeed, numerous sitmulating conversations were had during these years. I would like the thanks my family and friends for further support and encouragement over years. The chemisty faculty at Gustavus Adolphus College have also given support and inspiring my interest in chemistry. I would like the thank Dr. Ilia A. Guzei for the crystallographic work and Dr. Dave Eckels and Prof. Victor Lin for allowing me to use their scanners. Dr. Attila Nemes was of great help for sharing some of his computer knowledge with me. Dr. Dave Scott and Dr. Shu Xu were certainly of great assistance in recording NMR spectra over the years, as well.

This work was performed at Ames Laboratory under Contract No. W-7405-Eng-82 with the U. S. Department of Energy. The United State government has assigned the DOE Report number IS-T 2114 to this thesis.